Rockefeller University
Digital Commons @ RU

Student Theses and Dissertations

2011

Studies of the Kinetics of Cell Cycle Processes in S. Cerevisiae: The Molecular Basis of Start Irreversibility and Cyclin-Cdk Ordering of Mitotic Events

Catherine Oikonomou

Follow this and additional works at: http://digitalcommons.rockefeller.edu/student_theses_and_dissertations

 Part of the Life Sciences Commons

Recommended Citation
Oikonomou, Catherine, "Studies of the Kinetics of Cell Cycle Processes in S. Cerevisiae: The Molecular Basis of Start Irreversibility and Cyclin-Cdk Ordering of Mitotic Events" (2011). *Student Theses and Dissertations.* Paper 149.

This Thesis is brought to you for free and open access by Digital Commons @ RU. It has been accepted for inclusion in Student Theses and Dissertations by an authorized administrator of Digital Commons @ RU. For more information, please contact mcsweej@mail.rockefeller.edu.

STUDIES OF THE KINETICS OF CELL CYCLE PROCESSES IN *S. CEREVISIAE*: THE MOLECULAR BASIS OF START IRREVERSIBILITY AND CYCLIN-CDK ORDERING OF MITOTIC EVENTS

A Thesis Presented to the Faculty of

The Rockefeller University

in Partial Fulfillment of the Requirements for

the degree of Doctor of Philosophy

by

Catherine Oikonomou

June 2011

© Copyright by Catherine Oikonomou 2011

STUDIES OF THE KINETICS OF CELL CYCLE PROCESSES IN *S. CEREVISIAE*: THE MOLECULAR BASIS OF START IRREVERSIBILITY AND CYCLIN-CDK ORDERING OF MITOTIC EVENTS

Catherine Oikonomou, Ph.D.

The Rockefeller University 2011

The cell cycle machinery of *Saccharomyces cerevisiae* consists of a central negative feedback oscillator comprising cyclin-CDK and its antagonist, APC^{Cdc20}. This oscillator is stabilized and tuned by positive feedback loops, and its frequency is modulated by checkpoint controls. Either by directly triggering events, or by entraining independent oscillators controlling events, the cyclin-CDK oscillator regulates the key events of the cell cycle. These events have an established order and timing within the overall cycle.

The work I describe in this thesis concerns two fundamental questions: how is the order and timing of cell cycle events controlled, and what sets the intrinsic frequency of the cell cycle oscillator? I describe work on two major processes in the cell division cycle that reveals two very different modes of regulation. The first of these processes – Start – represents a pivotal commitment to divide. In collaboration with Gilles Charvin, I demonstrate that positive feedback in the molecular machinery underlying Start acts as a bistable switch that renders this regulatory transition irreversible.

The second major process is Mitosis, a set of events all triggered by the same class of cyclin-CDKs and yet occurring in a set and reproducible order. I describe an

ordering mechanism underlying this choreography that relies on the natural ramping-up of cyclin-CDK activity level. The observation that different events require different levels of cyclin-CDK activity leads to the question of how these thresholds are set. To begin to answer this, I discuss how mitotic cyclin-CDK triggers two different events – depolarization of growth and formation of the mitotic spindle – in two very different ways. The first relies on entrainment of an independent oscillator controlling growth polarization; the other may involve the simultaneous regulation of multiple targets.

The observation that cyclin-CDK is rate-limiting for mitotic events suggests that increasing the level of this key cell cycle regulator above its endogenous range should accelerate Mitosis, and I show evidence that this is the case. Quite surprisingly, this increase in cyclin-CDK abundance also accelerates the frequency of the cell cycle oscillator as a whole through its effect on growth. This provides an intriguing new answer to the question of what sets the intrinsic frequency of the cell cycle oscillator.

Together, this work underscores the central role of the mitotic cyclin-CDK regulator, which controls not only the relative timing of individual cell cycle events, but also the growth rate of the cell, and the overall frequency of the cell cycle oscillator.

For those who gave magic to science – my mother, Patricia Malone;

my brother, Andrew Lookingbill; and my husband, Grigori.

ACKNOWLEDGMENTS

I wish to thank the many contributors to this work. I am indebted to those who contributed reagents and advice: Gilles Charvin, Eric Siggia, Jamie Bean, Stefano di Talia, Nick Buchler, Lea Schroeder, Ben Drapkin, Andrea Procko, Amy Ikui, Joanna Bloom, Jon Robbins, and Ying Lu. I am further indebted to Gilles Charvin for his teaching and discussions during a fruitful collaboration discussed in this thesis. I am thankful for all past and present members of the Cross laboratory, including Lucy Bai, Kresti Pecani, Frej Tulin, Jess Rosenberg, and Andrej Ondracka, for contributing advice, support, and good humor. I am deeply grateful for my mentor, Fred Cross, who taught through demonstration the practice of science, the idea of scientific method, and clarity of thinking. And I am infinitely and happily indebted to Grigorios Oikonomou for his patience, his always wise advice, and his optimism.

TABLE OF CONTENTS

Dedication iii
Acknowledgments iv
Table of Contents v
List of Figures vii
List of Tables ix
Chapter 1 – Introduction 1
- Outputs of the Cell Cycle Oscillator 1
- A Negative Feedback Oscillator at the Heart of the Cycle 5
- Stabilization and Tuning by Positive Feedback 8
- Intrinsic Frequency Control of the Cell Cycle Oscillator 11
- Entrainment Between the Cell Cycle and Other Oscillators 15
- The Cyclin-CDK Oscillator Entrains Peripheral Cell Cycle Oscillators 16
- Scope of the Thesis Work 22

Chapter 2 – The Molecular Architecture that Makes Start Irreversible 24
- A Sharp Nonlinearity in Start Activation 28
- Positive Feedback of G1 Cyclins Makes Start Irreversible 36
- Whi5 Mediates the Irreversibility of Start 43
- Cln2 Controls the Dynamics of Budding 45

Chapter 3 – Graded Cyclin-CDK Levels Order Mitotic Events 48
- A System to Measure Mitotic Cyclin-CDK Requirements 51
- Increasing Cyclin-CDK Levels Order Mitotic Events 57
  - Growth Depolarization 59
  - Spindle Formation 61
  - Spindle Elongation/ Anaphase 69
- Swe1 Modulates Event Timing in Early Mitosis 71
- Testing a Mathematical Cell Cycle Model 72

Chapter 4 – Mechanistic Bases of Mitotic Cyclin-CDK Requirements 76
- Clb2-CDK Control of Growth Depolarization 78
- The Molecular Basis of the Threshold for Clb-CDK-Mediated Spindle Formation 81
  - Sfi1, a SPB Bridge Protein 81
  - Cin8, a Kinesin-5 Motor 86

Chapter 5 – Mitotic Cyclin-CDK Modulates the Frequency of the Cell Cycle Oscillator 93
- Increased Clb2 Level Accelerates Cell Cycle Timing 93
- Clb2 Overexpression Imposes a Fitness Cost 99

Chapter 6 – Discussion 103
- Molecular Architecture of Cell Cycle Transitions 103
  - Start: an Irreversible Switch 103
  - Mitosis: an Ordered Program of Events 105
- Setting Thresholds for Clb-CDK Activity 108
- Setting the Frequency of the Cell Cycle Oscillator 111

Appendix – Materials and Methods 113
I. Experimental Procedures 113
II. Experimental Materials 122
References 126

LIST OF FIGURES

1-1 Major processes of the cell division cycle in *S. cerevisiae* 2
1-2 A negative feedback loop lies at the core of the cell cycle oscillator....7
1-3 Positive feedback loops stabilize the cyclin-CDK oscillator....9
1-4 G1 size control in *S. cerevisiae* 13
1-5 Molecular mechanism of the Cdc14 release oscillator....18
1-6 Phase-locking entrains multiple peripheral oscillators to the cyclin-CDK oscillator....20
2-1 The molecular machinery underlying the Start transition 25
2-2 Schematic of bistable and irreversible system behavior....27
2-3 Passage through Start in response to *CLN2* pulses of various lengths 30
2-4 Correlation of expression of Venus and mCherry fluorophores driven by the *MET3* promoter in the same cell....32
2-5 Measurement of nonlinearity in Start activation 34
2-6 *MET3* promoter transcription rate as a function of –Met pulse duration 35
2-7 Start activation and *MET3* transcription rate following a *MET3:CLN2* pulse are independent of cell size....37
2-8 *CLN1,2*-mediated positive feedback renders Start irreversible....40
2-9 Whi5 mediates Start irreversibility....44
2-10 Polarized growth in the presence and absence of *CLN1,2* positive feedback ..46
3-1 Quantitative model for ordering events....50
3-2 Timing difference between CLB^{WT} and *clb1Δ clb3Δ clb4Δ* cells....52
3-3 Experimental protocol to measure Clb2-CDK requirements 54
3-4 Clb2-CDK inhibition by Swe1 in early Mitosis....56
3-5 Clb2-CDK activity ramps up over a period of 40 minutes....58
3-6 Relative timing of growth depolarization and spindle formation....60
3-7 Polarized growth cycles in the absence of Clb2-CDK 62
3-8 Clb2-CDK requirement for growth depolarization 63
3-9 Clb2-CDK requirement for spindle formation 65
3-10 Validation of experimental protocol for assaying spindle formation....66
3-11 Relative Clb2-CDK requirements for growth depolarization and spindle formation....68
3-12 Clb2-CDK requirement for anaphase....70
3-13 Swe1 raises the Clb2 requirement for spindle formation 73
3-14 Comparison of published ODE model for spindle formation with experimental results 74
4-1 A model for Clb2-CDK phase-locking of an independent growth polarization oscillator....80
4-2 Schematic of SPB-mediated spindle assembly....82
4-3 CDK consensus sites in the SPB bridge protein Sfi1 84
4-4 Clb2-CDK phosphorylation of Sfi1 promotes efficient spindle formation 85
4-5 Kinesin-5 motor activity generates outward force on SPBs....87

4-6 Clb2-CDK-mediated Cin8 accumulation is not rate-limiting for spindle formation....89
4-7 Increased Cin8 can rescue the spindle formation defect of *sfi1-120*....90
4-8 Combination of potential Clb-CDK bypass mutations in *SFI1* and *CIN8* does not affect Clb2 requirement for spindle formation....91
5-1 Clb2 is rate-limiting for cell cycle frequency....95
5-2 Clb2 overexpression accelerates individual mitotic events....96
5-3 Clb2 overexpression increases the rate of increase of cellular area through premature growth depolarization....98
5-4 *clb2::GALL:CLB2* does not exhibit synthetic lethality with *mad2Δ*....100
5-5 Clb2 overexpression imposes a fitness cost....101

LIST OF TABLES

1 Yeast strains used in this study 122
2 Plasmids used in this study 125

CHAPTER 1 – INTRODUCTION

Oscillatory networks underlie much of biology: the beating of our hearts, the circadian clock which couples our behavior to the light-dark cycle of the planet, and, most fundamental of all, the cycle of cell division, which creates two cells from one and thus drives the reproduction and development of all living systems. Oscillators can be characterized by the order and timing of specific outputs from the cycle, as well as by their overall operating frequency (how often the cycle occurs). My interest here is in what controls these aspects of the cell cycle oscillator, which I study in the unicellular budding yeast.

Outputs of the Cell Cycle Oscillator

In each round of cell division, the contents of the mother cell are replicated, and a faithful copy distributed to each of the two daughter cells. This entails several major processes, schematized in Figure 1-1 and discussed below.

First, the cell must commit to division. In budding yeast, this decision is based on nutrient availability, sufficient cell size, and, in haploid cells, the absence of pheromone signals from cells of the opposite mating type. This regulatory transition into the division cycle is known as "Start" and is an irreversible commitment (Cross, 1995). I will discuss the regulatory machinery of Start in Chapter 2. Once committed, the cell must replicate its various components. These components can be classed generally into two categories: those present at high copy number, and those present at low copy number. Fairly

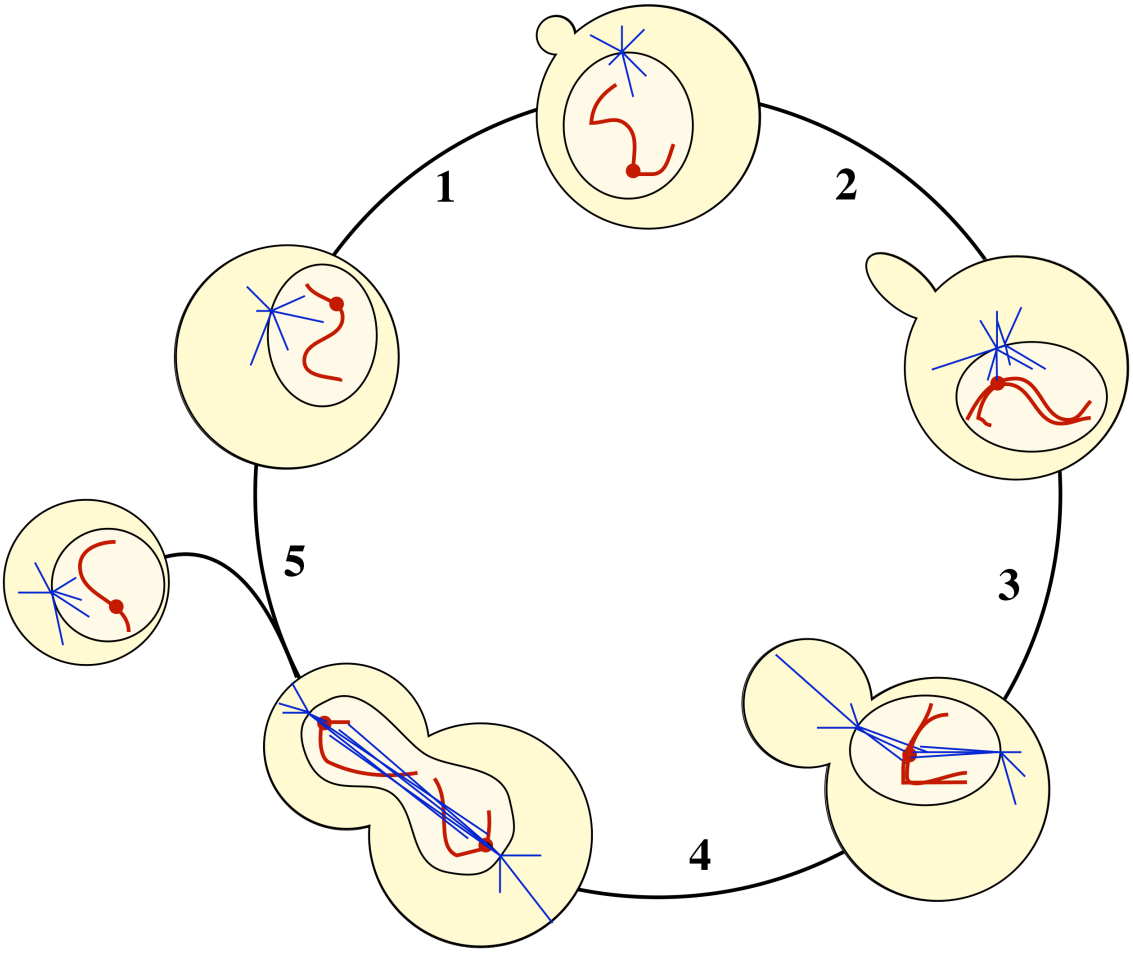

Figure 1-1 Major processes of the cell division cycle in *S. cerevisiae* **1** The cell commits to a complete round of division at Start. Soon after Start, the bud (future daughter cell) begins to form. **2** Two major single-copy components are duplicated: the chromosomes (one of 16 is shown, in red), containing the cell's genomic information; and the SPB (shown in blue with nucleated microtubules), which organizes microtubules. **3** The mitotic spindle forms within the nucleus (unlike many other eukaryotes, *S. cerevisiae* undergoes a closed Mitosis, with no breakdown of the nuclear envelope); sister chromatids attach to opposite SPBs. **4** The mitotic spindle elongates in anaphase, pulling one set of separated chromosomes to each pole. **5** The nucleus divides (karyokinesis) and the daughter cell pinches off (cytokinesis), completing the replicative cycle.

abundant structures, such as ribosomes and mitochondria, increase in abundance as the cell grows and can simply be partitioned by the division plane – each resulting cell will get enough. In segregating lower-abundance items, however, the cell cannot rely on chance: one progeny may get too many copies and the other none.

One such low-copy number item is the nuclear DNA, the genetic content of the cell, present as a single copy. Two special portions of the cell cycle deal with genomic duplication and segregation. First is the Synthetic phase, or S-phase, in which a full copy of the genome is synthesized. The second is Mitosis, a remarkable, choreographed routine resulting in precise separation of the two copies. I will discuss how this set of events is regulated in Chapters 3 and 4. In the metaphase portion of Mitosis, a structure known as the spindle is assembled between two scaffolding points: the centrosomes or Spindle Pole Bodies (SPBs), as they are known in yeast. (Interestingly, some organisms can assemble spindles even without centrosomes.) The spindle consists of filamentous microtubules extending from the SPBs to the duplicated chromosomes (16 in budding yeast). At this point, each chromosome consists of two copies known as chromatids. Each chromatid is physically linked to its duplicated "sister." To ensure that one copy goes to each cell, the two sisters of each chromosome connect to opposite SPBs. Once all attachments are correctly made, the anaphase portion of Mitosis begins. The tethers between sister chromatids release and the spindle rapidly extends, pulling one SPB and its full set of associated chromosomes past the division plane and into the daughter cell, while leaving the other SPB and chromosome set in the mother cell (Morgan, 2007).

A second low-copy number item is the SPB itself. It takes two poles to assemble the spindle, and more than two SPBs could result in aberrant separation of chromosomes.

After cell division, each daughter cell contains one set of genomic DNA, and one associated SPB. Around the time of S-phase, this SPB is duplicated, and the two copies remain tethered to one another until it is time to separate and form the spindle (Haase et al., 2001; Simmons Kovacs et al., 2008).

In many organisms, the mother cell grows to a sufficient size and then splits down the middle to produce two symmetric cells by fission. In budding yeast, however, division is asymmetric, resulting in a larger mother (the original cell) and a smaller daughter. The incipient daughter cell is visible throughout most of the cell cycle in the form of a growing bud attached to the mother cell. Cortical growth continues throughout the cell cycle (expanding the cell's surface), but nearly all such growth is concentrated in the bud. Soon after Start, bud morphogenesis begins as the cell's actin-mediated cortical growth redirects to a single site, establishing the new bud. This polarized growth continues to push out the bud tip until about the beginning of mitosis, when a switch occurs from polarized growth to isotropic growth, in which growth is redistributed over the full cortex of the bud so that it rounds out in all directions. Growth is still concentrated in the bud, however, until around the time of anaphase when growth redistributes evenly between the mother and daughter cortex (Lew and Reed, 1993). Following segregation of a SPB and a set of chromosomes into the bud, cytokinesis occurs, pinching off the bud to create an autonomous daughter cell.

A Negative Feedback Oscillator at the Heart of the Cycle

The machinery governing the ordered execution of the events described above is a biochemical oscillator. In principle, simple genetic circuits can give rise to oscillations. For example, the negative feedback loop X → R —| X (protein X activates an inhibitor R, which inhibits X, so that R goes down, so that X goes back up…) can yield oscillations. To continue oscillating, however, such a circuit requires significant non-linearity or a time delay to introduce an overshoot to keep the system from settling to a constant steady state (Novak and Tyson, 2008). The molecular nature of this negative feedback oscillator differs between prokaryotes and eukaryotes. In the bacterium *Caulobacter crescentus*, phospho-signaling cascades control cell cycle progression. Cell cycle oscillations are proposed to arise from a negative feedback loop involving the master regulator CtrA and DivK, which indirectly triggers CtrA destruction. A time delay is introduced by the dependency of DivK accumulation on cell division (Biondi et al., 2006). In the eukaryotic cell cycle, the central oscillator consists of a negative feedback loop comprising the cyclin-Cyclin Dependent Kinase (CDK) complex and its antagonist, the Anaphase Promoting Complex (APC) (Felix et al., 1990; Morgan, 2007). A time delay is introduced by additional molecular components, as discussed below.

CDKs, the main regulatory kinases of the eukaryotic cell cycle, are enzymes that add phosphate groups to specific Serines or Threonines (minimal recognition sequence [S/T P], full consensus sequence [S/T P X K/R]) of substrate proteins (Morgan, 2007). These phosphorylations can modify the activity or localization, or trigger the degradation, of the substrates. CDKs on their own are inactive. They rely on the binding of a second

protein for activity. These activators, called cyclins for their cyclical expression pattern (Evans et al., 1983), confer not only activity, but also determine the localization of the complex and its specificity for targets (Loog and Morgan, 2005; Bloom and Cross, 2007). In budding yeast, there is one major CDK responsible for most cell cycle events (and sufficient for cell cycle progression): Cdc28. It is activated variously by nine different cyclin subunits, which are expressed at different times during the cycle and regulate different events (Bloom and Cross, 2007). At the beginning of the cell cycle, cyclin-CDK activity is low, and ramps up over most of the cycle. Early cyclins trigger production of later cyclins and these later cyclins turn off the earlier cyclins, so that control passes from one set of cyclin-CDKs to the next (Morgan, 2007). The last set of cyclins to be activated, the mitotic cyclins, initiate Mitosis, the separation of genetic material into the two daughter cells, and also initiate their own destruction by activating the APC (Rudner and Murray, 2000; Rudner et al., 2000).

The APC is a multi-subunit complex that similarly relies on the binding of one of two alternative activating subunits for activity and specificity. When active, the complex catalyzes the transfer of ubiquitin molecules to target substrates. Chains of ubiquitin act as signals to degrade the protein, an action carried out by a giant protein complex known as the proteasome (Morgan, 2007). Temporally, the APC is first bound by Cdc20, and it is this complex which is activated by mitotic cyclin-CDK activity and which targets the mitotic cyclins for destruction, resetting the cell to a low-CDK activity state. This interplay between cyclin-CDK and APC activities forms the negative feedback loop that lies at the heart of the cell cycle oscillator (Figure 1-2).

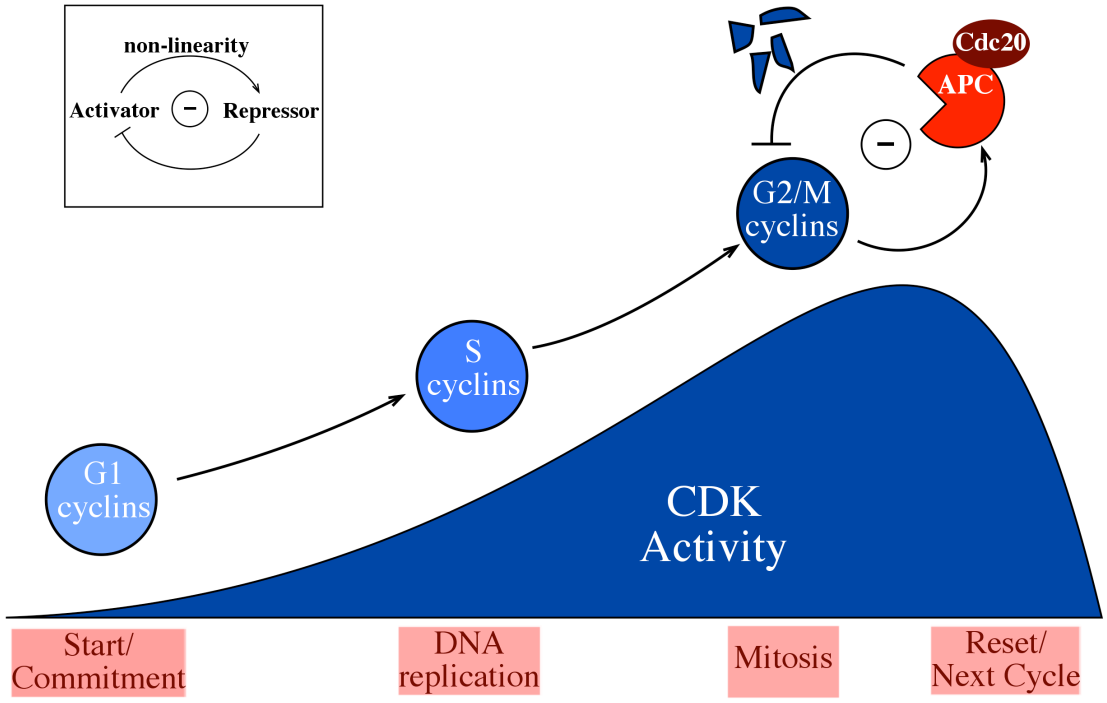

Figure 1-2 A negative feedback loop lies at the core of the cell cycle oscillator. Inset: a simple negative feedback loop that can give rise to oscillations. The circled minus sign indicates a negative feedback loop, and I will use this convention throughout. Below: CDKs, present throughout the cell cycle, require the binding of a cyclin subunit for activity. These cyclin partners can also determine the localization of the complex and its specificity for targets. At the beginning of the cell cycle, cyclin-CDK activity is low, and ramps up over most of the cycle. Early cyclins trigger production of later cyclins and these later cyclins subsequently turn off the earlier cyclins, so that control passes from one set of cyclin-CDKs to the next. The last set of cyclins to be activated, the G2/M-phase cyclins, initiate Mitosis, and also initiate their own destruction by activating the APC^{Cdc20} negative feedback loop. APC^{Cdc20} targets the G2/M-phase cyclins for destruction, resetting the cell to a low-CDK activity state, ready for the next cycle.

Stabilization and Tuning by Positive Feedback

Negative feedback oscillators form the core not just of the cell cycle, but of many biological clocks, including multiple independent circadian systems, each operating with different biochemical machinery (King and Takahashi, 2000; Dunlap et al., 2007; Markson and O'Shea, 2009). A synthetic "repressilator" has even been constructed using a three-negative-feedback genetic architecture and shown to oscillate (Elowitz and Leibler, 2000). This "repressilator" architecture, however, is relatively unstable and has not been observed in any natural system, to my knowledge. In natural cases of negative feedback oscillators, the "low X" and "high X" states are stabilized by the addition of positive feedback elements. While these positive feedback loops in principle are not essential for oscillations, empirically they appear to increase greatly the reliability and robustness of the oscillator (Cross, 2003).

In the cell cycle, there are multiple positive feedback loops stabilizing the central negative feedback oscillator, schematized in Figure 1-3. A highly conserved but non-essential mechanism is the handoff of cyclin proteolysis from APC^{Cdc20} to APC^{Cdh1}. Cdh1 is a homolog of Cdc20 that activates the APC late in mitosis and into the beginning of the next cell cycle. Cdh1, unlike Cdc20, is inhibited by cyclin-CDK activity, resulting in mutual inhibition (a double-negative that is logically equivalent to positive feedback) (Zachariae et al., 1998). Another positive feedback loop involves a set of cyclin-CDK Inhibitors (CKIs), including Sic1 in budding yeast, that inhibit the kinase through a stoichiometric interaction. Cyclin-CDKs in turn inhibit the CKIs, thereby closing the mutual inhibition loop. These two positive feedback circuits stabilize high- and low-

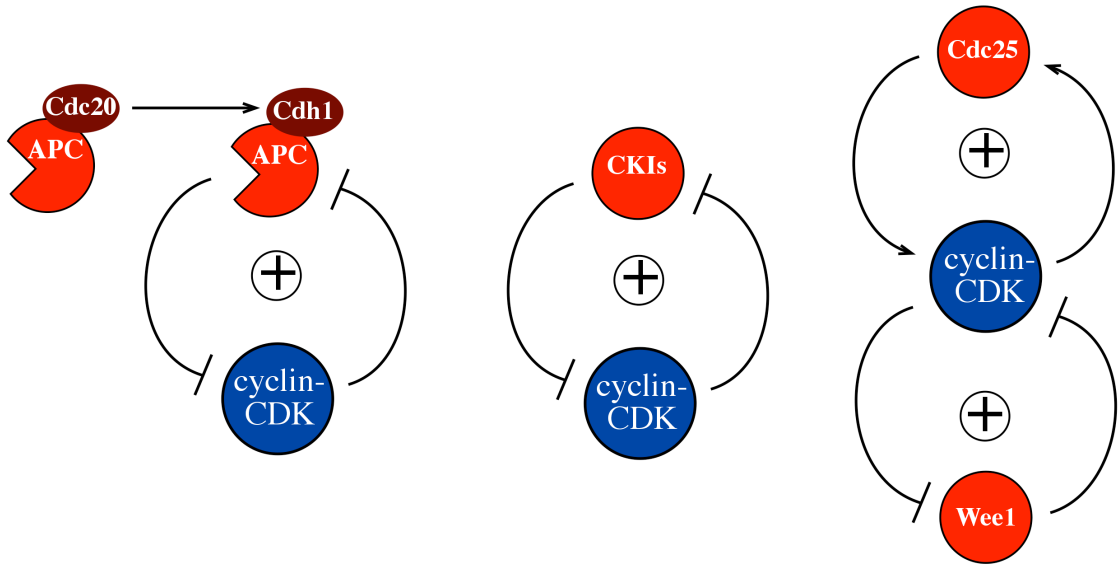

Figure 1-3 Positive feedback loops stabilize the cyclin-CDK oscillator. Left: handoff of cyclin proteolysis from APC^{Cdc20} to APC^{Cdh1}. Cdh1 is a homolog of Cdc20 that activates the APC late in Mitosis and into the ensuing G1. Cdh1 is inhibited by cyclin-CDK activity, resulting in mutual inhibition. Middle: antagonism between cyclin-CDKs and stoichiometric CDK inhibitors (CKIs) results in logical positive feedback. Right: a double positive feedback loop comprises CDK-mediated inhibition of the Wee1 kinase (which inhibits CDK) and activation of the Cdc25 phosphatase (which activates CDK by removing the inhibitory phosphorylation added by Wee1).

CDK activity states (Cross, 2003). An additional positive feedback mechanism stabilizes the intermediate CDK activity found in mid-cycle, as well as an alternative stable state of high mitotic CDK activity. This mechanism consists of two positive feedback loops controlling an inhibitory phosphorylation on the CDK itself. The kinase, Swe1 (Wee1 in other organisms), that adds this phosphorylation (thus inhibiting the CDK) is inhibited by cyclin-CDK activity; the phosphatase, Cdc25, that removes the phosphorylation (thus activating the CDK) is activated by cyclin-CDK activity (Pomerening et al., 2003; Harvey et al., 2005).

Positive feedback loops can also contribute to the irreversibility or coherence of specific processes within the cell cycle. In Chapter 2, I will discuss a positive feedback loop that makes commitment to the division cycle at Start irreversible, and leads to the near-simultaneous activation of hundreds of genes (Skotheim et al., 2008; Charvin et al., 2010b). Similarly, a positive feedback loop was recently shown to function during the separation of sister chromatids at anaphase. The links between sister chromatids are severed by a protease called separase. Separase is activated by a positive feedback loop that creates a switch-like transition to high levels of activity, ensuring that all 16 sets of chromatids are separated at nearly exactly the same time (Holt et al., 2008).

Positive feedback may serve other purposes as well. Theoretical comparison of negative-feedback-only and negative-plus-positive-feedback models of a cell cycle oscillator suggests that positive feedback dramatically increases the functional frequency range of the oscillator without significantly altering its amplitude. Thus, positive feedback may be a source of elasticity to accommodate a broad range of frequencies (cell cycle times in the same organism can vary from minutes to hours or days) using the same

fundamental machinery. This in turn could promote the evolvability of the system (Tsai et al., 2008).

Intrinsic Frequency Control of the Cell Cycle Oscillator

Theoretically, the cell cycle control system should oscillate with a frequency that is determined by the timescales of protein synthesis, inhibition, and degradation. However, in most cells the observed cell cycle frequency is highly variable. As an extreme example, the cell cycle in the early embryo of the fly can oscillate with a frequency of approximately ten minutes, while later somatic cells have frequencies measured in hours or days. Multiple mechanisms contribute to this tuning of the oscillator's frequency.

One crucial modulator of the inherent frequency of the cell cycle is a set of controls designed to ensure the integrity of cell replication. These controls ensure that division does not occur under non-optimal conditions, for example with insufficient cell size, errors in cell morphogenesis, incomplete DNA replication, DNA damage, or partially-assembled mitotic spindles. This is accomplished by halting the cell cycle machinery at set points until all requirements have been met (Hartwell and Weinert, 1989).

In budding yeast, however, checkpoint controls, for the most part, do not contribute to the timing of individual cell cycle events (they are not activated in an unperturbed cycle), and the cycle proceeds normally in their absence (Weinert et al., 1994; Cross et al., 2002). The notable exception is cell size, which has a clear effect on

cell cycle frequency. In most cells (with the exception of embryonic cells resulting from the rapid division of very large fertilized eggs), cell growth is coordinated with cell division. This is intuitive, as a population of ever-larger or ever-smaller cells is unsustainable. In budding yeast, it was long ago observed that growth is rate-limiting for cell division (Johnston et al., 1977). In practice, the coupling of cell growth and cell division results because cells in the G1 phase (the first phase of the cell cycle, during which cells grow and perhaps commit to a round of division) encounter a size control (Figure 1-4). Cells of increasing size are increasingly likely to initiate Start (Bean et al., 2006; Di Talia et al., 2007). Actual size measurement was recently proposed to operate through direct binding of the most upstream G1 cyclin – Cln3 – to the target sequence of a critical G1/S-phase regulatory transcription factor (Wang et al., 2009). Unlike other cyclins, whose levels oscillate throughout the cell cycle, Cln3 is fairly constantly expressed, scaling with overall protein level in the cell (which increases as cells get bigger) (Cross, 1995; Schneider et al., 2004). The genes for the next cyclins in the progression, the G1/S cyclins – Cln1 and Cln2 – which trigger Start and other early events of the cell cycle, are controlled by two transcription factors: SBF (made up of the Swi4 and Swi6 proteins) and MBF (made up of Swi4 and Mbp1) (Bean et al., 2005). In G1, SBF transcription factors are bound by a repressor, Whi5, which is exported from the nucleus by Cln3, resulting in expression of *CLN1* and *CLN2* (Costanzo et al., 2004; de Bruin et al., 2004). It was recently shown that Cln3 binds directly to the target sequences of SBF (known as SCB sites) and Start activation may occur when all of these sites are titrated by Cln3. Remarkably, when the number of SCB sites in the genome is increased, the size of cells undergoing Start is similarly increased, in a Cln3-dependent manner.

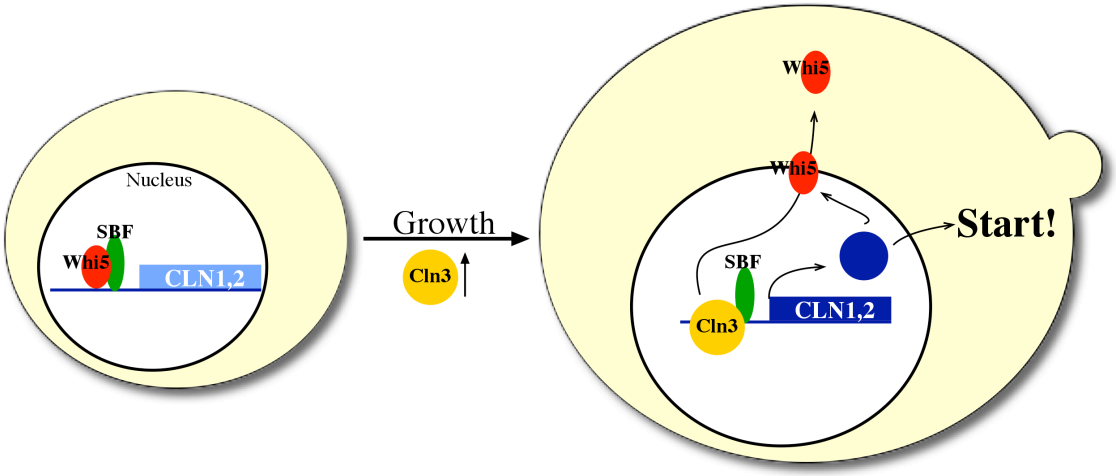

Figure 1-4 G1 size control in *S. cerevisiae*. Transcription of many genes, including the G1/S-phase cyclins (*CLN1* and *CLN2*) is controlled by the SBF (made up of Swi4 and Swi6) transcription factor. The Whi5 repressor inhibits this transcription until it is exported from the nucleus by the most upstream G1 cyclin – Cln3 – in response to sufficient cell size. Cln3 thus relieves transcriptional inhibition, promoting *CLN1,2* expression and subsequent cell cycle Start. Cln1 and Cln2 then promote their own transcription (a positive feedback loop). Actual size "measurement" was recently proposed to operate through direct binding of Cln3 to the SCB target sequences of SBF, with Start occurring upon titration of these sites by Cln3.

Thus size measurement may occur through a direct comparison between the size of the cell (reflected by Cln3 protein levels) and a fixed reference – the number of SCB sites in the genome (Wang et al., 2009).

Budding yeast undergo asymmetric cell division, resulting in a larger mother cell and a smaller daughter cell (the pinched-off bud). This unusual mode of division means that mother cells retain their size from previous cycles. Mothers have already "passed" size control during their previous cycle (Hartwell and Unger, 1977). Interestingly, mothers and daughters were recently reported to experience different transcriptional control of *CLN3*, the size-sensing cyclin (Di Talia et al., 2009). Mothers exhibit a pulse of *CLN3* immediately after cell division, which may drive a prompt and largely size-independent Start. Daughter cells lack this pulse. Hence they are subject to the tight size control described before. This explains the observed regular and rapid cell divisions of mother cells, compared to the much slower divisions of daughter cells. The difference appears to be largely due to the need for an extended growth period in daughter cells to catch up to the mothers' size (Di Talia et al., 2009).

The observation that growth is rate-limiting for division (Johnston et al., 1977) suggests that the oscillator's frequency can only be increased through added nutrients, not through any tinkering with the regulatory mechanism of the oscillator. However, recently it has been observed that while the growth rate controls cell cycle progression, the converse may be true as well, since the growth rate is lower and higher at different points in the cell cycle (Mitchison, 1958; Goranov et al., 2009). In Chapter 5, I will discuss work suggesting that, in fact, a key component of the cell cycle oscillator helps to set the oscillator's frequency by affecting the cell's growth rate.

Entrainment Between the Cell Cycle and Other Oscillators

The cell cycle is not the only oscillatory system present in cells, and under certain circumstances, its frequency appears to be linked to these other cycles. Metabolic cycles regulate modes of nutrition in single-celled organisms under nutrient-limited conditions (Richard, 2003; Silverman et al., 2010) and there is evidence in budding yeast that, under chemostat conditions where cells are induced to undergo synchronized oxido-reductive metabolic cycles, DNA replication (S-phase) may be restricted to the reductive portion of the cycle. This may limit DNA damage caused by reactive oxygen during this sensitive period (Klevecz et al., 2004; Tu et al., 2005; Chen et al., 2007).

Additionally, in organisms other than budding yeast, circadian rhythms influence cell cycle frequency, although this restriction operates differently in different systems. In many proliferating mammalian tissues and in zebrafish embryos, S-phase is gated by the circadian clock, by an unknown mechanism, perhaps in order to prevent DNA damage from UV exposure during the day (Bjarnason et al., 2001; Bjarnason and Jordan, 2002; Smaaland et al., 2002; Dekens et al., 2003). In mouse fibroblasts and regenerating liver cells, though, the gating occurs not before S-phase, but rather at a later point (Matsuo et al., 2003; Nagoshi et al., 2004). In this case, core components of the circadian oscillator control the transcription of Wee1, the cyclin-CDK inhibitor, and thus the timing of Mitosis (Matsuo et al., 2003). Recent work in the cyanobacterium *Synechococcus elongatus* indicates that circadian gating in that organism occurs at the time of cytokinesis, perhaps in order to ensure the synchronization of the two daughter clocks (Dong et al., 2010; Yang et al., 2010). The variety of gating mechanisms in different

organisms suggests multiple roles for this input. Perhaps different control points reflect different selective pressures (e.g. between single-celled organisms, plants, and metazoans).

The Cyclin-CDK Oscillator Entrains Peripheral Cell Cycle Oscillators

The cell cycle has so far been described as the oscillation of a master regulatory cyclin-CDK activity circuit, which triggers events at the correct time. But even when the cyclin-CDK oscillator is stalled at a constant high (but physiological) level, the cell cycle progresses with surprising efficiency (Drapkin et al., 2009). This observation may be explained by the functioning of another class of oscillators whose frequency is set by the master cyclin-CDK oscillator. These peripheral oscillators may control the execution of specific events within the cell cycle. For instance, continuing cycles of centrosome duplication occur in the absence of cell cycle progression in yeast, sea urchins, *Drosophila*, *Xenopus*, and Chinese Hamster Ovary (CHO) cells (Sluder and Lewis, 1987; Gard et al., 1990; Sluder et al., 1990; Haase et al., 2001; Durcan et al., 2008; McCleland and O'Farrell, 2008). In budding yeast, additional independent event oscillators have been observed. Polarization of cellular growth (responsible for producing the bud, as described previously) exhibits periodic cycles in the absence of S/M-phase cyclin-CDK activity and cell cycle progression (Hartwell, 1971; Haase and Reed, 1999). I will discuss this oscillator further in Chapters 3 and 4. Recently, an oscillator controlling the activity of the mitotic phosphatase Cdc14 (a protein that specifically removes the phosphorylations added to substrates by cyclin-CDK) was shown to continue cycling at

locked high levels of cyclin-CDK activity (Lu and Cross, 2010). In addition, almost 70% of cell cycle-regulated genes continue their periodic and timely expression in the absence of S/M cyclin-CDK activity or cell cycle progression, suggesting an independent transcriptional oscillator (Orlando et al., 2008).

These events, which have the potential to oscillate in the absence of cyclin-CDK activity oscillations, are nevertheless tightly controlled to occur once per cell cycle in normally cycling cells, even at vastly different cell cycle frequencies. How does the cyclin-CDK oscillator, almost surely the primary driver (Thornton and Toczyski, 2003), coordinate these peripheral oscillators? Recent experimental and theoretical work suggests that coordination may occur through a phase-locking mechanism in which the master cyclin-CDK oscillator can force peripheral oscillators, either advancing them or delaying them within a sensitive period, to ensure that they fire once and only once in each execution of the master cycle (Lu and Cross, 2010). This mechanism, phase-locking, is the same one responsible for entrainment of otherwise free-running circadian oscillators to a light-dark cycle. The frequency of the main cyclin-CDK oscillator can also be slowed by phase-locking to an external signal (Cross and Siggia, 2005; Charvin et al., 2009).

A phase-locking model was quantitatively shown to account for the activation of Cdc14 once per cell cycle, with the strength of the coupling between the oscillators measured experimentally. At the molecular level, the Cdc14 oscillator consists of a negative feedback loop, shown in Figure 1-5. Cdc14 is sequestered into a substructure of the nucleus, the nucleolus, for much of the cell cycle. In late Mitosis, it is released to dephosphorylate its targets. Cdc14 release, promoted by the Polo-like kinase Cdc5,

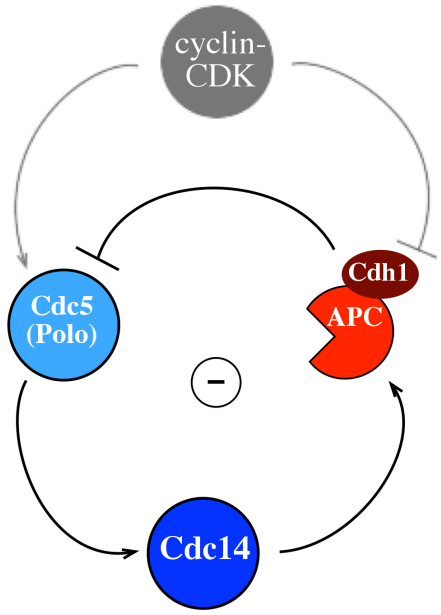

Figure 1-5 Molecular mechanism of the Cdc14 release oscillator. The mitotic phosphatase Cdc14 is activated upon release from sequestration in the nucleolus. This release is controlled by a negative feedback loop in which Cdc14 release, promoted by the Polo-like kinase Cdc5, activates APC^{Cdh1}, which then promotes Cdc5 degradation, allowing Cdc14 resequestration. This negative feedback oscillator is entrained to the cyclin-CDK cycle at multiple points, both by cyclin-CDK promotion of *CDC5* transcription and Cdc5 kinase activation, and by cyclin-CDK inhibition of APC^{Cdh1} activity.

activates APC^{Cdh1}, which then promotes Cdc5 degradation and thus Cdc14 resequestration (Lu and Cross, 2010; Manzoni et al., 2010). This oscillator is entrained to the cyclin-CDK oscillator at multiple points. Cyclin-CDK activity promotes both the transcription of *CDC5* and the activation of the Cdc5 kinase. Cyclin-CDK activity also inhibits APC^{Cdh1}, as discussed above.

To generalize this phase-locking idea, a single master cyclin-CDK oscillator could entrain multiple independent oscillators controlling individual cell cycle events (e.g. Cdc14 release, periodic transcription, SPB duplication, and budding), as in Figure 1-6. If this were the case, decreasing the amplitude of cyclin-CDK oscillations should weaken the entrainment of peripheral oscillators, leading to disorder of the events they control (due to different intrinsic frequencies of the oscillators). It was shown experimentally that this is the case; reducing the amplitude of cyclin-CDK oscillations in freely cycling cells leads to alterations in relative timing as well as sporadic skips or extra executions of normally strictly-ordered, once-per-cycle events (Lu and Cross, 2010).

A phase-locking mechanism can account for results that otherwise seem contradictory. For example, periodic once-per-cell-cycle transcription seemed well accounted for by the known cyclin-CDK regulation of various transcription factors, until the transcriptional cycle was reported to cycle autonomously, independent of the cyclin-CDK cycle (Orlando et al., 2008). Phase-locking models account for this discrepancy by proposing that the known regulatory links between cyclin-CDK and transcription factors constitute couplings between the two individual cycles, rather than the oscillatory mechanism itself. In the case of transcription, the intrinsic oscillatory mechanism could be the sequential activation of transcription factors in a wave-like fashion

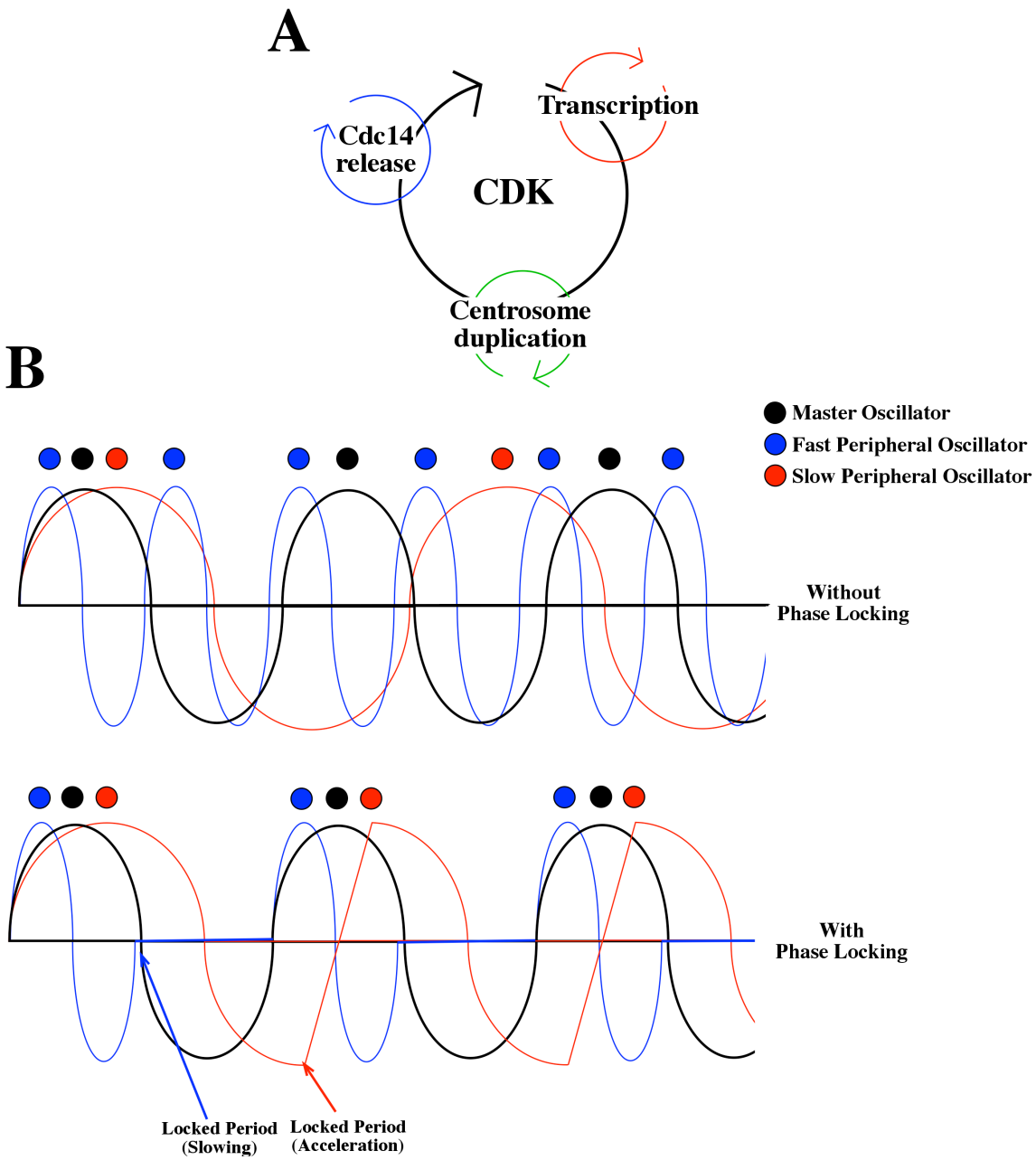

Figure 1-6 Phase-locking entrains multiple peripheral oscillators to the cyclin-CDK oscillator, as shown in **A**. Peripheral oscillators also feed back on the cyclin-CDK oscillator. **B** Three hypothetical oscillators are shown: a master cycle in black, a faster peripheral cycle in blue, and a slower peripheral cycle in red. Top: in the absence of phase-locking, the oscillators trigger events (colored circles) without a coherent phase relationship. Bottom: in the presence of coupling, the peripheral oscillators are slowed or accelerated within their critical periods to produce a locked phase relationship, with events occurring once and only once within each master cycle.

(Lee et al., 2002). Coupling could come about through the additional regulation of these factors by the cyclin-CDK cycle (Wittenberg and Reed, 2005).

I have described the non-CDK oscillators as peripheral, yet all of them feed back, directly or indirectly, on the cyclin-CDK oscillator itself, resulting in two-way coupling. For example, genes in the periodic program of transcription include most cyclins, as well as *CDC20* (the APC activator involved in the central negative feedback loop of the cyclin-CDK cycle) and *CDC5*. Cdc14 directly promotes the establishment of the low-cyclin-CDK positive feedback loop described above by activating Cdh1 and Sic1 (the stoichiometric CKI). Less directly, Cdc14 antagonizes cyclin-CDK activity by dephosphorylating its targets. The SPB duplication and budding cycles could communicate with the cyclin-CDK cycle via the spindle integrity and morphogenesis checkpoints. This two-way communication almost surely tightens oscillator coordination. It could also account for the robust cycling observed in the absence of checkpoint controls or upon ablation of transcriptional controls. (As a striking example, the entire G1/S transcriptional program can be made constitutive at a low level without preventing viability, provided one G1 cyclin – Cln2 – is constitutively expressed (Koch et al., 1993).)

It becomes increasingly clear, as more cell cycle mechanisms are understood, that coupled oscillators, both within the cell cycle and between the cell cycle and external clocks, are a common mode of cell cycle regulation. While the Cdc14 oscillator has been well characterized, many details of the strength and timing of oscillator coupling between cyclin-CDK and other peripheral oscillators remain unknown. An intriguing idea is that these peripheral cell cycle oscillators may have originally evolved independently in order

to promote cyclic events in primitive cells, and then been yoked to a later-evolving CDK cycle for a fitness advantage (Lu and Cross, 2010).

Scope of the Thesis Work

In this introduction, I hope to have described the basic features of the cell cycle oscillator: a central negative feedback oscillator, stabilized and tuned by positive feedback loops, cycles with an intrinsic frequency. Either through direct triggering of events, or through entrainment of independent oscillators controlling events, this cyclin-CDK oscillator triggers a series of ordered outputs. These outputs are the key events of the cell cycle. These events, in turn, have an established order and timing within the overall cycle.

The work I describe in this thesis concerns two fundamental questions: how is the order and timing of cell cycle events controlled, and what sets the intrinsic frequency of the cell cycle oscillator? I will describe work on two major processes in the cell division cycle that reveals two very different modes of regulation. The first of these processes, Start, represents a pivotal commitment to divide; in Chapter 2, I will discuss a collaboration with Gilles Charvin demonstrating that positive feedback in the molecular machinery underlying Start acts as a bistable switch to provide irreversibility to this regulatory transition. The second major process is Mitosis, a set of events all triggered by the same class of cyclin-CDKs and yet occurring in a set and reproducible order. In Chapter 3, I will discuss an ordering mechanism underlying this choreography that relies on the natural ramping-up of cyclin-CDK activity level. The observation that different

events require different levels of cyclin-CDK activity leads to the question of how these thresholds are set. In Chapter 4, I will discuss how mitotic cyclin-CDK triggers two different events – depolarization of growth and formation of the mitotic spindle – in two very different ways. The first relies on entrainment of an independent oscillator controlling growth polarization; the other may involve the simultaneous regulation of multiple targets.

The observation that cyclin-CDK level is rate-limiting for mitotic events suggests that increasing the level of this key cell cycle regulator above its endogenous level should accelerate Mitosis. In Chapter 5, I show evidence that this is the case. Quite surprisingly, this increase in cyclin-CDK abundance also accelerates the frequency of the cell cycle oscillator as a whole through its effect on growth. This provides an intriguing new answer to the question of what sets the intrinsic frequency of the cell cycle oscillator.

CHAPTER 2 – THE MOLECULAR ARCHITECTURE THAT MAKES START IRREVERSIBLE

Early studies of the cell division cycle identified a regulatory step controlling entry to the cycle. In budding yeast this step, called Start, was identified as a point of arrest for cells exposed to mating pheromone, deprived of nutrients, or lacking CDK activity (Pringle and Hartwell, 1981). Start, as described in the introduction, is also the point of size control in budding yeast (Johnston et al., 1977). Once cells pass this step, they are irreversibly committed to division; they will complete the cell cycle even in the absence of nutrients or the presence of mating signals.

The molecular machinery of Start involves the most upstream G1 cyclin, Cln3. Cln3 removes a transcriptional inhibitor, Whi5, in order to promote transcription of a gene regulon activated by the SBF and MBF transcription factor complexes. Included in this regulon of approximately 200 genes are the G1/S cyclins, *CLN1* and *CLN2*, which are responsible for many events of the early cell cycle: budding, SPB duplication, and activation of the cyclin-CDK complexes responsible for DNA replication and events beyond (Spellman et al., 1998). This machinery is schematized in Figure 2-1.

The Start transition is quite interesting from a regulatory point of view. A graded signal (Cln3 protein) is translated into an all-or-none decision that, once made, is irreversible. How is this achieved? In principle, irreversibility can arise from a bistable system (Figure 2-2). Increasing levels of input cross a threshold that switches the system from a low to a high state. Decreasing the input switches the system back to the low state, but only at a much lower threshold. Thus, for critical levels of input, the system

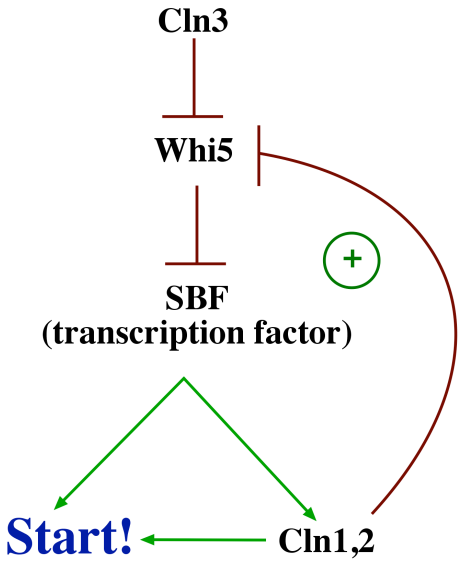

Figure 2-1 The molecular machinery underlying the Start transition. (See also Figure 1-4.) The most upstream G1 cyclin, Cln3, triggers the expulsion of the Whi5 repressor from the nucleus, thus relieving inhibition of the SBF transcription factor. This allows transcription of many genes that are responsible for early cell cycle events and passage through the Start transition, including *CLN1* and *CLN2*. Cln1 and Cln2 further promote their own activation through a positive feedback loop.

can exist in either the high or low state, depending on its history; if the level is increasing from a low value, the system will remain in the low state. If the level is decreasing from a high value, however, the system will remain in the high state. If this lower threshold is shifted to the left (by increasing the strength of positive feedback) so that it occurs at a negative value of input, the system becomes irreversible; even if the input level is reduced to zero, the system remains in the high state (Figure 2-2). There are two requirements for generating such a bistable system: positive feedback and significant nonlinearity.

Previous work identified a positive feedback loop in the Start machinery in which the G1/S cyclins Cln1 and Cln2 positively regulate their own transcription. Skotheim *et al*. compared the activation time of the *CLN2* promoter in the presence or absence of the *CLN1* and *CLN2* genes. The presence of the G1/S cyclins accelerated the activation of the *CLN2* promoter, and increased the coherence of the regulon, demonstrating positive feedback. This positive feedback is partially mediated by fast Cln1,2-dependent phosphorylation of Whi5 (leading to its removal from the nucleus), compared to slower Whi5 removal by Cln3-CDK.

The loss of coherence of the G1/S transcriptional regulon in *cln1*Δ *cln2*Δ cells has drastic consequences. Some cells apparently activate S-phase and mitotic B-type cyclin (Clb)-CDK complexes before earlier events (such as budding) have occurred, resulting in a fatal arrest of unbudded cells with high Clb-CDK levels. Clb-CDKs inactivate SBF and MBF complexes, turning off expression of the G1/S regulon (Amon et al., 1993) and, due to the lack of timely budding in *cln1Δ cln2Δ* cells, creating a dead-end for the cell. Positive feedback of *CLN1* and *CLN2* thus coordinates the coherent expression of a large

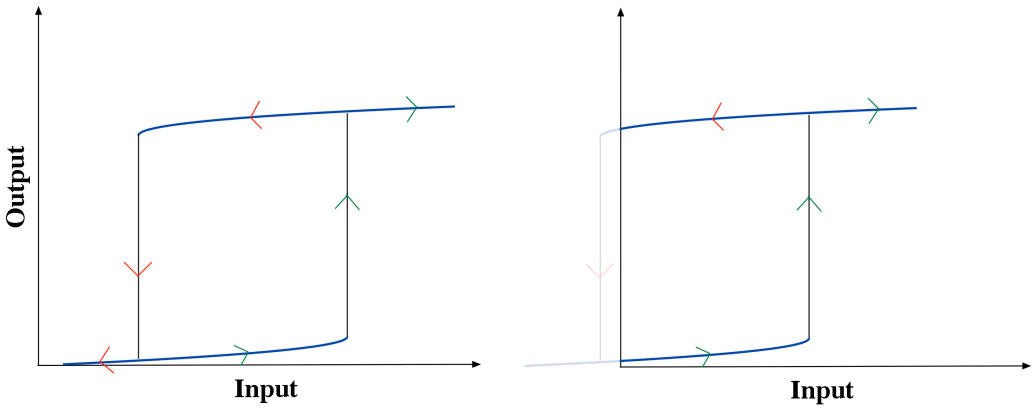

Figure 2-2 Schematic of bistable and irreversible system behavior. Left: Positive feedback and nonlinearity can generate a bistable system. Increasing the level of input (green arrows) past a certain high threshold can trigger a switch to the "on" state. Once the system is in the "on" state, input levels must be decreased (red arrows) past a lower threshold in order to trigger a switch back to the "off" state. Thus, for certain levels of input, the system can exist in either of two stable states, depending on its history. Right: If the response curve is shifted to the left, the lower threshold can effectively disappear (since it now occurs at a negative value of input), rendering the "on" state irreversible once achieved.

number of genes, as well as Cln1,2-CDK-dependent functions in processes like budding, to efficiently trigger early cell cycle events before the ensuing wave of Clb-CDK activity begins and the window of opportunity is closed (Skotheim et al., 2008).

Does this positive feedback also make the Start transition irreversible? To answer this question, I collaborated with Gilles Charvin to further examine the molecular network underlying Start (Charvin et al., 2010b). In this chapter, I discuss our findings in response to the following questions. First, is there significant nonlinearity in the system (the additional requirement for bistability)? Second, does the presence of nonlinearity and positive feedback lead to bistability in this case? And finally, what is the molecular basis for this positive-feedback-mediated irreversibility of Start? The following text in this chapter has been modified from Charvin et al., 2010b.

A Sharp Nonlinearity in Start Activation

To determine whether or not there is significant nonlinearity in the Start regulatory module, G. Charvin had measured the activation of Start (output) in response to graded levels of G1 cyclin (input). To bypass the positive feedback loop discussed above, he used a strain in which *cln1, cln2,* and *cln3* have all been disrupted, and the sole source of G1 cyclin is a copy of *CLN2* expressed from the methionine-repressible *MET3* promoter. This strain has been previously characterized (Charvin et al., 2008): first, these cells are stably blocked in a pre-Start state when grown in the presence of methionine, and exhibit a normal Start when triggered with a 20-minute pulse of *CLN2* gene expression (accomplished by removing methionine from the media). Second, the

amount of transcription from the *MET3* promoter can be controlled by varying the duration, τ, of the no-methionine (-Met) pulse. Finally, the lifetime of the Cln2 protein is on the order of 5-10 minutes, so –Met pulses provide reversible expression of Cln2. (The stock of protein is rapidly depleted once transcription is halted.) He used a microfluidic system in combination with timelapse microscopy to provide pulses of Cln2 expression and monitor resulting cell fates in real time.

To determine whether or not cells passed the Start transition, he used two fluorescent markers. Cdc10, a septin which localizes to the bud neck between mother and daughter cells, was tagged with YFP to track bud formation. Whi5, the transcriptional repressor, was tagged with GFP to track its nuclear localization (Whi5 is localized to the nucleus prior to Start, and is exported to the cytoplasm at Start, as previously discussed). Cells were pregrown in the microfluidic device and depleted of Cln2 (+Met) to uniformly arrest cells pre-Start. Cells were then given a –Met pulse of varying duration, τ, and followed by timelapse microscopy to assay Whi5-GFP export and bud formation (Figure 2-3). High Cln2 pulses (τ = 20 minutes) gave a uniform response: Whi5-GFP exited the nucleus around 18 minutes after the beginning of the pulse, buds formed (assayed by Cdc10-YFP signal), and cells eventually divided. Low Cln2 pulses (τ = 2.5 minutes) also gave a fairly uniform response: the vast majority of cells retained Whi5-GFP in the nucleus and remained unbudded. Intermediate Cln2 pulses (τ = 5 minutes) yielded a bimodal behavior: ~40% of cells underwent Start and completed their cycles, and ~40% remained blocked pre-Start. Interestingly, the remaining 20% of cells displayed a partial and temporary Whi5-GFP nuclear export,

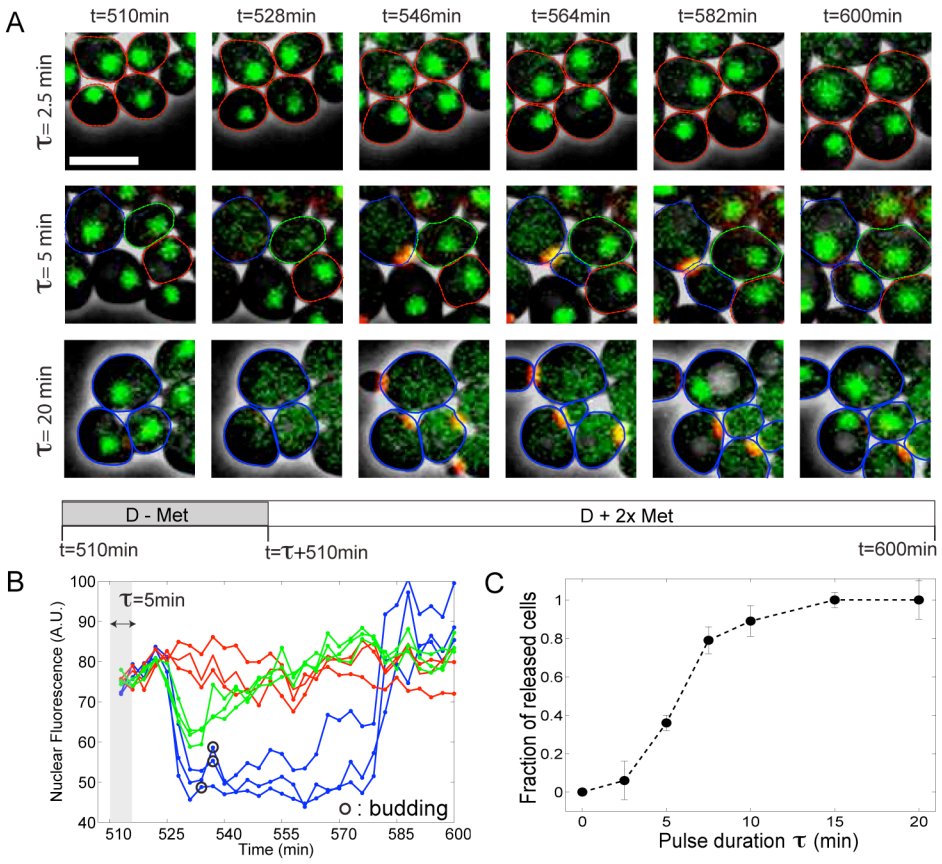

Figure 2-3 Passage through Start in response to *CLN2* pulses of various lengths. A Timelapse images (overlaid phase, GFP, and YFP (false-colored red) channels) of *cln1Δ cln2Δ cln3Δ* cells undergoing Start following a –Met pulse to induce *MET3:CLN2*. Pulse duration, τ, is indicated on left, and the time of media switches is indicated by the schematic below. Cell contours are color-coded to reflect fates: blue indicates cells that undergo Start, bud, and subsequently complete the cell cycle; red indicates cells that remain blocked in G1; green indicates cells that display partial and transient Whi5-GFP nuclear exit without budding. Scale bar represents 5μm. **B** Quantification of nuclear Whi5-GFP fluorescence intensity (arbitrary units, A.U.) as a function of time for the experiment shown in A, with τ = 5 minutes indicated by grey box. Colors as in A, with time of budding indicated by black circles. **C** Fraction of cells undergoing Start (released cells) as a function of pulse duration, τ. Error bars indicate standard error of the mean (s.e.m). Experiment conducted by Gilles Charvin alone.

which did not lead to budding or subsequent cell cycle progression. This implies that there is a non-zero threshold of Cln2 required for successful initiation of Start.

As he varied the pulse duration, τ, he observed that the fraction of released cells (cells undergoing Start) increased quite sharply from zero, at short τ, to one, at long τ. This suggested that Start is highly sensitive to Cln2 level. However, the amount of Cln2 protein produced may not necessarily scale linearly with the duration of the –Met pulse. Therefore, we wanted to correlate the likelihood of undergoing Start with the actual Cln2 level. All experiments discussed in the rest of this chapter were conducted jointly by G. Charvin and myself.

The extremely short lifetime of Cln2 compared to the maturation time of a fluorescent protein meant that we could not detect any fluorescent signal from a Cln2-YFP fusion protein. Therefore, we used an indirect measure – a reporter of transcription from the *MET3* promoter, *MET3pr:Venus*, in cells also carrying *MET3pr:CLN2*. To determine whether or not Venus fluorescence was a good indicator of *CLN2* expression in the same cell, we determined the correlation of expression between two different fluorescent proteins (Venus and mCherry) driven by the *MET3* promoter (Figure 2-4). The intrinsic noise (inherent stochasticity in gene expression) of the two reporters was determined to be 0.17, while the extrinsic noise (fluctuations in conditions within a given cell, compared to other cells in the population) was determined to be 0.37, calculated as in Elowitz et al., 2002. In practical terms, this implies that *Venus* expression correlates with simultaneous *CLN2* expression in >80% of cells, making it a useful reporter.

In order to have low background levels of Venus fluorescence prior to the –Met pulse, we integrated a second inducible G1 cyclin construct, *GAL1pr:CLN1*. Expression

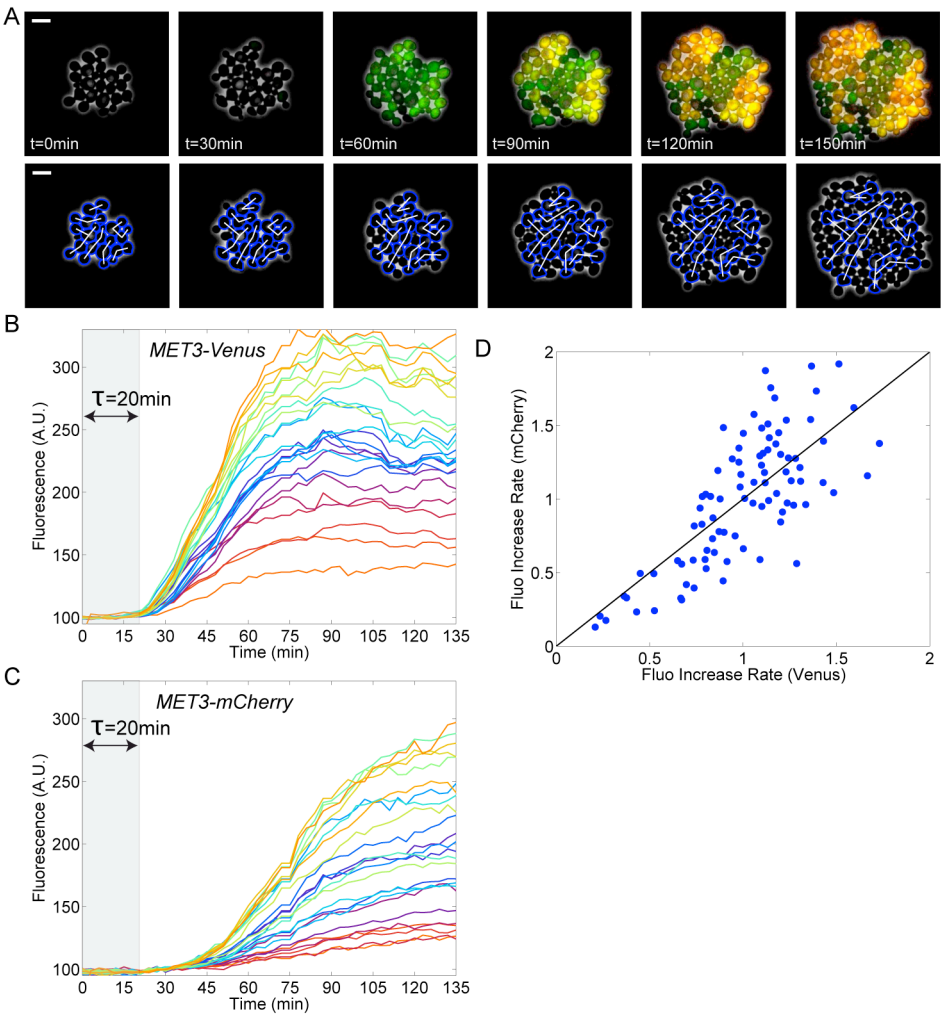

Figure 2-4 Correlation of expression of Venus and mCherry fluorophores driven by the *MET3* promoter in the same cell. **A** Top: timelapse images (overlaid phase, YFP (false-colored green), and mCherry channels) of cells following a 20 minute –Met pulse to induce expression of *MET3:Venus* and *MET3:mCherry*. Bottom: phase channels of timelapse images shown above, with segmented cell contours indicated in blue. White lines indicate cell parentage. **B** YFP fluorescence traces of individual cells from the experiment shown in A as a function of time. The shaded area represents the –Met pulse. **C** mCherry fluorescence traces of same cells. Note longer maturation time of fluorophore (~45 minutes for mCherry, versus 18 minutes for Venus). **D** Correlation of Venus and mCherry transcription rates for single cells (defined by the rate of fluorescence increase in the linear part of the curves in B and C, normalized to the mean of each distribution). The black line indicates the diagonal.

of *CLN1* allowed cells to cycle in the absence of *CLN2* expression. We pre-grew cells in media containing galactose (to induce *CLN1*) and a saturating concentration of methionine (10X Met) so that very little cytoplasmic fluorescence accumulated prior to the Cln2 pulse. Cells were blocked in glucose media with methionine (*GAL1* and *MET3* promoters off) and given a pulse of –Met to induce *CLN2* expression as before. This approach allowed us to detect small increases in Venus fluorescence resulting from short –Met pulses, with a high signal-to-noise ratio.

Using this system, we repeated the timelapse experiment described above (Figure 2-5). As before, intermediate pulses (τ = 8-15 minutes) yielded a bimodal response in cell fates. For each cell, we measured the slope of the Venus fluorescence increase following the pulse to infer the *MET3pr:CLN2* transcription rate. Overall, increasing the pulse length increased the average transcription rate. As expected, cells that remained blocked had, on average, lower expression from the *MET3* promoter than cells that successfully passed Start (assayed by budding). In fact, we observed a fairly sharp threshold level of *MET3pr:CLN2* expression required for passing Start. Increasing the duration of the pulse increased the average *MET3* expression (Figure 2-6) but did not affect the observed threshold for budding.

It was possible that the bimodality we observed was due to the *MET3* promoter turning on in some cells and not others, with increasing lengths of –Met pulses increasing the likelihood of turn-on. However, the fact that we observed cells with significant *MET3* transcription rates (implying production of Cln2) that did not pass Start excluded this possibility.

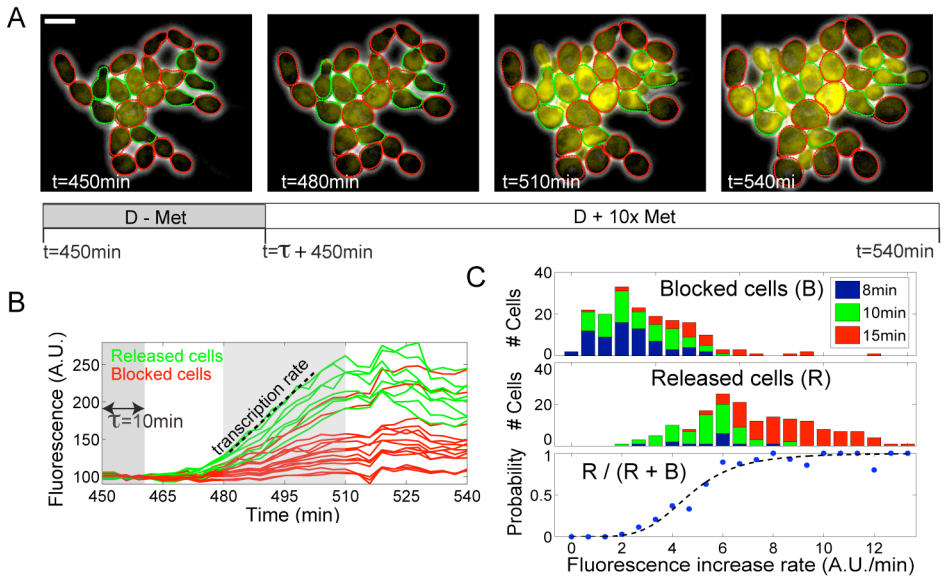

Figure 2-5 Measurement of nonlinearity in Start activation. **A** Timelapse images (overlaid phase and YFP channels) of *cln1Δ cln2Δ cln3Δ* cells following a –Met pulse to induce *MET3:CLN2* and *MET3:Venus* expression. Cell contours color-coded to reflect fates: green indicates released cells (those that pass Start, assayed by budding), and red indicates blocked cells (those that remain in G1). Scale bar represents 5μm. **B** Quantification of cytoplasmic YFP fluorescence (A.U.) as a function of time following a 10 minute –Met pulse. Colors as in A. The transcription rate was measured from the linear period of rising fluorescence followed by the pulse, indicated by the second grey box. **C** Top two panels show histograms of transcription rates, measured as shown in B, for blocked cells (top panel) and released cells (middle panel), for –Met pulses of various durations. Blue, 8 minutes; green, 10 minutes; red, 15 minutes. N = 342. The bottom panel shows the probability of undergoing Start (number of released cells divided by total number of cells) as a function of the transcription rate. The dashed line indicates the best fit of a Hill function with Hill coefficient $n = 4.8 \pm 0.3$.

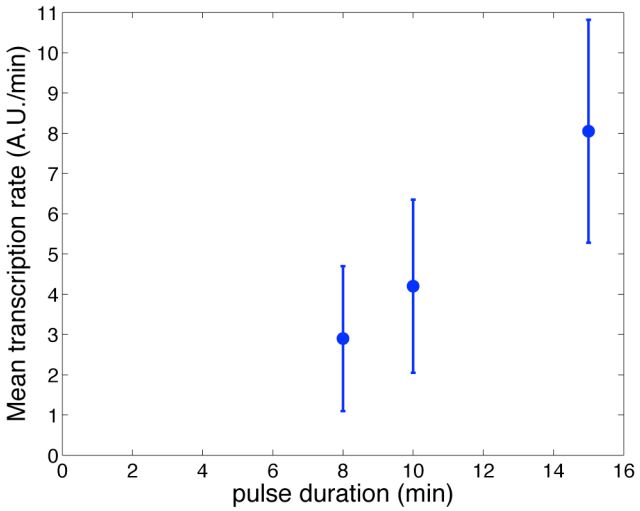

Figure 2-6 *MET3* promoter transcription rate as a function of –Met pulse duration. Points indicate the mean transcription rate, measured as in Figure 2-5, from *MET3:Venus* (A.U.) as a function of pulse duration for pools of approximately 100 cells. Error bars indicate standard deviation (s.d.).

Due to the size control mechanism described in the introduction, it was also possible that some of the observed effect could be due to differences in cell size. Perhaps smaller cells exhibited lower levels of transcription and took longer to bud due to the necessity for extra growth to achieve the minimum size required for Start. However, we observed no correlation between cell size and the probability of budding after a –Met pulse (Figure 2-7). This is not unexpected, as cells continue to grow during the blocking period (without Cln activity), and are therefore larger than wild-type cells at the time of budding. (The imaged area of blocked cells is, on average, around 1.8 times that of wild-type cells at budding.) We also observed no correlation between the size of a cell and its Venus fluorescence intensity following a –Met pulse. Finally, we repeated these experiments using Whi5-GFP exit from the nucleus (rather than budding) as a marker for Start, and observed identical results.

To quantify the sharpness of the response to Cln2 level, Gilles fit the probability of budding to a Hill function, which yielded a Hill coefficient of 4.8. This indicates a strong nonlinearity in Start activation, even in the absence of *CLN1,2* positive feedback.

Positive Feedback of G1 Cyclins Makes Start Irreversible

Does this sharp nonlinearity of Start activation, combined with previously identified positive feedback, yield bistability? To examine the long-term stability of the system, we needed to halt further cell cycle progression. In the experiments described above, once cells passed Start, B-type cyclin-CDK (Clb-CDK) activity was rapidly induced, which then repressed SBF-mediated transcription, turning off the G1 regulon

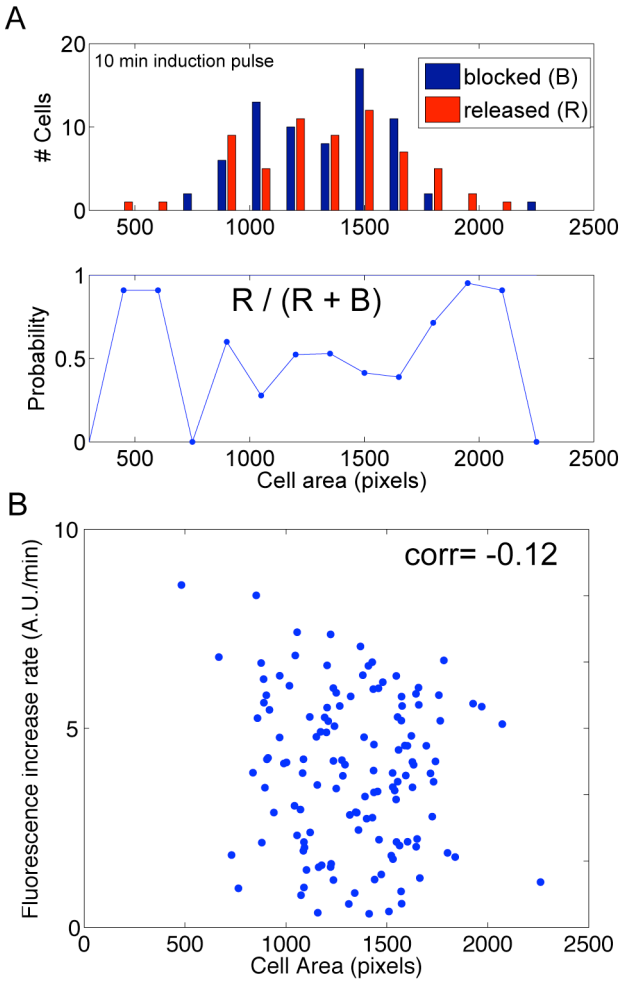

Figure 2-7 Start activation and *MET3* transcription rate following a *MET3:CLN2* pulse are independent of cell size. **A** Top: histogram of cell area (imaged pixels) of blocked (blue) and released (red) cells following a 10 minute –Met pulse. Bottom: probability of passing Start as a function of cell area, calculated as in Figure 2-5. **B** Lack of correlation between *MET3:Venus* transcription rate and cell area (imaged pixels) for individual cells, quantified by the low coefficient of correlation ("corr").

(Amon et al., 1993). To prevent Clb-CDK activation, we took advantage of an endogenous stoichiometric inhibitor, Sic1. Sic1 binds and effectively inhibits Clb-CDK complexes early in the cell cycle to stabilize the low-CDK state (one of the positive feedback loops described in the Introduction). It is normally phosphorylated by Cln1,2-CDK, which targets it for proteolytic degradation and allows Clb-CDK activity to accumulate for S-phase and subsequent cell cycle progression. However, mutating three target sequences for Cln1,2-CDK phosphorylations (*SIC1-Δ3P*) effectively blocks its degradation. Expressing the *SIC1-Δ3P* allele from a strong inducible promoter, *GAL1*, stably arrests cells post-Start with low Clb-CDK levels (Verma et al., 1997).

Using the microfluidic timelapse setup described in the last section, we used media containing methionine (+Met) to block cells in G1 as before, then added galactose (G+Met) to accumulate a high level of stable Sic1-Δ3P. After sufficient accumulation, we switched cells to glucose media (D+Met), because cells grow faster in glucose than in galactose and sufficient Sic1-Δ3P had accumulated to inhibit Clb-CDKs for the remainder of the experiment. Once the blocking procedure was completed and cells were loaded with Sic1-Δ3P, we provided a 15-minute –Met pulse to induce *MET3pr:CLN2* expression.

To assay Start events, we used several markers. As before, we used Cdc10-YFP to track bud formation and Whi5-GFP to follow the nuclear localization of Whi5. We also followed *CLN2* promoter activity using a fluorescent reporter, *CLN2pr:Venus-CLN2*$_{PEST}$. The *CLN2*$_{PEST}$ sequence is a "degron," a C-terminal sequence in *CLN2* that targets the protein for degradation. In this case, it destabilizes the fluorescent protein, allowing us to track the turn-on and turn-off of the promoter with reasonable time

resolution (Mateus and Avery, 2000; Bean et al., 2006). Previous work has shown that degradation of the Venus-CLN2$_{PEST}$ fusion is not affected by cell cycle stage (Charvin et al., 2008). In order to reliably separate the Whi5-GFP and Venus-CLN2$_{PEST}$ signals, we used narrow band-pass filters and image processing, as described, and validated, in Charvin et al., 2008. Essentially, the contribution of the YFP fluorescence to the GFP measurement, and vice versa, was computationally subtracted using linear algebra.

We first examined the stability of the Start transition in the absence of *CLN1,2* positive feedback. The strain was as described above: *cln1Δ cln2Δ cln3Δ MET3:CLN2 GAL1:SIC1-Δ3P*, with the three fluorescent markers. Cells were blocked as described, loaded with stable Sic1-Δ3P, and pulsed with Cln2 (Figure 2-8 A,E,I). As expected, the Cln2 pulse resulted in the exit of Whi5-GFP from the nucleus (approximately 20 minutes after the beginning of the pulse), followed by budding and an increase in Venus fluorescence from the *CLN2* promoter. Interestingly, about 45 minutes from the beginning of the pulse, Whi5-GFP re-entered the nucleus, and Venus fluorescence decayed, indicating turn-off of the *CLN2* promoter. This suggested that cells had reverted to a pre-Start state. Consistent with this idea, if cells subsequently received a second –Met pulse (150 minutes after the first), Start was again observed: Whi5-GFP exited the nucleus, Venus fluorescence from the *CLN2* promoter began to accumulate, and (already budded) cells rebudded. This second Start was similarly reversed about 45 minutes from the beginning of the pulse. The 45-minute delay in Whi5 re-entry to the nucleus and repression of the *CLN2* promoter is significantly longer than the ~10-minute half-life of the Cln2 protein. This suggests some other, slow, step in reversion to a pre-

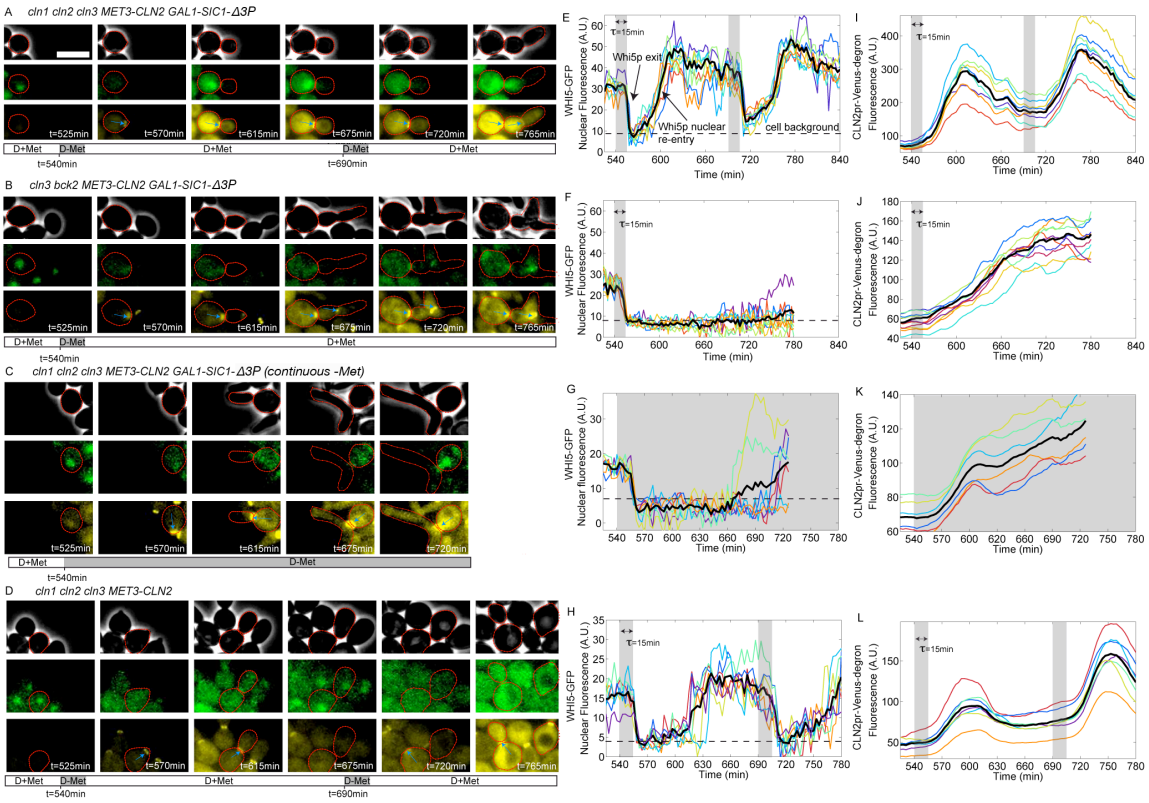

Figure 2-8 ***CLN1,2*-mediated positive feedback renders Start irreversible. A-D** Timelapse images (phase, GFP [marking Whi5], and YFP [marking Cdc10] channels) of cells of the indicated genotypes at indicated timepoints following various protocols of –Met pulses, as indicated by schematics below. Blue arrows indicate bud necks and scale bars correspond to 5μm. **E-H** Whi5-GFP nuclear fluorescence (A.U.) as a function of time for individual cells (conditions described in corresponding row of A-D). Grey boxes indicate –Met pulses, and solid black lines indicate the average of the displayed single traces. **I-L** *CLN2pr:Venus-degron* fluorescence as a function of time for individual cells (conditions described in corresponding row of A-D). Conventions as in E-H.

Start state. We speculate that it could reflect the time required for dephosphorylation of Whi5, but we do not know.

Together, these results suggest that, in the absence of endogenous G1 cyclins, and therefore in the absence of a positive feedback loop, the Start transition is fully reversible. What happens in the presence of the *CLN1,2* positive feedback loop?

To answer this, we repeated the experiment with a strain carrying functional *CLN1* and *CLN2* (*cln3Δ*). In order to arrest these cells pre-Start, we also disrupted *bck2*. The exact function of Bck2 is not well understood, but it allows *cln3Δ* cells to fire *CLN1* and *CLN2* spontaneously (Epstein and Cross, 1994; Di Como et al., 1995). *cln3Δ bck2Δ* cells arrest stably pre-Start, and any *CLN1,2* expression depends on *MET3:CLN2* induction. To ensure that *bck2Δ* did not have unexpected effects, we first performed the experiment, as described above, with a *bck2Δ cln1Δ cln2Δ cln3Δ* strain and observed identical results.

We next repeated the experiment with a *bck2Δ CLN1 CLN2 cln3Δ* strain (Figure 2-8 B,F,J) and observed strikingly different results. Following the –Met pulse, Whi5-GFP exited the nucleus as usual, but remained in the cytoplasm. In 12 of 15 cells examined, Whi5-GFP remained cytoplasmic for at least 5 hours. In three cells, Whi5-GFP did reenter the nucleus, but only after several hours, and reentry was markedly slower than in *cln1,2Δ* cells. Similarly, the *CLN2* promoter was activated as before, but it remained on for at least 3 hours following the –Met pulse. To compare this phenotype with a known continuous *CLN2* expression phenotype, we repeated the assay with the *cln1Δ cln2Δ cln3Δ* strain, this time providing continuous *MET3:CLN2* expression by leaving the cells in –Met media (Figure 2-8 C,G,K). We observed the same result: an

extended period of Whi5-GFP exclusion from the nucleus, and continued expression from the *CLN2* promoter. This implies that *CLN1* and *CLN2*, once activated, can maintain their own expression.

One caveat of these experiments is the relatively uncharacterized nature of the *bck2* mutation. Perhaps *CLN1,2* can only maintain their expression in the absence of *BCK2*. This seems unlikely, since Bck2 is a Cln-independent activator of *CLN1,2* expression. However, to control for an unexpected effect of *bck2* disruption, we blocked wild-type cells prior to S-phase (post-Start) using *GAL1:SIC1-Δ3P*, and observed continued expression from the *CLN2* promoter.

As a final control, we assayed the effect of a Cln2 pulse in *cln1Δ cln2Δ cln3Δ* cells without first inducing *GAL1:SIC1-Δ3P* (Figure 2-8 D,H,L). Following a –Met pulse, these cells underwent a normal, complete division cycle. Interestingly, Whi5-GFP re-entered the nucleus 60-80 minutes after the beginning of the pulse, significantly longer than the 45 minutes observed in the presence of stable Sic1. This delayed reentry is likely due to continued phosphorylation of Whi5 by Clb-CDKs after disappearance of Cln2-CDK(Costanzo et al., 2004), and presents an interesting distinction between initiation of Start and, for wild-type cells, maintenance of the post-Start state.

These experiments indicate that, following transient activation, continued expression of SBF-regulated genes requires transcriptional positive feedback by *CLN1* and *CLN2*. Amazingly, the presence of this positive feedback maintains the state over a timescale well beyond the duration of the cell cycle, creating an irreversible transition. Thus, the Start regulatory module acts as a ratchet, ensuring one-way passage through Start.

Whi5 Mediates the Irreversibility of Start

Why is the *CLN1,2* positive feedback loop required for the irreversibility of Start? Since, in the absence of positive feedback, a pulse of *MET3:CLN2* produced a transient activation of SBF-dependent gene expression, which was promptly reversed, we hypothesized that Whi5 was re-entering the nucleus and repressing transcription. To test this, we repeated the no-positive-feedback experiment described in the last section (*cln1Δ cln2Δ cln3Δ* cells blocked, loaded with Sic1-Δ3P, and pulsed with Cln2) with the additional disruption of *whi5* (Figure 2-9). Whereas in the presence of *WHI5*, cells rapidly reverted to a pre-Start state, *whi5Δ* cells exhibited continued expression of *CLN2pr:Venus-CLN2$_{PEST}$*. Since the degradation rate of Venus-CLN2$_{PEST}$ was shown to be invariant throughout the cell cycle (Charvin et al., 2008), we believe that the plateau level of Venus fluorescence observed in this experiment represents a balance between continuing (though lessened) synthesis and degradation. Compare to the rapid loss of signal in the *WHI5* background (Figure 2-8 I).

This result supports the idea that Whi5 is a powerful repressor of SBF-controlled genes which can only be countered by positive feedback of the G1 cyclins. In the absence of *whi5*, SBF activation (once triggered by a pulse of G1 cyclin) is irreversible, continuing to promote transcription over a very long timescale (longer than the length of the cell cycle). Thus, Whi5 imposes the requirement for *CLN1,2* positive feedback in making Start an irreversible cell cycle transition.

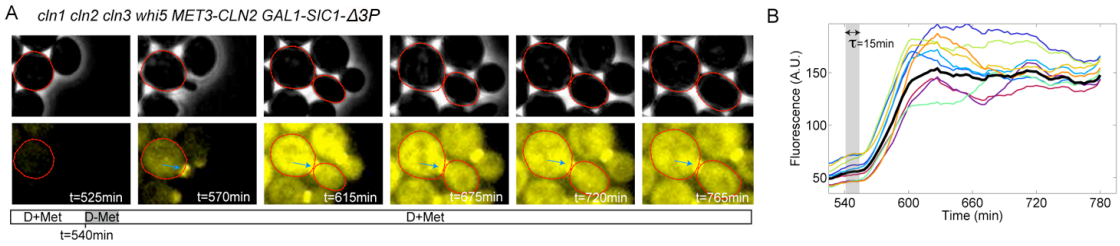

Figure 2-9 Whi5 mediates Start irreversibility. **A** Timelapse images of cells of the indicated genotype (phase and YFP [Cdc10-YFP and *CLN2pr:Venus-degron*] channels) following a 15-minute –Met pulse, as schematized below. The red contour indicates a typical cell, and the blue arrow indicates the bud neck. **B** YFP fluorescence reflecting *CLN2pr:Venus-degron* expression (A.U.) in single cells from experiment shown in A. The black line indicates the average of the displayed single traces.

Cln2 Controls the Dynamics of Budding

An interesting observation from the previous experiments was that cells, once budded and induced to revert to a pre-Start state, could successfully form a second bud. Additionally, we observed a clear difference in bud morphology between protocols in which cells were exposed only briefly to G1 cyclins (e.g. Figure 2-8 A,D and Figure 2-9 A) and those in which cells were exposed to G1 cyclins for an extended period of time (e.g. Figure 2-8 B,C). In the former case, buds were relatively round; in the latter, buds were extended and/or branched. This led us to examine more closely the effect of Cln2 on the dynamics of bud morphogenesis.

G1 cyclin-CDK (Cln-CDK) activity has been shown to be responsible for triggering bud formation by inducing polarized growth shortly after Start (Lew and Reed, 1993). More recent work has suggested a continued involvement of Cln-CDK activity in bud growth; CDK inactivation (through inhibition of an engineered analogue-sensitive *CDK1* allele, *cdk1-as*) in small-budded cells halted further bud growth(McCusker et al., 2007). (This result was complicated by the fact that overall cell growth was reported to be highly impaired upon Cdk1-as inactivation.) We therefore used our experimental system to test the continuing requirement for endogenous Cln-CDK activity in the maintenance of polarized growth.

To quantify polarized growth, we calculated the ratio of the imaged area of the bud to that of its mother, as a function of time. We first assayed polarized growth in the presence of *CLN1,2* positive feedback (*CLN1 CLN2 cln3Δ bck2Δ*). We blocked cells as before, loaded them with Sic1-Δ3P, and gave a brief pulse of *MET3:CLN2* expression

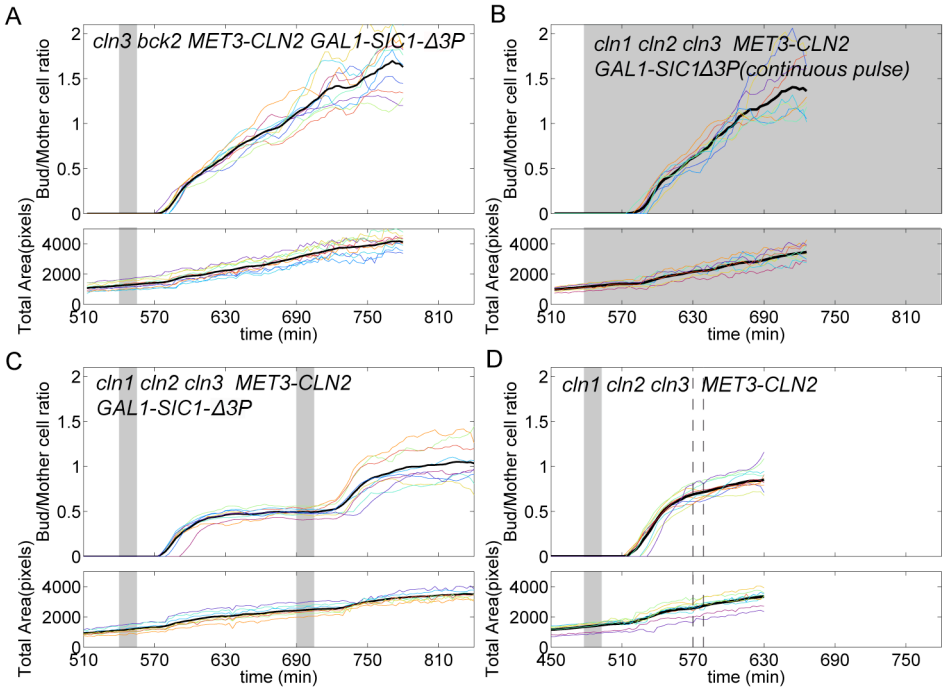

Figure 2-10 Polarized growth in the presence and absence of *CLN1,2* positive feedback. A-D Top panels indicate the ratio of bud to mother area (imaged pixels), and bottom panels indicate the total area (imaged pixels) of mother and bud combined for individual cells of the indicated genotypes in response to a single –Met pulse (A, D), subsequent –Met pulses (C), or continuous –Met induction of *MET3:CLN2* (B). Black lines indicate the averages of the displayed single traces. Grey boxes indicate –Met pulses and, in D, the time interval between the two dashed lines indicates the completion of division for the majority of cells in that experiment.

(Figure 2-10 A). We observed a strongly polarized growth pattern, consistent with continuous Cln2-CDK activity. Similarly, in the absence of positive feedback (*cln1Δ cln2Δ cln3Δ* cells, blocked and loaded with Sic1-Δ3P) but with continuous expression of *MET3:CLN2*, we observed the same pattern of extended, highly polarized growth (Figure 2-10 B).

In contrast, if we provided a 15-minute pulse of Cln2 in the absence of positive feedback, we observed a limited period of polarized growth, lasting for approximately 45 minutes (Figure 2-10 C). A second Cln2 pulse in the same cells induced a second period of polarized growth (rebudding) that lasted the same amount of time. However, in contrast to the results of McCusker et al., 2007, overall cell growth, measured by the total area of mother and bud, continued even in the absence of significant CDK activity. To compare this result to a normal cell cycle in which Clb-CDK is activated, we repeated the experiment without *GAL1:SIC1-Δ3P* (Figure 2-10 D). Cells pulsed with Cln2 exhibited a similar period of polarized growth lasting about 45 minutes before depolarizing growth and completing their division cycles.

These results are consistent with a continuing requirement for Cln2-CDK activity for maintaining, not just triggering, polarized growth.

CHAPTER 3 – GRADED CYCLIN-CDK LEVELS ORDER MITOTIC EVENTS

As described in the introduction, various cyclin-CDK complexes trigger the events of the cell cycle. In budding yeast, a single essential CDK is activated alternately by nine cyclins in three functional/temporal categories: the G1 cyclins (Cln1-3), responsible for cell cycle entry as described in the last chapter; the S-phase cyclins (Clb5,6), responsible for DNA replication; and the mitotic cyclins (Clb1-4). These cyclins are differentially expressed, inhibited, and degraded, and their temporal order of activity contributes to the ordering of cell cycle events (Loog and Morgan, 2005; Bloom and Cross, 2007). To take an example from the last chapter, G1 cyclins initiate Start, trigger early events such as bud formation. They also trigger the production of B-type cyclins (Clbs). Clb-CDK activity turns off expression of the G1 cyclins, and also triggers later cell cycle events.

Within these classes, however, there is significant functional redundancy. A single cyclin-CDK complex can control multiple events. Strains containing a single Clb substituting for the full complement of S-phase (Clb5,6) and mitotic cyclins (Clb1,2,3,4) are viable (Haase and Reed, 1999; Hu and Aparicio, 2005). And Clb2, in the absence of the other mitotic cyclins, can promote all essential mitotic events with near-wild-type efficiency (Fitch et al., 1992; Richardson et al., 1992). Unlike the switch-like activation of Start discussed above, mitotic events are temporally separated and exhibit a stereotyped order. For example, growth is depolarized, spindles form, and then APC^{Cdc20} is activated and spindles elongate, separating chromosomes. How is the order of these events preserved in the absence of unique cyclin-CDK activators?

Possible ordering mechanisms include checkpoints, which halt cell cycle progression until certain conditions have been met (Hartwell and Weinert, 1989); mechanistic coupling, in which a later event is structurally dependent upon completion of an earlier event (Pringle and Hartwell, 1981); and a "quantitative model," proposed by Stern and Nurse, in which later events require higher CDK activity levels than earlier events (Stern and Nurse, 1996). In budding yeast, checkpoints are not essential for cell cycle progression under normal conditions (Weinert et al., 1994; Cross et al., 2002), and mechanistic coupling can only easily explain events that involve the same structure (e.g. formation and elongation of the spindle). I therefore wanted to test the "quantitative model" of control, in which increasing cyclin-CDK activity levels order events (Figure 3-1).

While this work was in progress, two studies of cyclinB1-CDK1 activation dynamics in HeLa cells and HeLa cell extracts provided support for this quantitative cyclin-CDK level model. It was shown that in prophase, later events require more cyclinB1-CDK1 activity than earlier events (Gavet and Pines, 2010). It was also shown, *in vitro*, that later-acting cyclinB1-CDK substrates require higher levels of cyclinB1 for phosphorylation than earlier-acting substrates (Deibler and Kirschner, 2010). Mitosis in budding yeast provides an ideal *in vivo*, organismal system to test these ideas further. A single cyclin, Clb2, can control all mitotic events, and the Wee1 and Cdc25 feedback loops that control CDK activation in higher eukaryotes are not essential for cell cycle progression in budding yeast (Amon et al., 1992), greatly simplifying the system. In addition, genetic tools allow me to titrate cyclin levels within the endogenous range. This

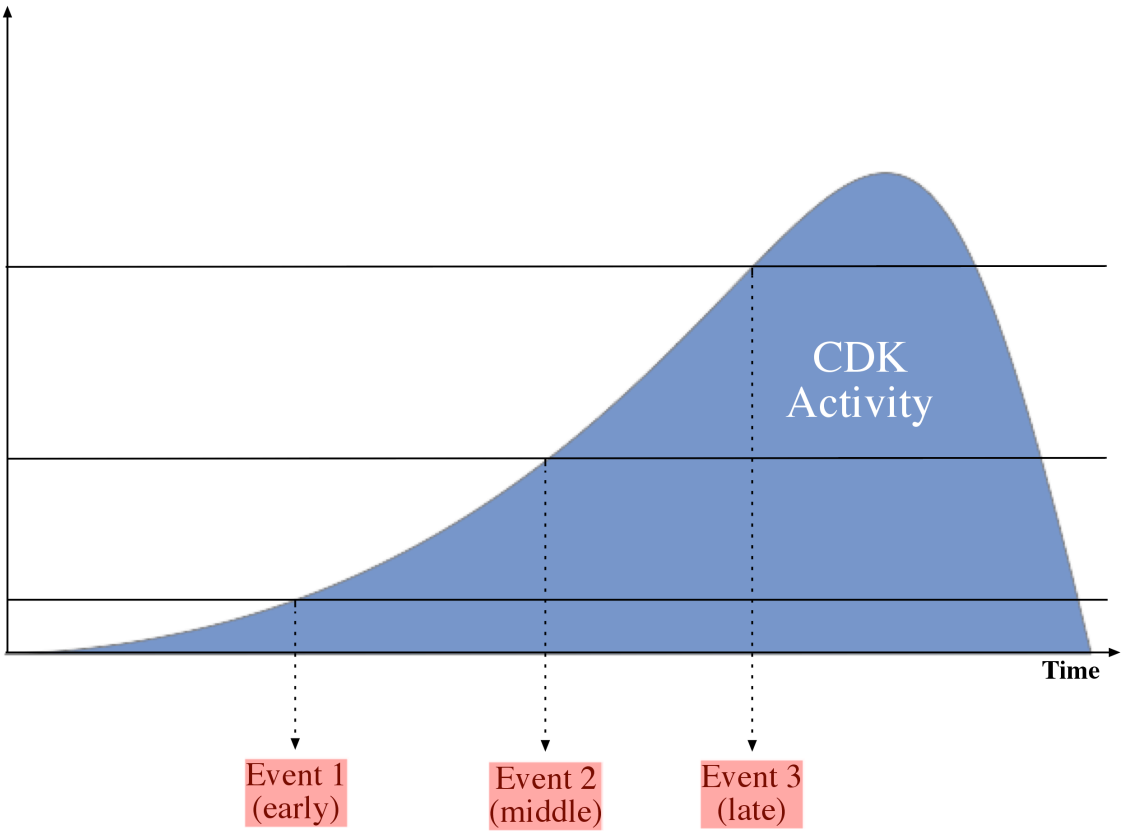

Figure 3-1 Quantitative model for ordering events. If cell cycle events are triggered by different threshold levels of cyclin-CDK activity (indicated by horizontal lines), the once-per-cycle rise and fall of cyclin-CDK activity can confer temporal order on the events. In this simple example, Event 1 requires less cyclin-CDK activity than Event 2, which requires less than Event 3. Thus, as cyclin-CDK activity ramps up, Event 1 will occur first, followed by Event 2, and finally Event 3.

titration, in combination with timelapse imaging, allows me to measure, quantitatively, thresholds for cyclin-CDK control of individual events.

A System to Measure Mitotic Cyclin-CDK Requirements

There are four, largely redundant mitotic cyclins in budding yeast: Clb1, Clb2, Clb3, and Clb4. In the absence of the other three, Clb2 can successfully promote all essential events with near-wild-type timing (Figure 3-2) (Fitch et al., 1992; Richardson et al., 1992). Taking advantage of this simplification, I built a *clb1Δ clb2::GALL:CLB2 clb3Δ clb4Δ* strain, in which *CLB2* is the sole source of mitotic cyclin and is expressed from a regulatable promoter (*GALL*, an attenuated form of the galactose-inducible *GAL1* promoter). This promoter, when activated by the addition of galactose to the growth media, was unsuitable for my studies: the expression level was higher than that of the endogenous *CLB2* promoter, and switching on and off expression required changing the carbon source available to the cells. This had significant effects on cell physiology. I therefore added a construct encoding a fusion of *GAL4* (the activator of the *GALL* promoter) with a mammalian mineralocorticoid receptor (Picard, 1999). *CLB2* expression was now dependent upon an exogenous hormone (deoxycorticosterone, DOC) so that experiments could be carried out in a single carbon source (glucose). The expression level achieved was now within the physiological range for *CLB2* (Drapkin et al., 2009). I provided pulses of *CLB2* expression by adding and washing out DOC, and titrated the expression by varying the duration of the pulse.

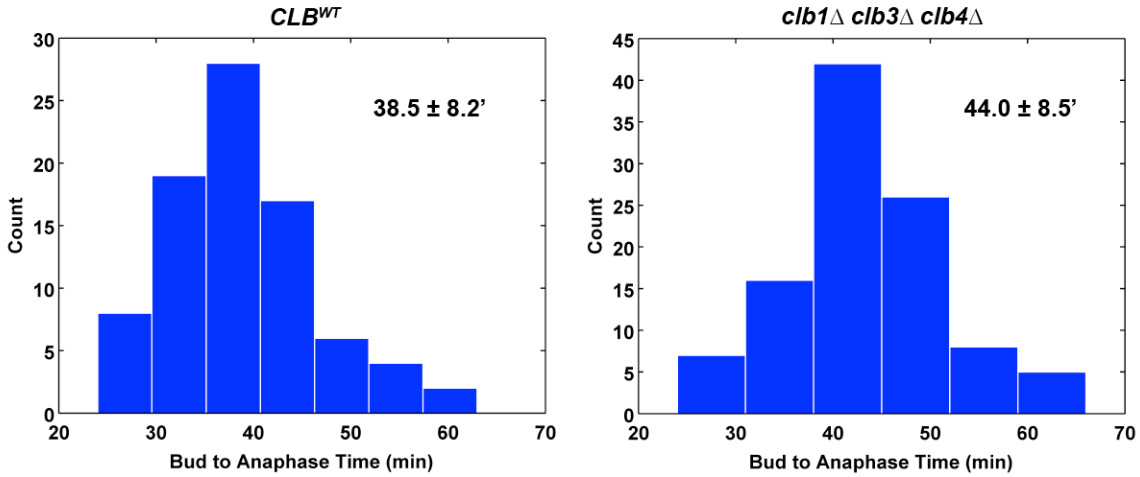

Figure 3-2 Timing difference between *CLB*^{WT} and *clb1Δ clb3Δ clb4Δ* cells. Cycling cells of the indicated genotypes (also containing Tub1-GFP) were followed by timelapse microscopy. Budding and anaphase were scored by eye from phase and GFP channels. Histograms show the length of the interval from budding to anaphase. Numbers indicate mean ± s.d.

To measure the Clb2 concentration in single cells, I used YFP-tagged Clb2, which is fully functional. Clb2 is predominantly localized to the nucleus (Hood et al., 2001), and nuclear size in budding yeast is tightly correlated with overall cell size (Jorgensen et al., 2007), so I used a histone H2B-mCherry fusion to mark the nucleus. I then measured the mean YFP intensity within this mask (and subtracted the background autofluorescence from unlabeled cells) to estimate the Clb2-YFP concentration in each cell.

To prevent degradation of the expressed Clb2-YFP, so that cells could be incubated for extended periods with a given titrated level (and so that the YFP could fully mature before measurement), I placed the APC activator *CDC20* under the control of a methionine-repressible promoter (*MET3*). Clb2-YFP pulses induced in the presence of methionine (and therefore in the absence of *CDC20* expression) were stable for at least two hours (Figure 3-3 C).

My experimental protocol was the following (Figure 3-3): 1. Proliferate cells in media containing hormone. 2. Deplete Clb2-YFP by washing out the hormone, uniformly arresting cells just before Mitosis. Deplete Cdc20 by adding methionine to the media. 3. Give a pulse of Clb2-YFP by adding and washing out the hormone. Use timelapse microscopy to correlate cell fate with the mean nuclear Clb2-YFP intensity in single cells. This mean nuclear Clb2-YFP intensity was then background-subtracted and normalized to the peak Clb2 expression in cycling cells (Drapkin et al., 2009). Previous studies have validated this quantification and shown the 'proportion of peak' units to have physiological meaning (Drapkin et al., 2009; Lu and Cross, 2010).

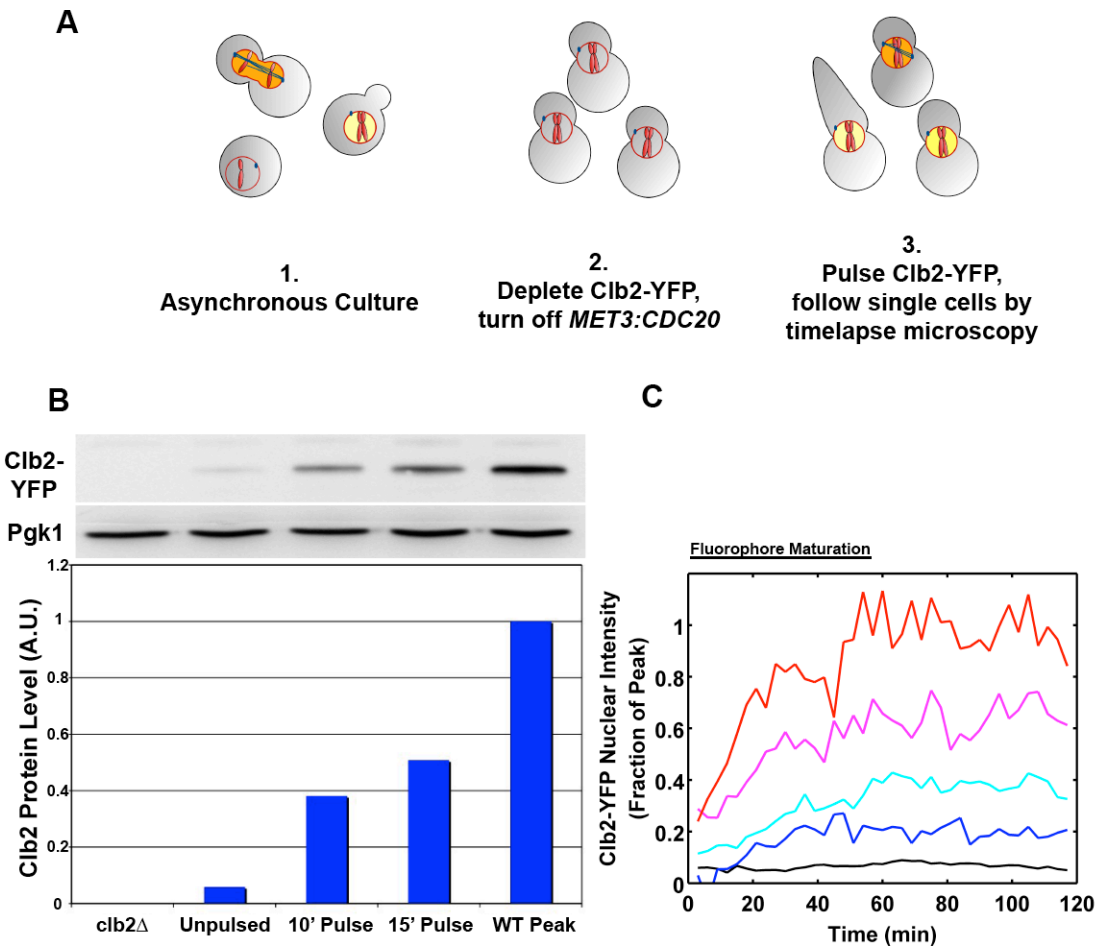

Figure 3-3 Experimental protocol to measure Clb2-CDK requirements. A Schematic of protocol. (1) *clb1Δ clb3Δ clb4Δ* cells expressing *CLB2-YFP* in response to deoxycorticosterone (DOC) are grown asynchronously in the presence of DOC. (2) DOC is washed out, arresting cells (by mitotic cyclin depletion) prior to Mitosis. Methionine is added to turn off *CDC20* (and thus Clb2-YFP degradation). (3) Cells are given a pulse of DOC and followed by timelapse microscopy. The execution of mitotic events is correlated with the Clb2-YFP level in single cells. **B** Top: Clb2-YFP protein and Pgk1 protein assayed by Western Blot from populations of cells either unpulsed or pulsed with 5mM DOC for 10 or 15 minutes, compared to the protein level in a *clb2Δ* strain (left) or the peak expression in a $CLB2^{WT}$ strain (right). Bottom: Quantification of top, with Clb2 protein levels normalized to Pgk1 levels. **C** Clb2-YFP nuclear intensity in individual cells as a function of time following a 15-minute pulse of DOC. Levels are normalized to Wild-type peak, and bar indicates approximate duration of fluorophore maturation.

One caveat of this approach is that I am using Clb2 level as a surrogate measure of Clb2-CDK activity. The stoichiometric Clb-CDK inhibitor Sic1 is almost surely absent in these cells, since they express a high level of the G1 cyclin Cln2 (Amon et al., 1993), which promotes efficient Sic1 degradation (Verma et al., 1997). However, the Clb2-CDK inhibitory kinase Swe1 is present and potentially active in these cells. Still, Swe1 activity might not be high because the cells are budded, so the 'morphogenetic checkpoint' should not activate Swe1 (Keaton and Lew, 2006).

To address directly the regulation of Clb2-CDK activity by Swe1, I measured Clb2-CDK kinase activity (assayed by phosphorylation of the histone H1 substrate) throughout the protocol, using *SWE1* and *swe1Δ* cells (Figure 3-4 A). I found that the presence of Swe1 approximately halves the kinase activity of Clb2-CDK for approximately the first 30 minutes after the expression pulse. To compare this to the situation in normally cycling cells (which is the system I am attempting to recapitulate), I used alpha factor (a mating pheromone that causes a G1 arrest) to synchronize otherwise wild-type *SWE1* and *swe1Δ* strains, and measured their Clb2-CDK kinase activity following release (Figure 3-4 B). I observed that Swe1 lowers Clb2-CDK kinase activity only in early mitosis. This is consistent with previous work showing slightly accelerated spindle formation in *swe1Δ* cells (Harvey and Kellogg, 2003), and indicates that my expression system faithfully recreates physiological conditions of partial kinase inhibition.

What about Sic1? Since, at later times in the *SWE1* timecourses and throughout the *swe1Δ* timecourses (both in the hormone induction protocol and the wild-type alpha-factor synchronization), the activity of Clb2-associated kinase closely paralleled Clb2

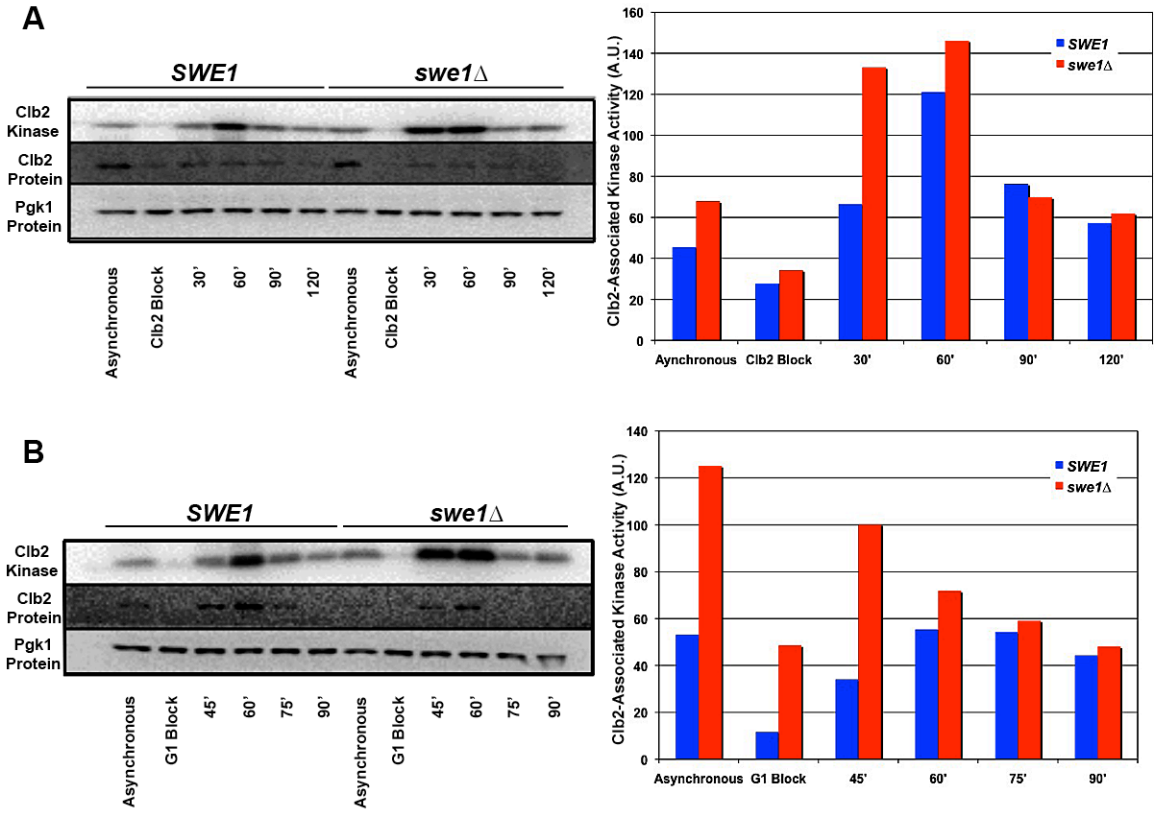

Figure 3-4 Clb2-CDK inhibition by Swe1 in early Mitosis. **A** Cells of the experimental strain, with (blue) or without (red) *SWE1*, were given a pulse of Clb2-YFP according to the protocol in Figure 3-3. Clb2-YFP protein level and associated kinase activity, as well as Pgk1 protein level, were assayed following the pulse. Right: quantification of Clb2-associated kinase activity (normalized to Pgk1 protein level). **B** Otherwise wild-type *SWE1* (blue) and *swe1Δ* (red) strains were synchronized with alpha-factor and released. Clb2-YFP protein level and associated kinase activity, as well as Pgk1 protein level, were assayed following release. Right: quantification of Clb2-associated kinase activity (normalized to Pgk1 protein level).

protein levels, it is unlikely that Sic1 is significantly regulating Clb2-CDK activity in these experiments. Sic1 is completely degraded by the middle of the cell cycle (Schwob et al., 1994). If it were inhibiting Clb2-CDK earlier, I should observe a change in specific activity at later timepoints, when this inhibition is lifted.

Therefore, in this system, Clb2-CDK seems to be inhibited only transiently by Swe1, resulting in an approximately two-fold reduction in activity, and likely not at all by Sic1. The Clb2 levels I measure thus reflect Clb2-associated kinase activity, at least within a factor of two.

Increasing Cyclin-CDK Levels Order Mitotic Events

The events of Mitosis are significantly separated in time, spanning about a quarter of the cell cycle. To test the 'quantitative model,' it is important to know how rapidly Clb2-CDK levels ramp up over the course of the cell cycle; if they rise too quickly, it is unlikely that they are directly responsible for the observed event timings. I used alpha-factor to synchronize a *clb1Δ clb3Δ clb4Δ* strain in G1 and followed cells through the ensuing cell cycle (Figure 3-5). I observed that Clb2 protein levels, and associated Clb2-CDK kinase activity, ramped up gradually over a period of about 40 minutes. Thus, if different activity levels promote different events, these events could be significantly separated in time.

To test this idea, I chose to measure the Clb2 requirement for three temporally-separated mitotic events: depolarization of growth, spindle formation, and spindle elongation. In an alpha-factor synchronized cell cycle, growth depolarization (measured

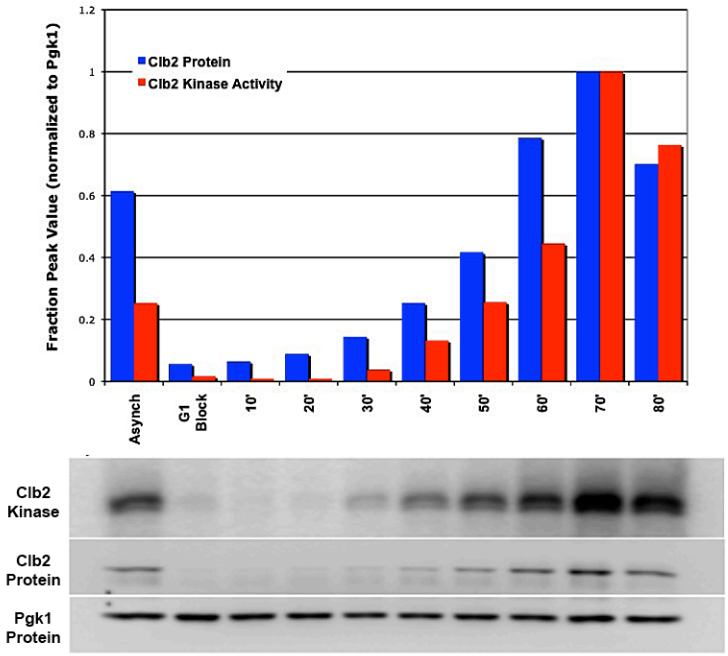

Figure 3-5 Clb2-CDK activity ramps up over a period of 40 minutes. *clb1Δ clb3Δ clb4Δ* cells were synchronized with alpha-factor and released. Clb2 protein levels, associated kinase activity, and Pgk1 protein levels were assayed at the indicated timepoints following release. Quantification of blots is shown above, with values normalized to Pgk1 and expressed as a fraction of the peak value at 70 minutes. "Asynchr" refers to a sample of asynchronous cells prior to addition of alpha-factor.

as the time of relocalization of actin filaments from the bud tip to the entire bud cortex (Lew and Reed, 1993)) occurs, on average, 20 minutes before spindle formation (Figure 3-6). Spindle formation, in turn, occurs approximately ten minutes before spindle elongation in anaphase. All three of these events occur as Clb2 levels are steadily increasing. Thus, they could, in principle, be ordered by their requirements for different amounts of Clb2-CDK.

Growth Depolarization

In budding yeast, cellular growth is polarized early in the cell cycle. At the time of bud initiation, all growth is focused to the bud tip, resulting in initial formation of an elongated bud with actin polarized to the bud tip ('polarized growth'). Later in the cell cycle, actin filaments redistribute within the bud and growth is depolarized in a Clb-CDK dependent manner, resulting in rounded bud growth ('isotropic growth')(Lew and Reed, 1993). Interestingly, however, in the absence of Clb-CDK activity, polarized growth does not appear to be continuous because cells exhibit multiple buds, rather than a single elongated bud (Haase and Reed, 1999). I wanted to use our experimental system to measure the dosage of Clb2 required for mediating the switch to isotropic growth.

To do that, I needed an assay for growth depolarization. It has previously been reported that Spa2 localizes to sites of polarized growth such as the bud tip, and may function as a scaffold for the cell wall integrity pathway (Snyder, 1989; van Drogen and Peter, 2002). Accordingly, I introduced a *SPA2-GFP* fusion construct into my experimental strain and observed its localization in response to Clb depletion (by DOC

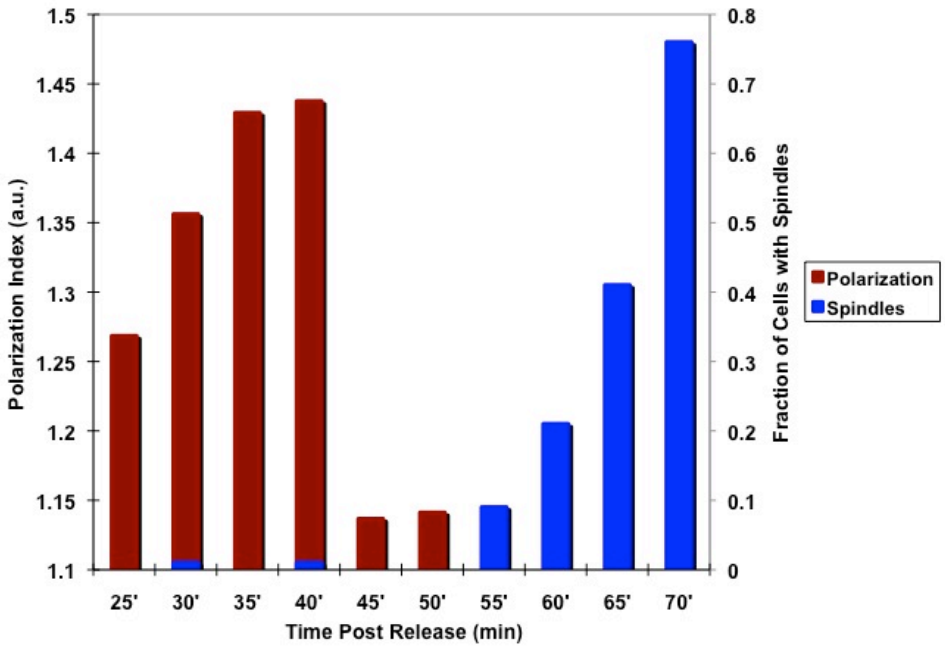

Figure 3-6 Relative timing of growth depolarization and spindle formation. *clb1Δ clb3Δ clb4Δ* cells were synchronized with alpha-factor and released. At the indicated timepoints, cells were scored for polarization (assayed by actin localization as described in Appendix I; values close to 1 indicate isotropic growth, while higher values indicate polarized growth) and spindle formation (assayed with Tub1-GFP).

washout). Remarkably, I observed robust alternating cycles of polarized and depolarized growth, each lasting approximately 40 minutes. During polarized growth, Spa2-GFP appeared tightly localized to the bud tip, and, during the same interval, the bud length rapidly increased. During isotropic growth, Spa2-GFP was delocalized, and the bud length increased at a dramatically slower rate (Figure 3-7). Since the emission spectra of GFP and YFP overlap, and since I was quantitatively measuring Clb2-YFP fluorescence, I conducted all subsequent experiments in a strain without *SPA2-GFP*, relying instead on the dramatic difference in rate of bud length increase to score polarized growth.

I next assayed growth depolarization following a pulse of Clb2-YFP using the protocol described above. In single cells, I correlated Clb2-YFP level with the fraction of time cells exhibited polarized growth (Figure 3-8). In unpulsed cells (no Clb2-YFP), I found that growth was depolarized about half the time (see Figure 3-7 B). Following a pulse, I observed a dose-dependent effect: the higher the Clb2-YFP level, the less time a cell exhibited polarized growth. I also found that relatively low levels of Clb2 were capable of inducing depolarized growth; around 10% of the peak level of Clb2 halved the average amount of time a cell spent in polarized growth, and growth was completely depolarized by 50% of the peak Clb2 level.

Spindle Formation

I next measured the amount of Clb2-YFP required for spindle formation. To track spindle morphology, I used fluorescently-labeled tubulin (*TUB1-CFP*). Spindle formation was marked by conversion of a tubulin dot (indicating unseparated SPBs) to a

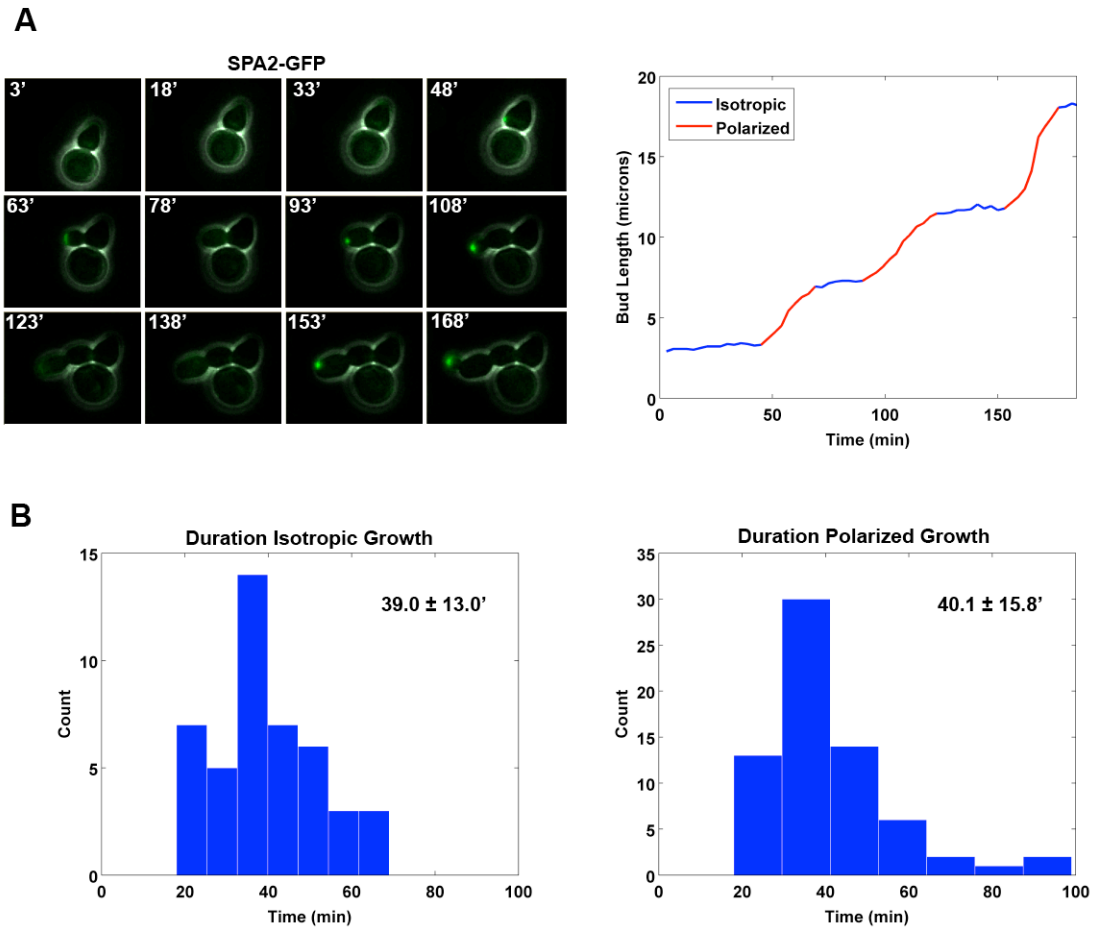

Figure 3-7 Polarized growth cycles in the absence of Clb2-CDK. **A** Left: timelapse images (overlaid phase and GFP channels) of a single cell of the experimental strain arrested by Clb2-YFP depletion (unpulsed) showing localization of Spa2-GFP. GFP images are composites of three z-stacks, 0.5μm apart. Right: bud length (μm) as a function of time for the same cell. Time periods for which growth was scored as isotropic (blue) or polarized (red) are indicated. **B** Histograms showing durations of isotropic (left) and polarized (right) growth for unpulsed cells such as the one shown in A. Inset numbers indicate mean ± s.d.

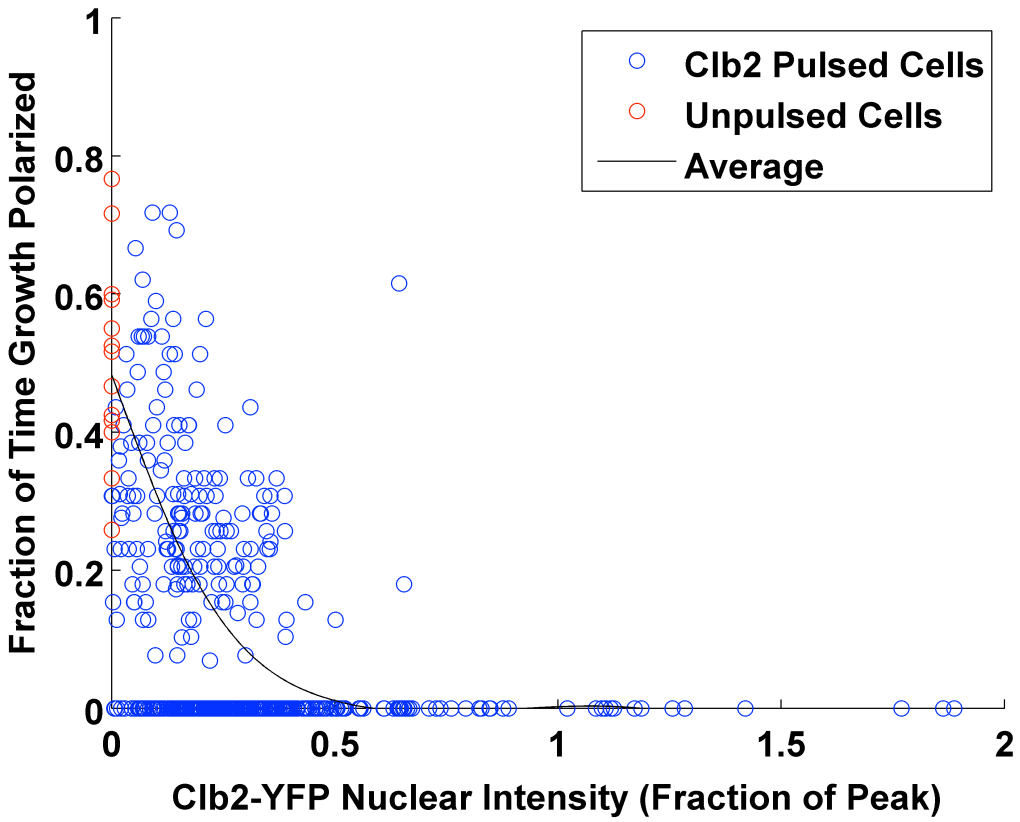

Figure 3-8 Clb2-CDK requirement for growth depolarization. The fraction of time a single cell exhibits polarized growth is shown as a function of Clb2-YFP level, normalized to the wild-type peak. Red points indicate examples of unpulsed cells (see Figure 3-7); blue points indicate cells that received a pulse of Clb2-YFP. The black line indicates the average. N = 538.

bar (indicating a short spindle). Using the same protocol as before, I observed that spindle formation exhibited a somewhat noisy but steep acceleration in response to increasing Clb2-YFP level (Figure 3-9). Cells with less Clb2 took, on average, much longer to form a spindle than cells with more. Interestingly, while cells with low Clb2 levels sometimes waited several hours before forming a spindle, the actual event almost invariably occurred within six minutes at all Clb2 levels. Another interesting observation was that in cells with continued low levels of Clb2-YFP, some cells formed a spindle without having depolarized their growth, indicating mis-ordering of these normally temporally separated events.

To confirm that the Tub1-CFP marker was accurately reporting spindles, I repeated the experiment with a similar strain containing a fluorescently-labeled component of the SPB (*SPC29-CFP*) instead. Since I could not follow SPBs reliably with timelapse microscopy (due to their small size and mobility), I fixed cells 60 minutes after a pulse of Clb2-YFP and correlated SPB separation (two distinct dots of Spc29-CFP) with Clb2-YFP level (Figure 3-10 A). I observed a Clb2 dose response that was consistent with the Tub1-CFP timelapse data at 60 minutes. Thus, Tub1-CFP seems to faithfully detect spindle formation. This experiment provided another useful control for my experimental system. Imaging of CFP fluorophores in yeast can cause toxicity, particularly over long timescales. The accordance of results from the fixed cell timecourse (in which cells were not imaged prior to fixation) with those from the timelapse setup indicates that the imaging conditions did not influence my results.

Finally, I determined the endogenous Clb2 level normally associated with spindle formation. To do this, I synchronized *clb1Δ clb3Δ clb4Δ CLB2-YFP* (endogenously

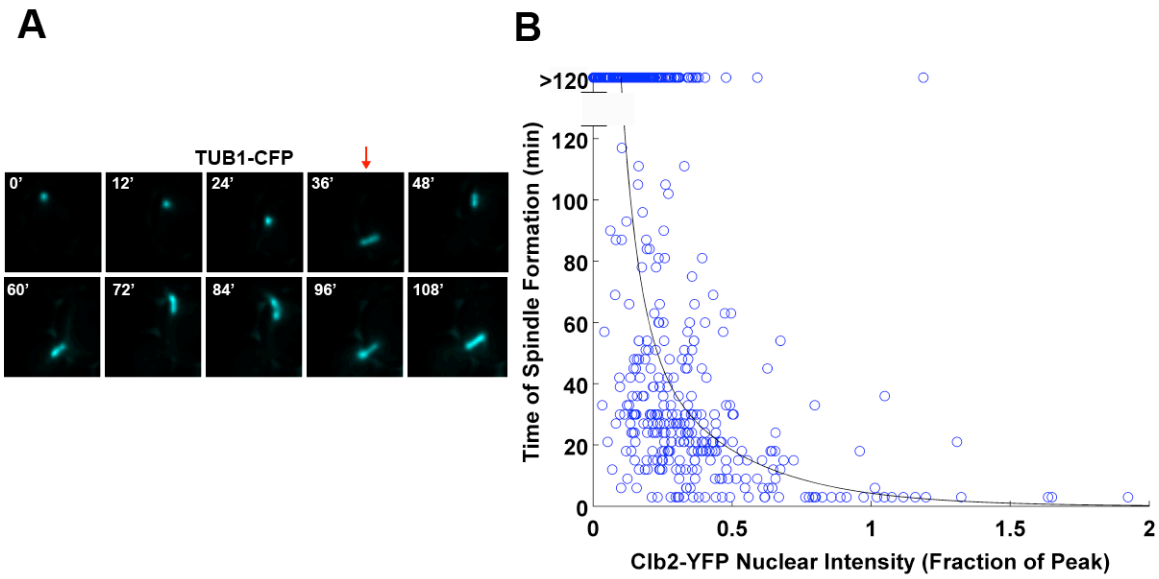

Figure 3-9 Clb2-CDK requirement for spindle formation. **A** Timelapse images (overlaid phase and CFP channels) of a single cell following a pulse of Clb2-YFP. Red arrow indicates scored time of spindle formation. **B** Time (minutes) at which spindle formation occurs as a function of Clb2-YFP level in single cells such as the one shown in A. Points above y = 120 indicate cells that failed to form a spindle within the two hour period of imaging. Black line shows exponential fit of median times of spindle formation for binned Clb2-YFP levels ($R^2 > 0.99$). N = 496.

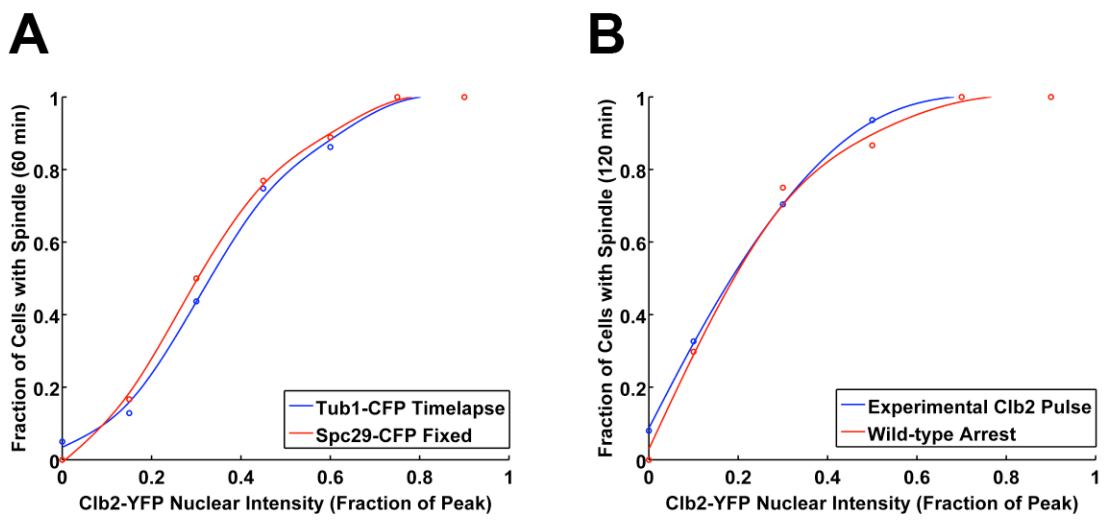

Figure 3-10 Validation of experimental protocol for assaying spindle formation. A Cells of the experimental strain containing Spc29-CFP in lieu of Tub1-CFP were pulsed with Clb2-YFP as before. Rather than undergoing timelapse imaging, cells were left in culture for 60 minutes, then fixed with formaldehyde for fluorescent imaging. Clb2-YFP nuclear intensity and spindle formation (defined as the appearance of two separated dots of Spc29-CFP signal) were assayed from images of the fixed cells. The fraction of cells that formed a spindle within 60 minutes as a function of Clb2-YFP level is shown for the Tub1-CFP timelapse experiments, described in Figure 3-9, (blue) and the Spc29-CFP fixation experiment, described here (red). N = 228. **B** *clb1Δ clb3Δ clb4Δ CLB2-YFP* cells were synchronized with alpha-factor and released. Cycloheximide was added between 45 and 55 minutes later to stop protein synthesis. One hour later, cells were fixed for fluorescent imaging. The fraction of cells with spindles (assayed by Tub1-CFP) as a function of Clb2-YFP level is shown, compared to the similar fraction of cells that formed a spindle within 120 minutes from the experimental timelapse data shown in Figure 3-9.

expressed) cells with alpha factor, turned off *MET3-CDC20* expression by adding methionine (so that I could observe Clb2-YFP levels without degradation), and added cycloheximide around 45 minutes after release from the alpha factor block. Cycloheximide, a potent inhibitor of translation, allowed me to wait for maturation of the YFP fluorophore without further protein synthesis, locking the Clb2-YFP level in each cell. After one hour, when maturation was complete, I fixed the cells and correlated Clb2-YFP level with spindle formation (assayed by Tub1-CFP) (Figure 3-10 B). I observed spindle formation only in cells that contained Clb2 levels similar to, or higher than, the threshold level measured in the pulsed cells described above. This result indicates that my measurements are physiologically relevant.

To compare the Clb2 requirements for growth depolarization and spindle formation, I calculated dose response curves for the two events. For growth depolarization, I determined the fraction of cells with a given binned Clb2-YFP value that completely depolarized their growth (fraction of time spent polarized = 0). For spindle formation, I calculated the fraction of cells with a given binned Clb2-YFP value that formed a spindle within 40 minutes. I chose 40 minutes because this is the average length of the polarized/depolarized phases of growth in unpulsed cells, and thus the limit of my resolution in detecting depolarization of growth. It is also the average amount of time that cells are exposed to Clb2-CDK activity in a normal cell cycle. Comparing these curves, I found that spindle formation required significantly more Clb2-YFP than did growth depolarization (Figure 3-11). This fact, combined with the gradual increase of Clb2 that I observed through a significant portion of the normal cell cycle, implies that rising cyclin-CDK levels control the relative timing of these two early mitotic events.

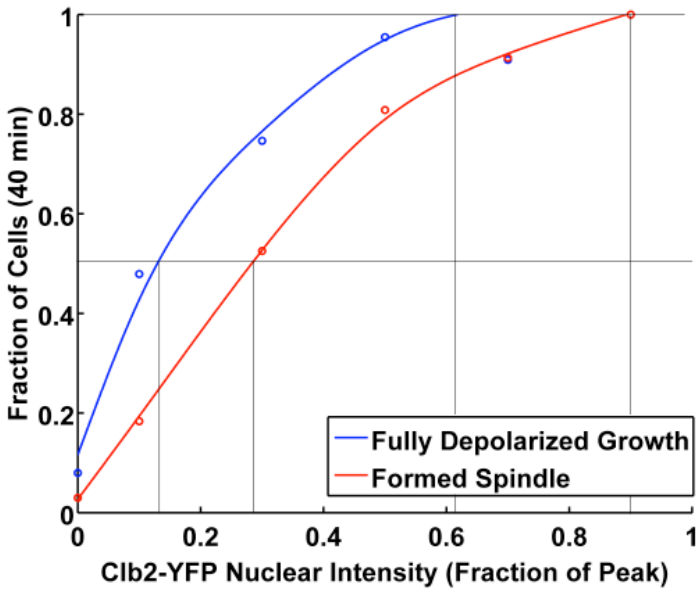

Figure 3-11 Relative Clb2-CDK requirements for growth depolarization and spindle formation. The fraction of cells that completely depolarized their growth (defined as exhibiting no polarized growth for the two hour duration of imaging, corresponding to y = 0 in Figure 3-8) is shown, as a function of Clb2-YFP level, in blue. The fraction of cells that formed a spindle within 40 minutes is shown, as a function of Clb2-YFP level, in red. Horizontal grey lines indicate 50% and 100%, and vertical grey lines indicate their intersection with the dose response curves.

Spindle Elongation/ Anaphase

Clb-CDK activity is required for promoting not just early mitotic events such as those discussed above, but also later events, such as the dramatic process of spindle elongation, or anaphase. As mentioned in the Introduction, replicated sister chromatids are held together by a protein called cohesin. At anaphase, APC^{Cdc20} drives the activation of the separase protease, which cleaves cohesin and frees the chromosomes for segregation to opposite poles of the mother and bud, ready for division to occur between them. Clb-CDK activity promotes this activation of APC^{Cdc20} (Rudner and Murray, 2000; Rudner et al., 2000). Clb-CDK activity also promotes spindle elongation through a less-understood APC-independent mechanism (Rahal and Amon, 2008).

To measure the Clb2 requirement for anaphase, I needed to modify my experimental protocol. Before, I assayed early mitotic events in the absence of *MET3:CDC20* expression. Cdc20, however, is required for anaphase. Therefore, I needed to add back Cdc20 after the Clb2-YFP fluorophore had matured. To do this, I depleted Clb2-YFP and Cdc20 as previously described (wash-out of DOC, followed by addition of methionine), pulsed the cells with Clb2-YFP as before (transient pulse of DOC), and then incubated the cells for two hours, still in methionine. This gave the Clb2-YFP time to mature, and also allowed the cells to form spindles. Finally, I washed out the methionine in the medium to allow Cdc20 reaccumulation, and followed single cells by timelapse microscopy (Figure 3-12 A). Since Clb2-YFP is degraded during anaphase, I correlated the time of anaphase with the pre-anaphase Clb2-YFP level in the same cell (Figure 3-12 B,C). I observed that spindle elongation (assayed with Tub1-

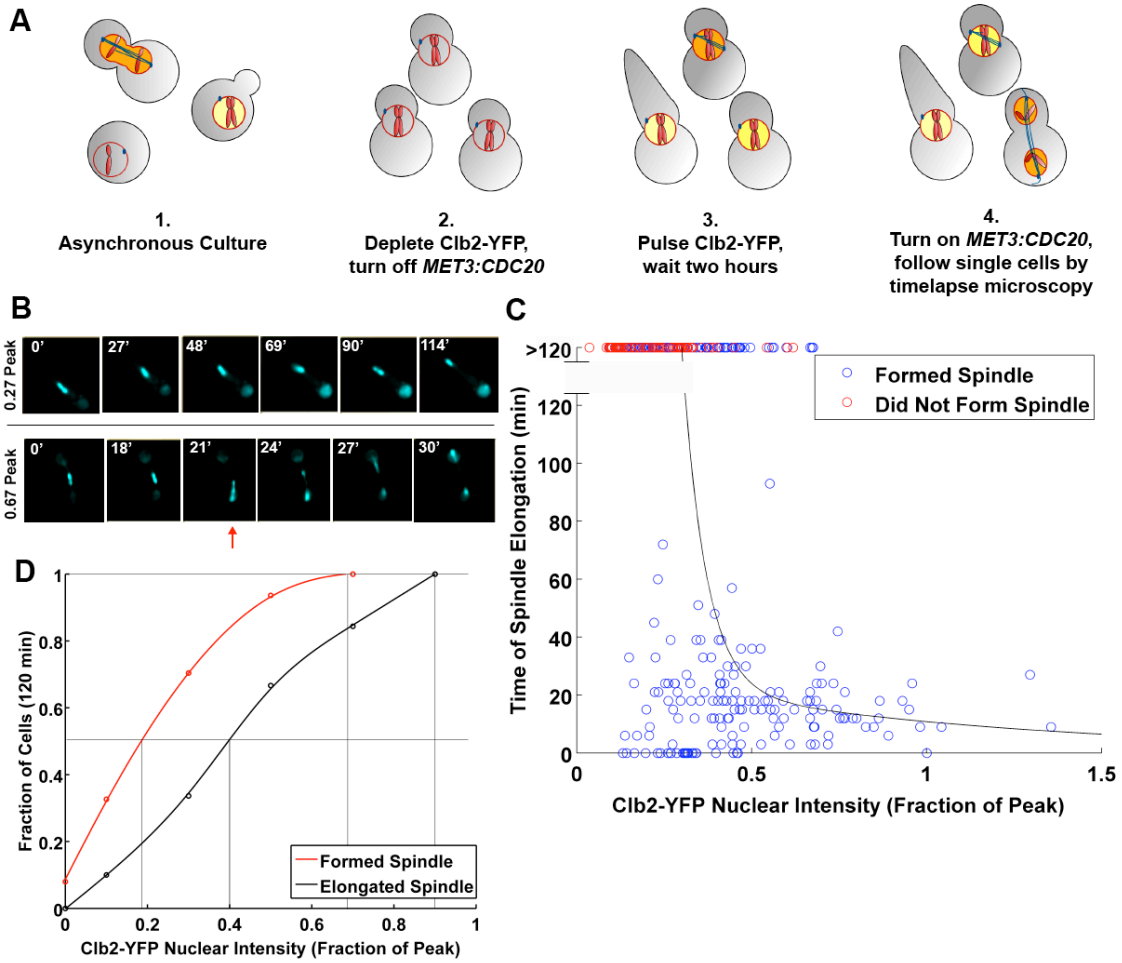

Figure 3-12 Clb2-CDK requirement for anaphase. **A** Schematic of protocol for assaying Clb2-YFP requirement for anaphase. (1), (2), and (3), are as described in Figure 3-3, but cells are left in culture for two hours following the DOC pulse. (4) Methionine is then washed out and cells are followed by timelapse microscopy. **B** Timelapse images of two cells following a pulse of Clb2-YFP and subsequent Cdc20 reintroduction. The top cell does not elongate its spindle, whereas the bottom cell does, with anaphase onset scored at the time indicated by the red arrow. Clb2-YFP levels for the two cells are indicated to the left. **C** Time of spindle elongation (minutes) as a function of Clb2-YFP level. Blue points above y = 120 indicate cells which formed, but did not elongate, a spindle; red points indicate cells which never formed spindles. Black line shows exponential fit of median times of spindle elongation ($R^2 > 0.99$). N = 239. **D** Dose response curves for spindle formation within 120 minutes (red) and spindle elongation (black) as a function of Clb2-YFP level. Grey lines are as in Figure 3-11.

CFP) occurred with increasing efficiency as a function of increasing Clb2-YFP level. Interestingly, I observed cells that had formed spindles successfully, but failed to elongate them. This indicates either that spindle formation and elongation are not ordered by mechanistic coupling alone, or that spindles formed with low Clb2 levels are somehow defective.

In order to compare the Clb2 requirements for spindle formation and elongation, I calculated dose response curves for the two events as before. A revision in the calculation was required: I calculated the fraction of cells with a given binned level of Clb2-YFP that executed each event within 120 minutes (Figure 3-12 D). I chose 120 minutes because this was the amount of time cells were given to form a spindle before restoring Cdc20 activity and allowing spindle elongation. I again observed that the later event (anaphase) required significantly more Clb2 than the earlier event (spindle formation). This rules out the possibility that these two structurally-related events (both involve the spindle) are simply mechanistically coupled. If that were the case, the threshold for the later event should be identical to that of the earlier event. These results are therefore consistent with increasing cyclin-CDK levels triggering cell cycle events in a conserved temporal order.

Swe1 Modulates Event Timing in Early Mitosis

Swe1, the kinase responsible for inhibitory phosphorylation of Clb-CDK complexes, is not required for normal cell cycle progression in yeast. However, as

discussed above, it does partially inhibit Clb2-CDK activity in early Mitosis. Moreover, in the absence of Swe1, spindle formation is slightly accelerated (Harvey and Kellogg, 2003). I therefore wanted to test the effect of Swe1 on the Clb2 requirement for an early mitotic event. Since Swe1 may function in a morphogenetic checkpoint in budding yeast, complicating its effects on growth depolarization (McNulty and Lew, 2005), I looked at spindle formation. I found that deletion of *SWE1* resulted in an approximately two-fold lower Clb2 requirement for spindle formation (Figure 3-13). This is consistent with the roughly two-fold increase in Clb2-CDK associated kinase activity that I observed in the absence of *SWE1*, and indicates that Swe1 normally affects the timing of spindle formation through partial and transient inhibition of Clb-CDK.

Testing a Mathematical Cell Cycle Model

A few years ago, Chen *et al.* published a quantitative ordinary differential equation (ODE) model of the budding yeast cell cycle (Chen et al., 2004). My quantitative measurement of the Clb2-CDK requirement for spindle formation allowed me to test the corresponding aspect of this model. To do this, I isolated the ODE module associated with spindle formation and simulated its response to various stable Clb2 concentrations, mimicking my experimental system of pulses. I observed a theoretical threshold for spindle formation corresponding to about 15% of the peak Clb2 level. This is around half the value I observed experimentally for a *SWE1* (wild-type) strain. Interestingly, though, it is very close to the threshold I observed experimentally in a *swe1Δ* strain (Figure 3-14). In fact, this is the more appropriate comparison, as the

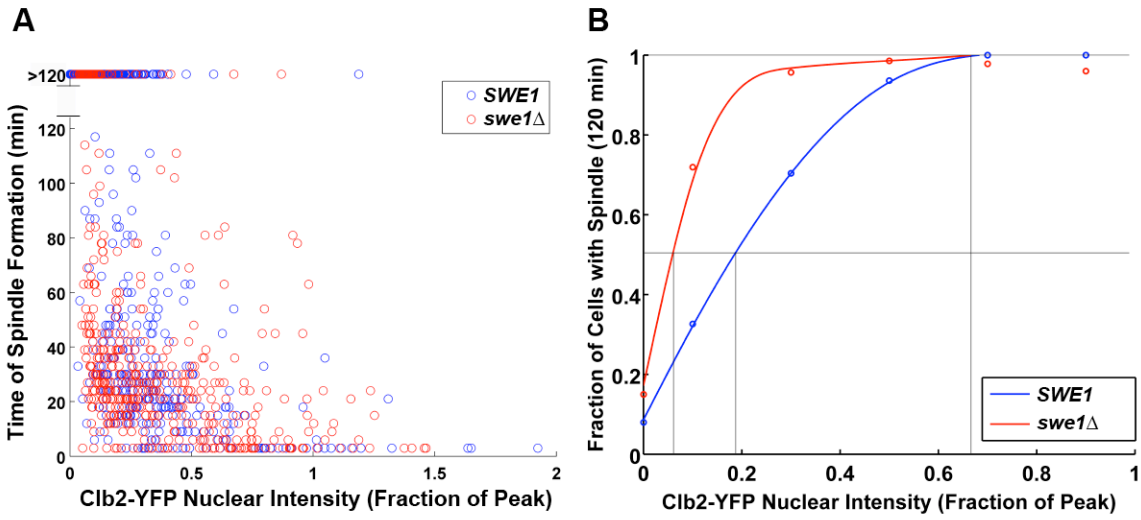

Figure 3-13 Swe1 raises the Clb2 requirement for spindle formation. **A** Time of spindle formation as a function of Clb2-YFP level for cells of the experimental strain (blue; repeated from Figure 3-9) or a similar *swe1Δ* strain (red). Points greater than y = 120 indicate cells that failed to form a spindle within the two hour period of imaging. *swe1Δ* N = 239. **B** Dose response curves for spindle formation within 120 minutes as a function of Clb2-YFP level for $SWE1^{WT}$ (blue) and *swe1Δ* (red) strains.

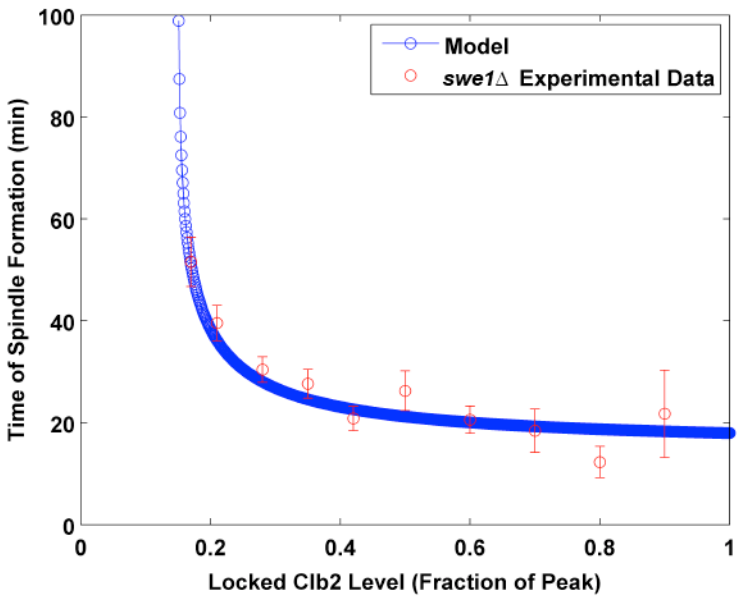

Figure 3-14 Comparison of published ODE model for spindle formation with experimental results. Time of spindle formation is shown in blue as a function of locked Clb2 level for simulation of a quantitative ODE model of the cell cycle (Chen et al., 2004). Corresponding experimental data for a *swe1Δ* strain (from Figure 3-13) is shown in red. Error bars indicate s.e.m.

computational model (Chen et al., 2004) did not include Swe1 inhibition of Clb2-CDK.

Even more strikingly, at critical values of Clb2 concentration (0.15 – 0.2 times the peak), the time of spindle formation predicted by the model increases dramatically from the normal 20-or-so minutes to nearly two hours. This is in accordance with the results I observed experimentally, and suggests that this relatively simple ODE model is a surprisingly good predictor of the complex cell cycle behavior of spindle formation.

CHAPTER 4 – MECHANISTIC BASES OF MITOTIC CYCLIN-CDK REQUIREMENTS

In the last chapter, I discussed how gradually increasing levels of the key regulator Clb-CDK can trigger the events of Mitosis in a reproducible order. This ordering mechanism relies on the ability of individual events to respond to different threshold levels of inducing Clb-CDK. It is of great interest to determine how these thresholds are set at the mechanistic level.

In theory, thresholds for kinase activity can be set in at least three ways. First, the kinase may have a different affinity for different substrates. For example, elegant work from David Morgan's group has illustrated two different strategies for the closely-related kinases Clb2-CDK and Clb5-CDK. While the later-acting (mitotic) Clb2-CDK has a significantly higher kinase activity than the earlier-acting (S-phase) Clb5-CDK, it is relatively nonspecific when it comes to substrates. In contrast, a hydrophobic patch in Clb5, lacking in Clb2, mediates interactions with a specific subset of cellular proteins (Archambault et al., 2005). The high concentration of general substrates in the cell means that initially Clb2-CDK is saturated, and the substrates are phosphorylated slowly. Clb5-CDK escapes this saturation through its lower affinity for general substrates, allowing it to focus on specific substrates, important for S-phase, for which it has a significantly higher affinity. This mechanism could result in ordered substrate phosphorylation even when both kinases are present at the same time; the specific substrates of Clb5-CDK (S-phase targets) would be rapidly phosphorylated, while bulk phosphorylation of general substrates (mitotic targets) would be delayed until Clb2 levels

rose and increasing phosphorylation relieved kinase inhibition (Loog and Morgan, 2005). This mechanism may order the relative progression of S-phase and Mitosis. However, within Mitosis, there appears to be little difference in the specificity of the kinase (Clb2-CDK) for its substrates, at least *in vitro* (Loog and Morgan, 2005).

Another possible mechanism for setting different kinase activity thresholds relies on the number of phosphorylation sites in the substrate. Mike Tyers' group has neatly demonstrated this mechanism at work in the hand-off of cell cycle control from Cln-CDKs to Clb-CDKs after Start. As discussed in Chapter 2, a stoichiometric inhibitor of Clb-CDK complexes, Sic1, is present during G1 to prevent premature activation of its sequestered targets. Cln-CDK phosphorylates Sic1, targeting it for degradation and allowing activation of the Clb-CDKs responsible for the next wave of activities in cell cycle progression (Schwob et al., 1994; Schneider et al., 1996; Verma et al., 1997). However, Sic1 contains not just one site for Cln-CDK phosphorylation, but nine. And rather than providing ideal recognition sites for the ubiquitin ligase responsible for Sic1 degradation, each is weakly recognized. Thus, phosphorylation on one site is not sufficient; multiple sites must be phosphorylated for the protein to be recognized by the degradation machinery. This cooperative phosphorylation generates a switch-like transition from a high-Sic1 (Clb-CDK inactive) state to a low-Sic1 (Clb-CDK active) state, at a high threshold level of Cln-CDK activity (Nash et al., 2001). Multiple phosphorylation sites are a common feature of CDK substrates (Holt et al., 2009), suggesting a widespread role for this mechanism.

Finally, observed thresholds for CDK activity may result from entrainment of peripheral oscillators (controlling individual cell cycle events) to the central CDK

oscillator. As discussed in the Introduction, some cell cycle events occur periodically in the absence of CDK activity cycles. These peripheral oscillators cycle with an intrinsic frequency, which may not match that of the cell cycle as a whole. This disparity may be corrected by entrainment, in which the master CDK input advances or delays the peripheral oscillator within a critical period, synchronizing the clocks (Lu and Cross, 2010). In this case, a minimum amount of CDK activity is required, during the window of sensitivity, to prevent the peripheral oscillator from cycling at its intrinsic frequency and mis-ordering cell cycle events.

In this chapter, I discuss my recent work in understanding the mechanisms by which the thresholds for two early mitotic events, growth depolarization and spindle formation, are set.

Clb2-CDK Control of Growth Polarization

As mentioned in Chapter 3, cells lacking Clb-CDK activity undergo repeated cycles of polarized and depolarized growth, each lasting approximately 40 minutes. This is consistent with a previous description of an intrinsic, Clb-CDK-independent, oscillator controlling budding (Haase and Reed, 1999). When I loaded cells with Clb2-YFP, I observed dose-dependent effects: the higher the Clb2-YFP level, the higher the degree of growth depolarization. Preliminary breakdown of this effect suggests that increasing Clb2 level decreases both the frequency of the oscillation, as well as the length of the polarized portion of the cycle. How could this be effected?

As discussed in the Introduction, recent work has supported a phase-locking mechanism by which Clb-CDK activity entrains an independent oscillator controlling Cdc14 localization, ensuring its execution once (and only once) per cell cycle (Lu and Cross, 2010). The finding that Clb2-CDK activity can modulate the frequency of the bud growth oscillator suggests that phase-locking may similarly constrain this oscillator to execute once per cell cycle. Lu and Cross described a simple mathematical model to describe phase-locking of the Cdc14 oscillator, based on the coupling between oscillators described in Strogatz, 1994 and modified for one-way phase-locking (the CDK oscillator can modulate the frequency of the peripheral Cdc14 oscillator, but not vice versa). I adapted this model to determine whether, theoretically, Clb2-CDK activity could similarly phase-lock an independent oscillator controlling growth polarization.

Such a model requires only three parameters: the frequency of the peripheral oscillator in the absence of Clb2-CDK activity, the period of the peripheral cycle in which it is sensitive (the window of opportunity for Clb2-CDK activity to force the cycle), and the strength of coupling between the two oscillators. I estimated the values of two of these parameters from my experiments. The frequency of the polarized growth oscillator is around 80 min^{-1}, and I assumed that the polarized growth cycle is sensitive to forcing during its polarized period, which is roughly half of the total cycle time. I then used these two parameters to estimate the third – the strength of coupling. This gave a behavior, in response to fixed levels of Clb2-CDK, that was quite similar to the behavior observed experimentally (Figure 4-1). This suggests that the levels and timing of Clb2 accumulation I observe experimentally are sufficient to effectively phase-lock the growth polarization oscillator, restricting its execution to once per cell cycle.

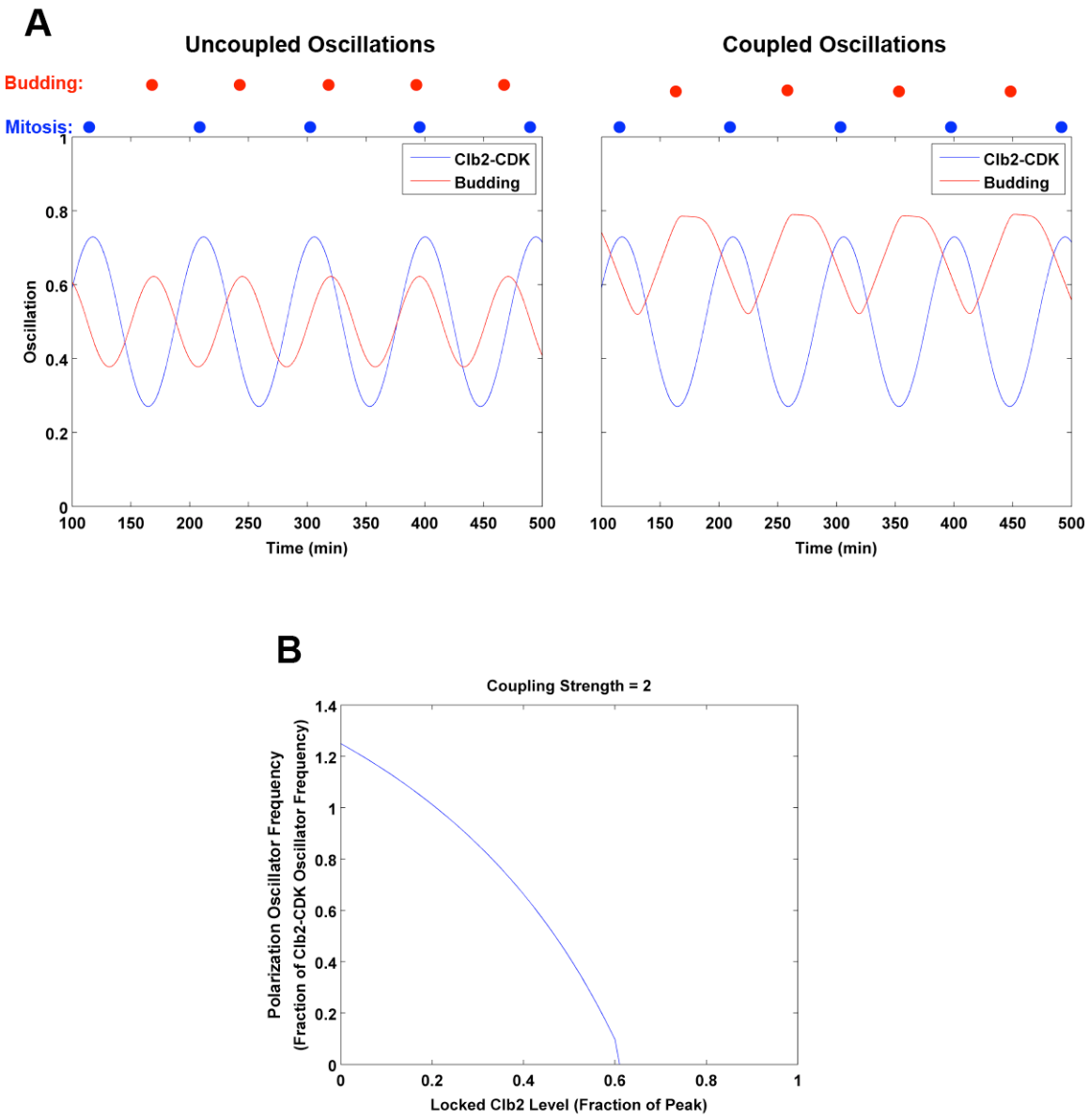

Figure 4-1 A model for Clb2-CDK phase-locking of an independent growth polarization oscillator. **A** Oscillations of Clb2-CDK activity (blue) and growth polarization (red) as modeled for uncoupled (left) and coupled (right) oscillators. Colored circles indicate times of Mitosis (blue) and budding (red) for illustrative purposes. Note the strict phase relationship imposed by phase-locking on the right. **B** The response of the growth polarization oscillator frequency (expressed as a fraction of the Clb2-CDK oscillator frequency) to fixed levels of Clb2, as provided experimentally. As discussed in the text, the strength of coupling was fit to 2.

The Molecular Basis of the Threshold for Clb-CDK-Mediated Spindle Formation

The requirement of Clb-CDK activity for spindle formation has been known for quite some time (Fitch et al., 1992; Richardson et al., 1992; Lim et al., 1996). However, the basis for this requirement is not well understood. The ability to measure a Clb2-CDK threshold provides a sensitive assay with which to test candidate targets that might promote spindle formation.

Budding yeast spindles consist of one microtubule attaching each chromatid's kinetochore to a SPB, as well as a small number of additional microtubules stretching between the two SPBs (Peterson and Ris, 1976; Winey et al., 1995). Prior to spindle formation, the SPBs (duplicated in a Cln-CDK-dependent manner early in the cell cycle (Haase et al., 2001)) lie embedded in the nuclear envelope and tethered to one another by a proteinaceous bridge. During early Mitosis, this bridge is severed and the SPBs move apart to opposite sides of the nucleus, arraying the spindle between them (Adams and Kilmartin, 1999), schematized in Figure 4-2.

At least two classes of mutants cannot separate SPBs in the presence of Clb-CDK activity: mutants of the Sfi1 protein, and mutants lacking kinesin-5 activity (encoded by *CIN8* and *KIP1*).

Sfi1, a SPB Bridge Protein

Sfi1 is a centrin-binding protein thought to form the structural basis for the SPB-tethering bridge (Kilmartin, 2003; Li et al., 2006). *sfi1Δ* cells arrest late in the cell cycle

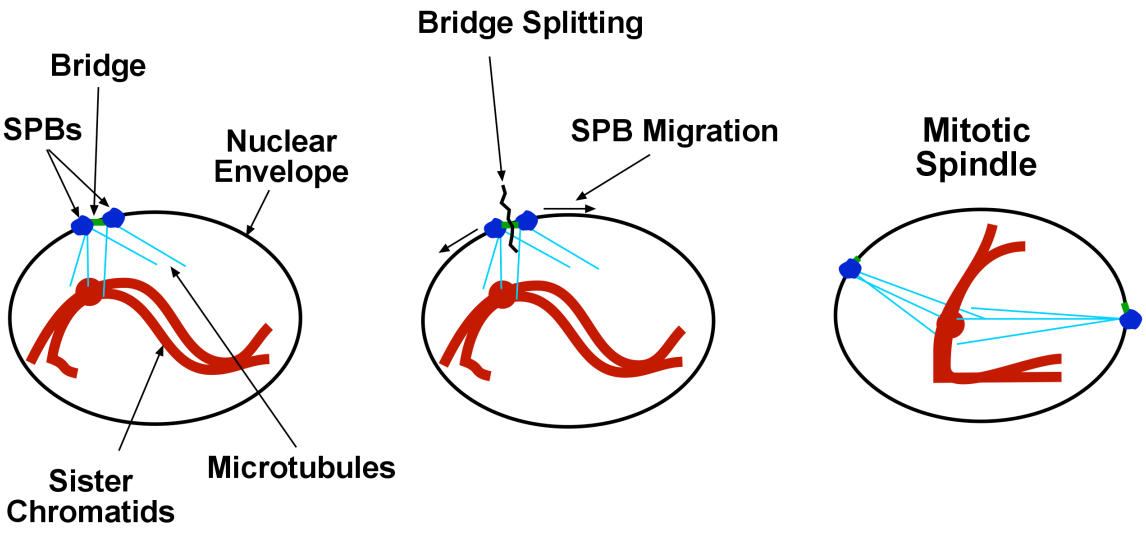

Figure 4-2 Schematic of SPB-mediated spindle assembly. Left: just prior to Mitosis, cells contain duplicated chromosomes and two SPBs, embedded in the nuclear envelope and tethered by a proteinaceous bridge. Middle: at the time of spindle formation, the bridge is severed and the SPBs move apart. Right: the completed mitotic spindle.

without spindles (Ma et al., 1999). Sfi1 contains five consensus CDK phosphorylation sites, all located in the C-terminus of the protein (Figure 4-3), and has been shown to be phosphorylated by Clb2-CDK *in vitro* (Ubersax et al., 2003). Interestingly, mutations in three of these consensus CDK sites have been isolated in screens for spindle assembly defects (assayed by synthetic lethality with either *mad1Δ*, a spindle checkpoint protein, or *bik1Δ*, a microtubule-associated protein) (Strawn and True, 2006; Anderson et al., 2007). The C-terminus of the protein is thought to mediate interactions with the C-termini of other Sfi1 molecules extending from the opposite SPB and overlapping in the middle of the bridge (Figure 4-3). Perhaps phosphorylation in this region weakens the interaction and allows splitting of the bridge?

I introduced one of these previously-described mutations, *sfi1-120*, into the Clb2 titration strain to determine its effect. This mutation inactivates a CDK consensus site: **S**^{857}PVK → **N**PVK (Anderson et al., 2007). I observed that the mutation greatly increased the Clb2 requirement for spindle formation. It also increased the variability of timing, even at high levels of Clb2 (Figure 4-4 A). To verify the importance of phosphorylation at this site, I created a phosphomimetic version of the protein by mutating S^{857} and the adjacent P^{858} to glutamates. This approach, in a different protein, has been shown to successfully mimic the double negative charge of a phosphorylation (Strickfaden et al., 2007). Cells with this mutation (*SFI1*$^{\boldsymbol{EE}VK}$) exhibited a Clb2 dose response nearly identical to that of *SFI1*^{WT} cells, supporting the importance of Clb2-CDK phosphorylation of this site (Figure 4-4 B). To determine whether Clb-CDK phosphorylation of Sfi1 was sufficient for spindle formation, I created a five-site phosphomimetic allele of *SFI1* using the same double glutamate approach to mimic

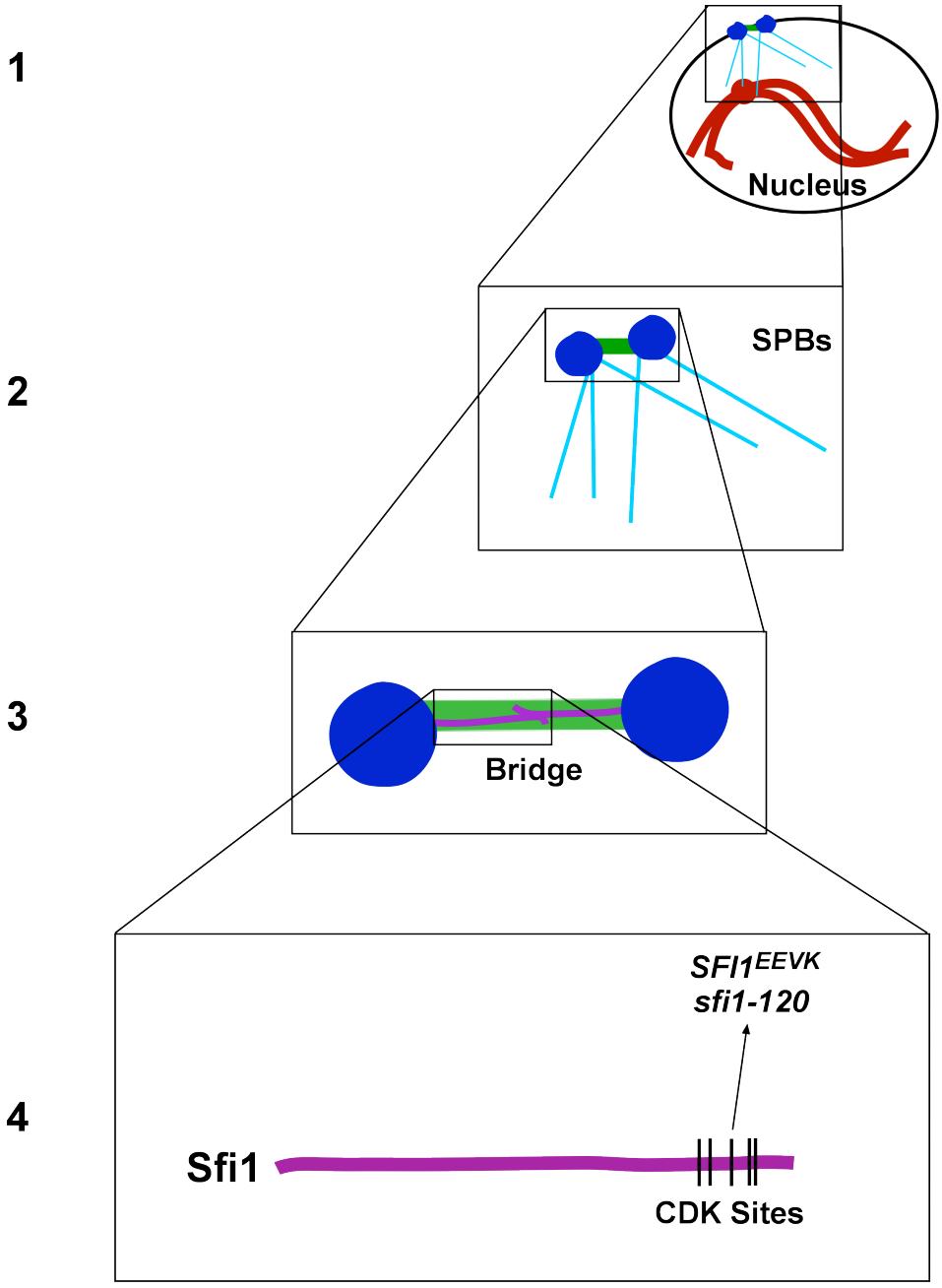

Figure 4-3 CDK consensus sites in the SPB bridge protein Sfi1. 1-3 Increasing magnification of the SPB bridge. Sfi1 localizes to the bridge, as filaments extending from each SPB, with their C-termini overlapping in the middle. **4** Schematic of the Sfi1 protein showing location of five consensus CDK sites in the C-terminus. The arrow indicates the site mutated in *sfi1-120* (and phospho-mimicked in $SFI1^{EEVK}$). All five sites contain phosphomimetic mutations in $SFI1^{5EE}$.

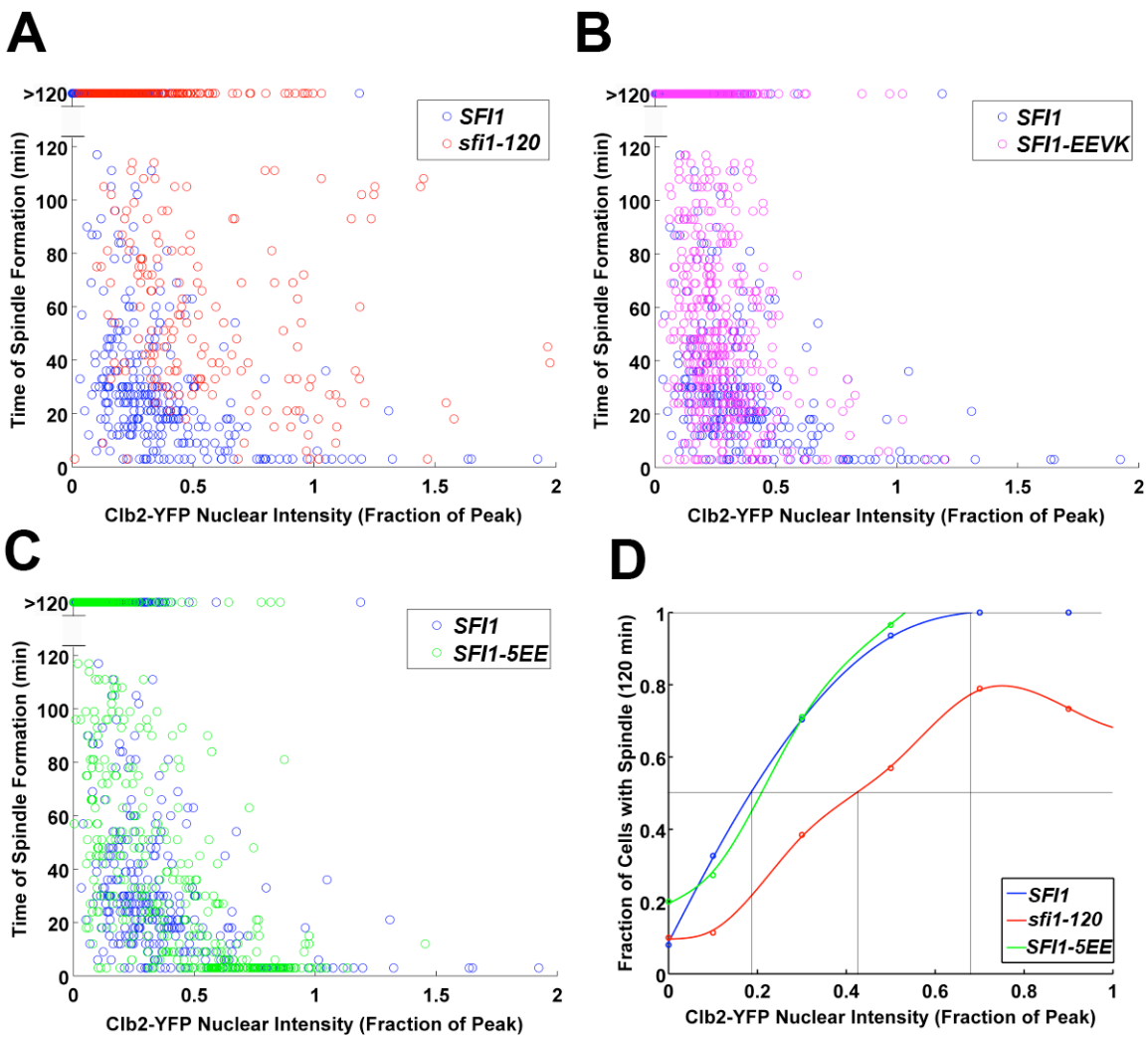

Figure 4-4 Clb2-CDK phosphorylation of Sfi1 promotes efficient spindle formation. **A** Comparison of the time of spindle formation, in minutes, as a function of Clb2-YFP level for the experimental strain (*SFI1* in blue, repeated from Figure 3-9) and a strain in which *SFI1* is replaced by the *sfi1-120* single phosphorylation site mutant allele (red, N = 400). Plotting conventions are as before. **B** Comparison of the time of spindle formation as a function of Clb2-YFP level for the *SFI1* experimental strain (blue) and the single-site phosphomimetic $SFI1^{EEVK}$ allele (purple, N = 738). **C** Comparison of the time of spindle formation as a function of Clb2-YFP level for the *SFI1* experimental strain (blue) and the five-site phosphomimetic $SFI1^{5EE}$ allele (green, N = 670). **D** Dose response curves for spindle formation within 120 minutes as a function of Clb2-YFP level for the *SFI1* (blue), *sfi1-120* (red), and $SFI1^{5EE}$ (green) strains shown in A and C.

phosphorylation on all five full consensus CDK sites. In this case, the Serine or Threonine residue of each site, as well as the adjacent Proline residues, were mutated to EE to give *SFI1*^{5EE}. Interestingly, *SFI1*^{5EE} cells also exhibited a near-wild type response to Clb2 titration (Figure 4-4 C,D). This suggests that while Sfi1 phosphorylation is important for spindle formation, it is not a rate-limiting target. There are likely other Clb-CDK targets for spindle formation, and these other targets are likely responsible for the observed kinetics in a wild-type cell cycle.

Cin8, a Kinesin-5 Motor

The formation of the mitotic spindle is, at heart, a mechanical process. The machinery responsible for pushing and pulling the spindle to its correct shape and orientation comprises a set of protein motors with both complementary and opposing roles (Hildebrandt and Hoyt, 2000). Two BimC/Kinesin-5 motors, Cin8 and Kip1, are thought to provide the initial push to separate the SPBs by sliding apart antiparallel microtubules. (These microtubules, whose (-) ends are associated with the SPBs, lie next to one another but are associated with opposite SPBs, explaining their antiparallel orientation.) Cin8 and Kip1 are (+) end-directed motors and are thought to operate as homotetramers; they can bind two antiparallel microtubules and, by walking toward the (+) ends of both microtubules, generate a relative outward force, pushing the SPBs to opposite sides of the nucleus (Hildebrandt and Hoyt, 2000), as illustrated in Figure 4-5. While each single mutant is viable, *cin8Δ kip1Δ* cells arrest with unseparated SPBs, and

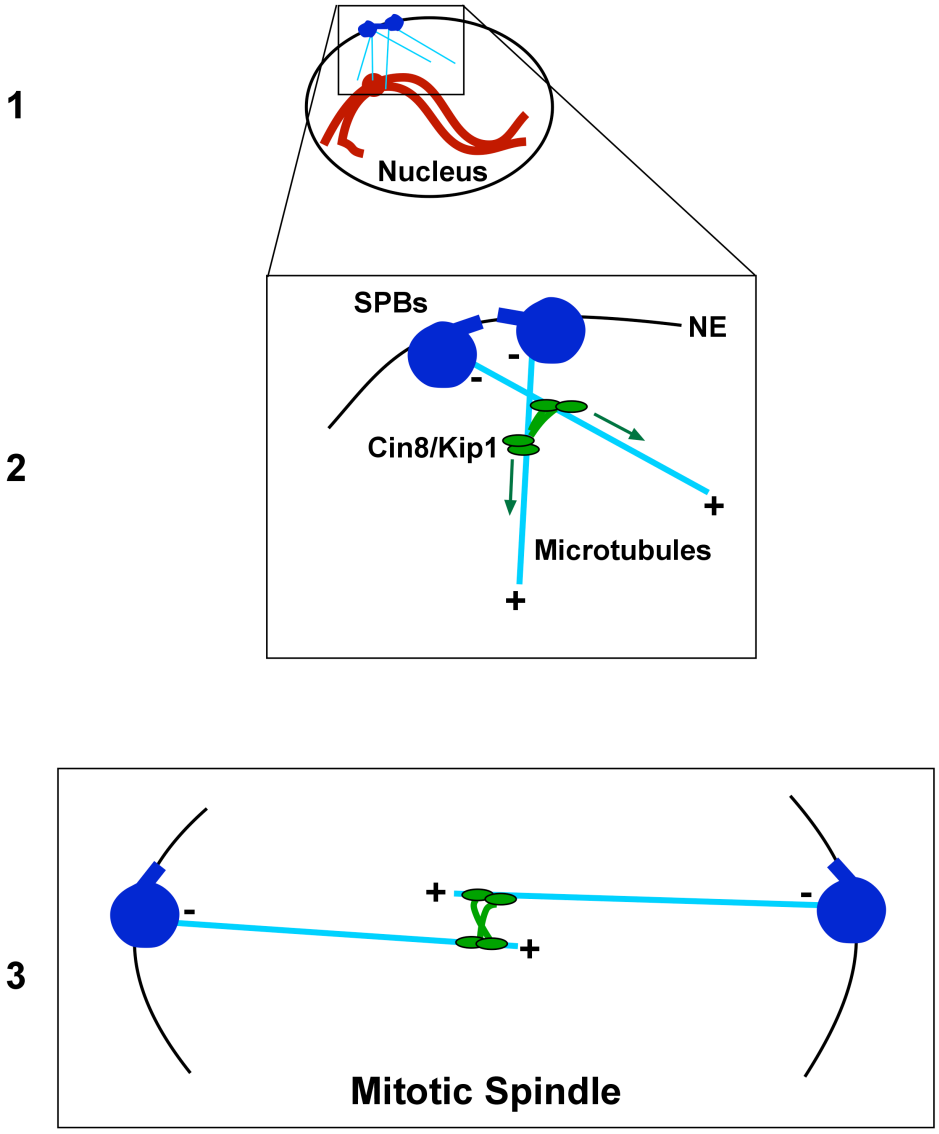

Figure 4-5 Kinesin-5 motor activity generates outward force on SPBs. 2 Magnification of SPBs and associated microtubules from **1**. Microtubule polarity is shown, with (-) ends associated with the SPBs and (+) ends extending outward into the nucleus. A cartoon of a kinesin-5 motor (Cin8 and Kip1; green) is shown binding two microtubules, one from each SPB. These motors are (+) end-directed and will move, relative to the SPBs, as shown by the green arrows. This generates force on the SPBs, which moves them into the opposing orientation shown in **3**.

Cin8 appears to play the more dominant role in spindle formation (Hoyt et al., 1992; Roof et al., 1992).

Cin8 protein levels vary throughout the cell cycle, and the protein is actively degraded early in the cycle in an APC^{Cdh1}- dependent manner (Hildebrandt and Hoyt, 2001). Clb-CDK activity contributes to Cdh1 inhibition, allowing accumulation of Cin8 and Kip1 (Yeong et al., 2001; Crasta et al., 2006; Crasta et al., 2008). It has been suggested that this Cin8/Kip1 protein stabilization is the only essential function of Clb-CDK activity in spindle formation (Crasta et al., 2006). These experiments, however, relied on significant overexpression of Cin8 and Kip1 to drive SPB separation. More recent work has suggested that Cin8 and Kip1 can accumulate in the absence of Clb-CDK activity (Chee and Haase, 2010), and that physiological levels of Cin8 are insufficient for SPB separation in the presence of sustained APC^{Cdh1} activity (and thus no Clb-CDK activity) (Robbins and Cross, 2010).

I used my experimental Clb2 titration system to test the effect of stabilized Cin8 on spindle formation. I added a single extra copy of the *CIN8* gene with its Cdh1 recognition site (KEN box) mutated (*CIN8-KED*), which renders the protein impervious to APC^{Cdh1}, and thus relatively stable (Hildebrandt and Hoyt, 2001). In the absence of Clb2 expression, greater than 90% of cells failed to make a spindle (similar to $CIN8^{WT}$), consistent with Cin8 stabilization not being the sole mechanism by which Clb2-CDK promotes spindle formation. Additionally, *CIN8-KED* had no effect on the kinetics of spindle formation in response to various Clb2 levels (Figure 4-6). This could be because Clb5-CDK, an S-phase cyclin which is undisturbed in my experimental strain, effectively

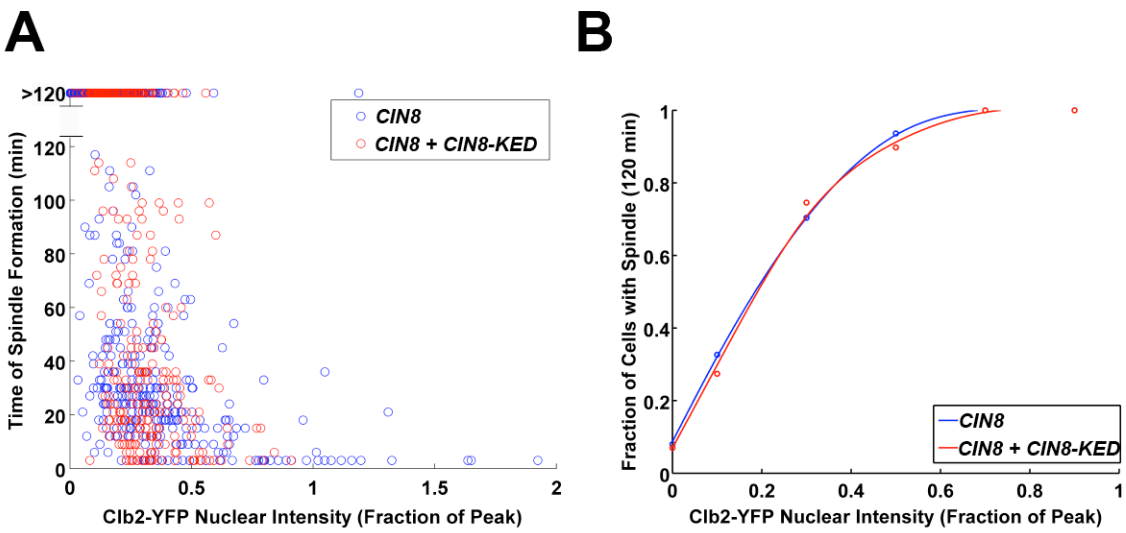

Figure 4-6 Clb2-CDK-mediated Cin8 accumulation is not rate-limiting for spindle formation. **A** Comparison of the timing of spindle formation, in minutes, as a function of Clb2-YFP level for the experimental strain (*CIN8* in blue, repeated from Figure 3-9) and a strain containing an extra copy of *CIN8-KED* with its APC^{Cdh1} destruction box mutated (red, N = 346). **B** Dose response curves for spindle formation within 120 minutes for the strains shown in A.

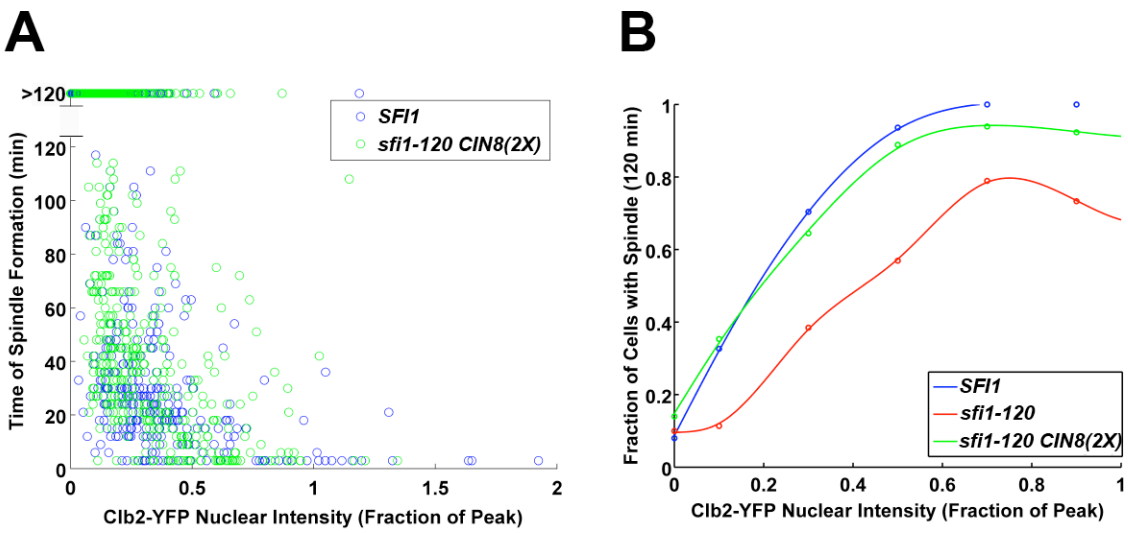

Figure 4-7 Increased Cin8 can rescue the spindle formation defect of *sfi1-120*. **A** Comparison of the timing of spindle formation, in minutes, as a function of Clb2-YFP level for the experimental strain (*SFI1* in blue, repeated from Figure 3-9) and a strain carrying the *sfi1-120* allele replacing the endogenous *SFI1* as well as an additional copy of normally-degradable *CIN8* (green, N = 654). **B** Dose response curves for spindle formation within 120 minutes for the *SFI1* (blue), *sfi1-120* (red), and *sfi1-120 CIN8* (2X) (green) strains shown in A and Figure 4-3 A.

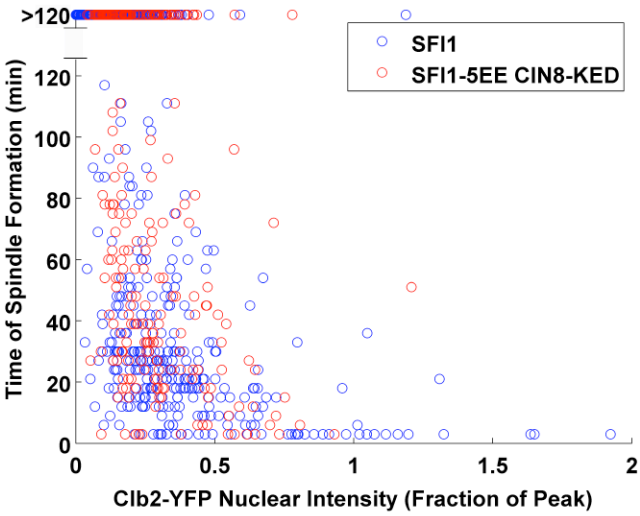

Figure 4-8 Combination of potential Clb-CDK bypass mutations in *SFI1* and *CIN8* does not affect Clb2 requirement for spindle formation. Comparison of the timing of spindle formation as a function of Clb2-YFP level for the experimental strain (blue, repeated from Figure 3-9) and a strain containing both the $SFI1^{5EE}$ allele (replacing *SFI1*) and the Cdh1-undegradable *CIN8-KED*, in addition to the endogenous *CIN8* (red, N = 253).

inactivates Cdh1 (and thus stabilizes Cin8), independently of Clb2-CDK activity (Yeong et al., 2001).

Interestingly, I observed that adding an extra copy of $CIN8^{WT}$ to *sfi1-120* ($sfi1^{NPVK}$) cells rescued the wild-type kinetics (Figure 4-7). This suggests that increased motor activity can overcome the defect of partially-unphosphorylatable Sfi1. The *KED* mutation in *CIN8*, conferring resistance to Cdh1, was not required for this effect. Again, this is likely because Cdh1 is efficiently inactivated in my experimental protocol, even without Clb2 induction.

Finally, I combined an extra copy of Cdh1-undegradable *CIN8-KED* with the five-site phosphomimetic $SFI1^{5EE}$. This combination did not bypass the Clb-CDK requirement for spindle formation, though, and cells exhibited similar dose-response kinetics of spindle formation following a pulse of Clb2-YFP (Figure 4-8). These results demonstrate the existence of at least one other essential, and likely rate-limiting, target of Clb2-CDK for spindle formation.

CHAPTER 5 – MITOTIC CYCLIN-CDK MODULATES THE FREQUENCY OF THE CELL CYCLE OSCILLATOR

A key prediction of the quantitative model of cell cycle control remains undemonstrated. If the level of a cell cycle regulator (Clb-CDK, in this case) controls the order and timing of events, it might be expected that increasing the level of that regulator above its endogenous level should accelerate the timing of the events it controls. Does Clb2 overexpression accelerate the timing of mitotic events?

One previous experiment has been carried out to address this question. In that work, cells were synchronized by nutrient deprivation (growth past the diauxic shift in respiration) and extremely high levels of *CLB2* were induced (at least eight copies of *GAL1-CLB2*). (Based on my results, this could result in expression levels several hundred-fold higher than from the endogenous *CLB2*.) Reentry to the cell cycle from such an arrest is quite slow, and execution of mitotic events (spindle formation and anaphase) was assayed with one-hour time resolution. No gross acceleration of events was observed (Surana et al., 1993), but given the nature of the synchronization and the extreme degree of *CLB2* overexpression, I felt that further investigation was warranted.

Increased Clb2 Level Accelerates Cell Cycle Timing

To determine whether increased levels of Clb2 can accelerate the timing of mitotic events, I replaced the endogenous *CLB2*, in an otherwise CLB^{WT} strain, with *CLB2* under the control of the *GALL* promoter. In galactose medium, *CLB2* expression

from this promoter is approximately five times that of the endogenous promoter. I used fluorescently-labeled tubulin (*TUB1-GFP*) and timelapse microscopy to score the time of anaphase in freely-cycling cells in galactose-containing media. I also scored the time of budding by eye. I observed that the budded period of the cell cycle (the time between budding and anaphase) was shortened in the *GALL:CLB2* strain, consistent with acceleration of mitotic events (Figure 5-1). I also observed a significant acceleration of the overall cell cycle time. *GALL:CLB2* mother cells took, on average, 80 minutes to progress from one anaphase to the next, while wild-type mother cells took an average of 133 minutes. These accelerated cell cycles were observed repeatedly when individual cells were followed; a short first cycle was not compensated for by a longer second cycle. Therefore, the intrinsic cell cycle frequency was significantly increased by *CLB2* overexpression.

To monitor the timing of individual mitotic events, I synchronized $CLB2^{WT}$ and *GALL:CLB2* strains in G1 using alpha-factor. After release, I took samples every ten minutes and used fixed-cell microscopy to assay cell cycle events (Figure 5-2). The time of budding is expected to be Clb2-independent (Cross, 1995); I therefore used it as an independent marker of release from alpha-factor block. Budding was scored from phase images. Growth polarization was determined from images of rhodamine-phalloidin by measuring a quantitative index of polarization with Matlab, as described in Appendix I. The timings of spindle formation and anaphase were determined from images of Tub1-GFP. In both strains, budding occurred approximately 40 minutes post-release. In *GALL:CLB2* cells, however, growth depolarization occurred at least 25 minutes earlier than in wild-type cells, and spindle formation and anaphase both occurred

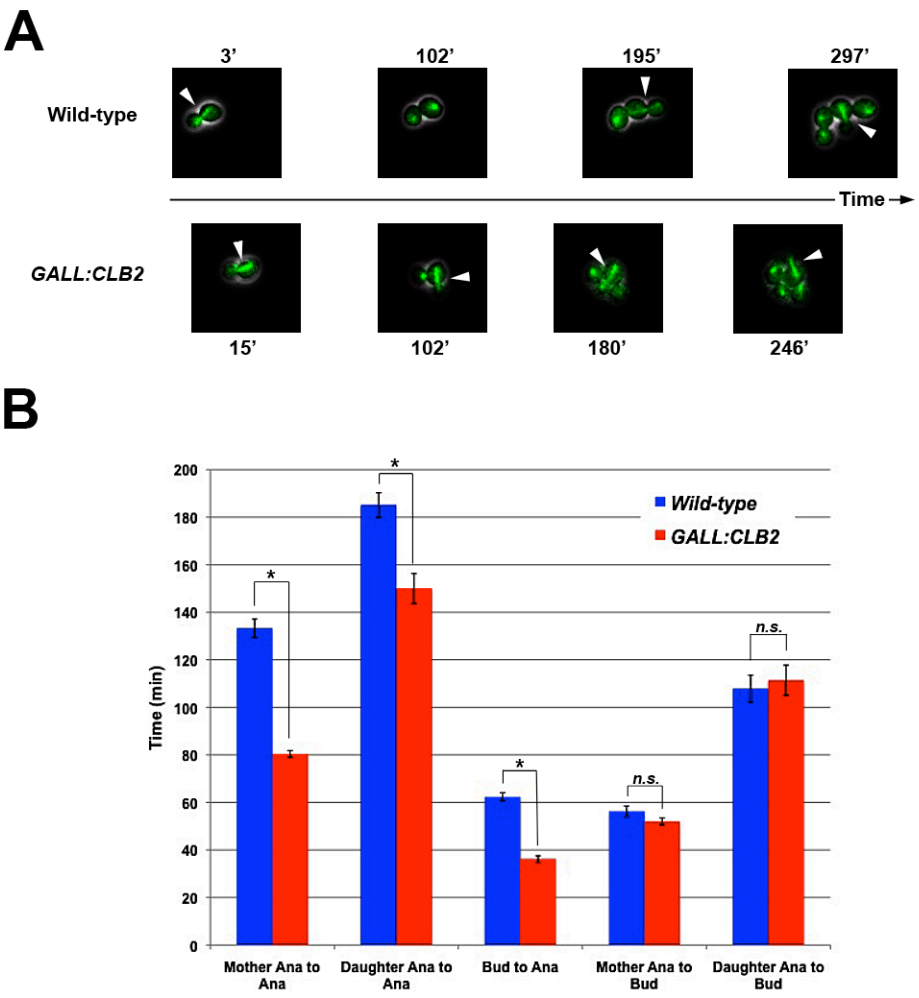

Figure 5-1 Clb2 is rate-limiting for cell cycle frequency. **A** Timelapse images (overlaid phase and GFP channels) of freely-cycling *CLB2*^{WT} (top) and *clb2::GALL:CLB2* (bottom) strains containing Tub1-GFP that were exposed to galactose. Arrowheads indicate sequential anaphases in the same cell. **B** Comparison of the average durations of various cell cycle intervals for freely-cycling *CLB2*^{WT} (blue) and *clb2::GALL:CLB2* (red) strains in galactose. Data were scored from timelapse images such as those shown in A. Intervals are, from left to right: anaphase-to-anaphase in mother cells, anaphase-to-anaphase in daughter cells, budding-to-anaphase in both mothers and daughters, anaphase-to-budding in mother cells, and anaphase-to-budding in daughter cells. Error bars indicate s.e.m. Data were compared using a student's unpaired t-test. * $p < .001$; n.s. not significant.

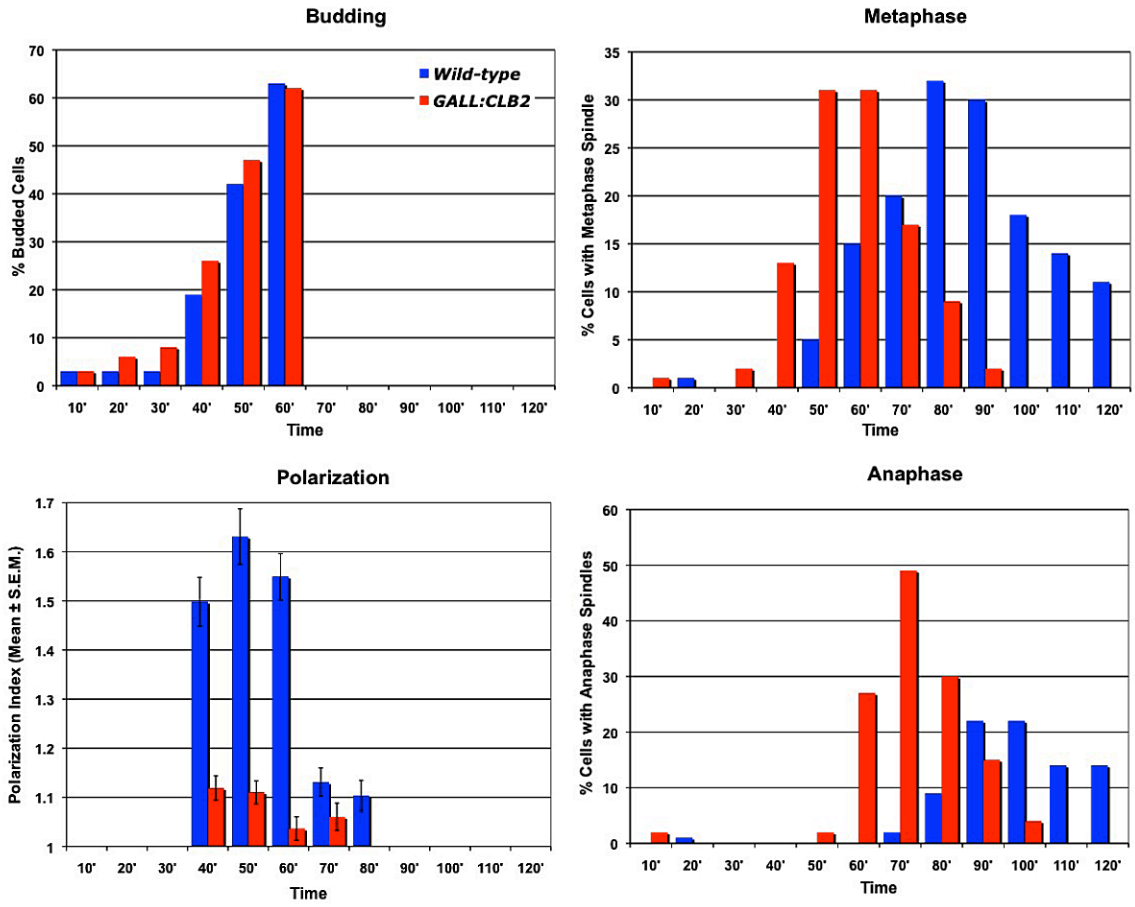

Figure 5-2 Clb2 overexpression accelerates individual mitotic events. *CLB2*^{WT} (blue) and *clb2::GALL:CLB2* (red) strains containing Tub1-GFP were synchronized in G1 with alpha-factor. Samples were fixed for fluorescent imaging at the indicated timepoints after release. Budding was scored by eye from phase images, polarization index was scored as described in Appendix I from rhodamine-phalloidin stained cells, and spindle formation (metaphase) and elongation (anaphase) were scored by eye from GFP images. Error bars in the plot of polarization index indicate s.e.m. In that plot, values close to 1 indicate isotropic growth, while higher values indicate polarized growth.

25 minutes earlier. The fact that budding occurred at the same time in both strains indicates that the acceleration of mitotic events was due specifically to premature Clb2 accumulation promoting mitotic events, rather than accelerating recovery from the alpha-factor block. Overall, these results indicate that Clb2 is, in fact, normally rate-limiting for Mitosis.

The accelerated cell cycles that I observed with timelapse microscopy of *GALL-CLB2* cells are surprising. It is a well-established view that growth, and not cell cycle regulation, is ultimately rate-limiting for division (Johnston et al., 1977). Is it possible that excess Clb2 accelerates cell growth as well as the cell cycle? I reasoned that this might be possible based on recent work showing that cell growth is faster during portions of the cell cycle when growth is depolarized (Goranov et al., 2009). Since growth depolarization is significantly advanced in strains overexpressing Clb2, it is possible that such cells spend a proportionally longer period of time in a higher growth rate regime. To test this, I calculated the bud size (measured as the length of the two-dimensional bud contour from phase images) as a function of time in the alpha-factor synchronized release experiment just described. I observed that bud growth was significantly faster in *GALL:CLB2* cells than in wild-type cells, precisely up until the time when the wild-type cells depolarized their growth (Figure 5-3). This is consistent with faster growth of *GALL:CLB2* cells during the window when overexpressed Clb2 has induced premature depolarization, preserving the coupling between growth and division.

Further evidence that this coupling is still intact in *GALL:CLB2* cells comes from the observation that the overall cell cycle time (measured as anaphase-to-anaphase) is

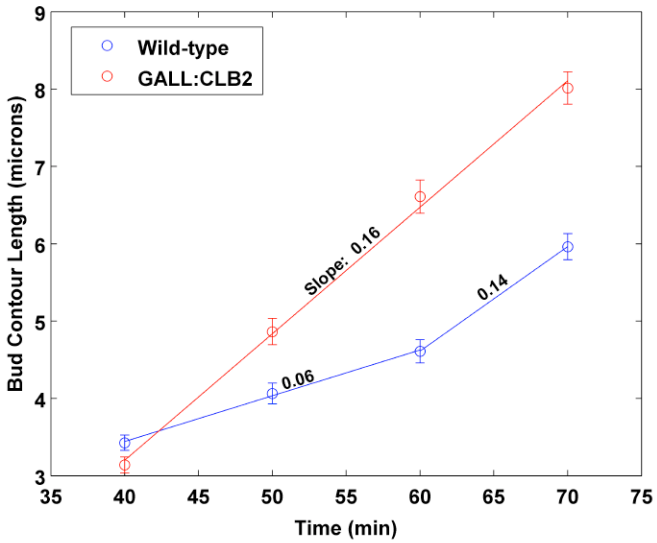

Figure 5-3 Clb2 overexpression increases the rate of increase of cellular area through premature growth depolarization. The mean two-dimensional bud contour length (μm; measured from phase images) is shown as a function of time following release for the *CLB2*^{WT} (blue) and *clb2::GALL:CLB2* (red) strains in the experiment shown in Figure 5-2. Error bars indicate s.e.m. The lines indicate linear fits of the data, with the indicated slopes.

decreased specifically by a reduction in the budding-to-anaphase time. The time from anaphase to subsequent budding, in both mother and daughter cells, is essentially identical to that of wild-type cells (Figure 5-1). As discussed in previous chapters, this pre-Start interval is the target of regulation coupling growth and division. The timing data therefore suggests that the coordination of growth and division at Start is intact, even with Clb2 overexpression.

Clb2 Overexpression Imposes a Fitness Cost

The observation that an increased Clb2 level can speed up the cell cycle is a bit puzzling. Such a speed-up should offer a fitness benefit; so why do wild-type cells not make more Clb2 than they do? In media containing galactose and lacking methionine (SCG-Met), the doubling time of the *GALL:CLB2* population was longer than the wild-type population (115 vs. 125 minutes), presumably due to an increased fraction of inviable cell divisions.

One possibility is that a faster Mitosis may result in an increase in chromosome segregation defects; perhaps cells need more time to ensure proper spindle attachments. If this were the case, the spindle assembly checkpoint should be activated more often than in wild-type cells. This checkpoint responds to defects in spindle formation or attachment to chromosomes and inhibits the APC^{Cdc20}, preventing anaphase until the spindle morphology is corrected. To determine whether *GALL:CLB2* cells rely on the spindle assembly checkpoint more heavily than wild-type cells, I deleted the checkpoint component *mad2Δ*. However, I observed no synthetic defect arising from the

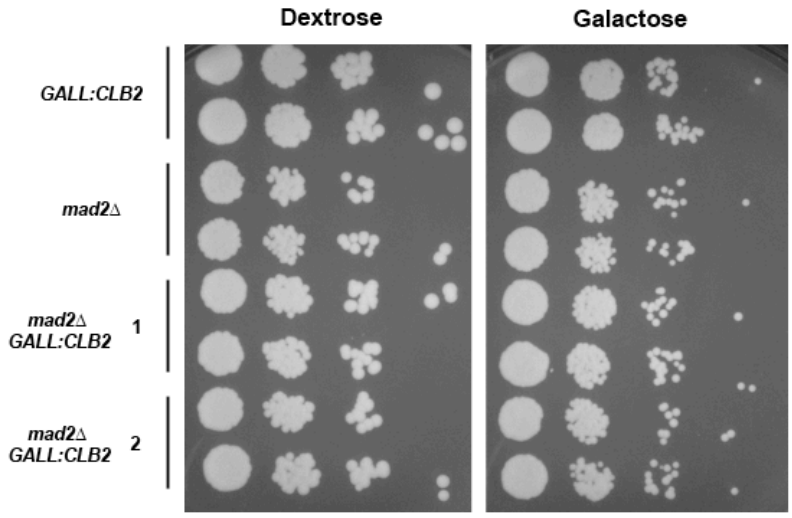

Figure 5-4 *clb2::GALL:CLB2* does not exhibit synthetic lethality with *mad2Δ*.
Strains of the indicated genotypes (the two bottom strains are separate transformants from the same transformation) were plated in 10-fold dilution series on dextrose-containing (left) and galactose-containing (right) plates. Images show two days of growth.

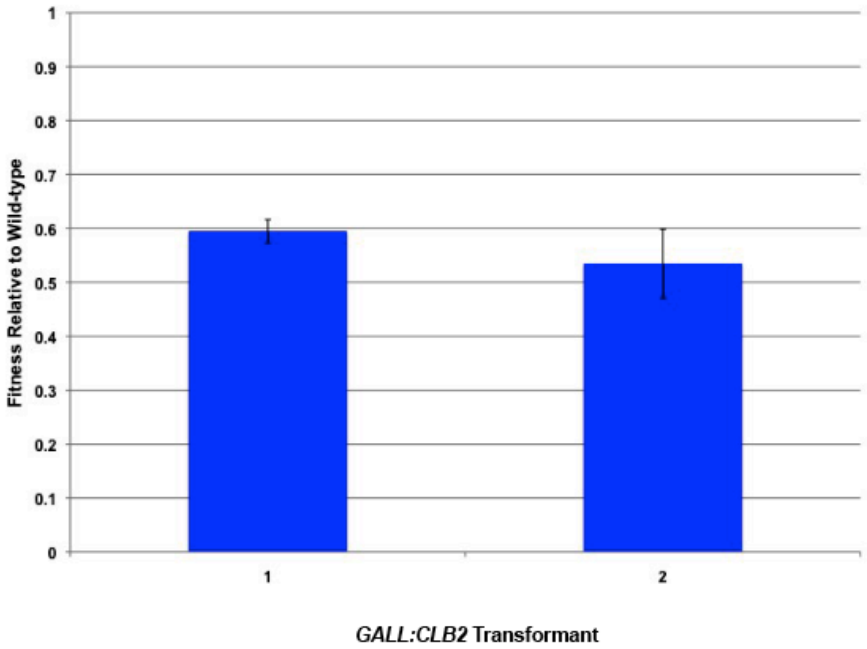

Figure 5-5 Clb2 overexpression imposes a fitness cost. Two *clb2::GALL:CLB2* strains (separate transformants from the same transformation) were competed against a $CLB2^{WT}$ strain in a single-step competition assay. Plot shows the mean fitness of each transformant as a fraction of the fitness of the $CLB2^{WT}$ strain. Error bars indicate s.d.

combination, indicating that Clb2 overexpression does not force cells to rely on the spindle assembly checkpoint for viability (Figure 5-4).

To determine whether there might be a fitness defect associated with Clb2 overexpression, I performed single-step competitive growth experiments, in which wild-type and *GALL:CLB2* strains compete in both log phase (exponential growth with excess nutrients) and growth past the diauxic shift (when sugar becomes limiting and cells switch from fermentation to respiration) (Herman, 2002). I found that wild-type cells out-competed *GALL:CLB2* cells in mixed culture, suggesting decreased fitness associated with Clb2 overexpression (Figure 5-5). The ability of *GALL:CLB2* cells to double faster in short-term log phase assays suggests that these Clb2-overexpressing cells are less adapted to growth in limiting nutrient conditions. It will be interesting to examine this further.

CHAPTER 6 – DISCUSSION

Molecular Architecture of Cell Cycle Transitions

In this work, I have discussed two phases of the cell cycle in which pivotal transitions are made. At Start, cells irreversibly commit to a round of division. In Mitosis, cells finish that round of division, taking steps to carefully segregate their genomic content. The two processes operate quite differently, however. Start is a quick and irreversible switch. Mitosis is an ordered series of events spread over a significant period of time. Accordingly, underlying the two processes are two very different machineries.

Start: an Irreversible Switch

In Chapter 2, I discussed work with Gilles Charvin elucidating the properties of the molecular network underlying Start. In order to isolate this pathway from the rest of the cell cycle machinery, we used genetics to partially rewire its connections. Using flow-cell timelapse microscopy, we observed single cells while triggering reversible pulses of gene expression. This allowed us to investigate the steady-state properties of the module in the absence of normal cell cycle progression.

At the heart of the regulatory module is a positive feedback loop of *CLN1* and *CLN2*. Previously, this feedback loop was shown to promote coherent and switch-like expression of a few hundred genes in the SBF/MBF regulon (Skotheim et al., 2008).

Here, we demonstrate another function of this feedback loop – to make the Start transition irreversible. We find that the Whi5 repressor mediates the requirement for the positive feedback loop; in its absence (*whi5Δ*), a pulse of *CLN2* expression results in sustained transcription, without positive feedback. However, an exogenous pulse of Cln2 is still required to trigger transcription in *cln1Δ cln2Δ cln3Δ whi5Δ* cells, which indicates that Whi5 inactivation cannot be the only essential step in transcriptional activation, consistent with previous conclusions (Costanzo et al., 2004; de Bruin et al., 2004; Skotheim et al., 2008).

To perform these experiments, we isolated the Start regulatory module from subsequent cell cycle progression, which raises the possibility that we are observing behavior that does not occur in wild-type cycling cells. Normally, Clb-CDK activity efficiently shuts off the Start module. Perhaps this turn-off occurs before the system reaches its stable, irreversible state. However, the kinetics of the regulatory module indicates that it does, in fact, reach steady-state in any given cell cycle. First, the time it takes to activate SBF-regulated transcription should be governed by the lifetime of Cln1 and Cln2, which is on the order of five-to-ten minutes. *CLN2*, however, is actively transcribed for 20-30 minutes each cell cycle, suggesting that the switch between stable states does occur in wild-type cell cycles. Secondly, Whi5 is rapidly exported from the nucleus (within about six minutes) (Bean et al., 2006), again consistent with the regulatory module reaching its steady state in any given cell cycle.

There may be several advantages associated with irreversible entry into the cell cycle. First, it allows a noisy signal to trigger a robust transition. Cln3 levels fluctuate little throughout the cell cycle, and the protein is both unstable and relatively non-

abundant (Cross, 1995; Schneider et al., 2004). Noise in gene expression has been shown to contribute to the timing variability of Start (Di Talia et al., 2007). The architecture of the Start module allows a transient above-threshold level of Cln3 to be translated into an all-or-none decision to enter the division cycle. The only criterion is that the duration of the Cln3 pulse be longer than the activation time of the *CLN1,2* positive feedback loop, which is likely on the order of a few minutes, as discussed above.

The all-or-none nature of the decision may be crucial to cell viability. Pre-Start cells are sensitive to mating pheromone, whereas post-Start cells are not. If Start were reversible, cells that had completed some steps of the division cycle (for instance, initiated DNA replication), could be reverted to a pre-Start state and induced to mate, with deleterious consequences. Alternatively, signal noise might cause a cell to undergo Start multiple times, perhaps initiating multiple buds or otherwise impairing fitness. Start thus stands as an interesting example of a graded signal being translated into an irreversible decision.

Mitosis: an Ordered Program of Events

Mitosis provides a compelling counterpoint to the switch-like Start transition. In Mitosis, the cell undertakes the steps necessary for division of the genomic contents and completion of the division cycle. In contrast to the coherence that characterizes Start, mitotic events are temporally separated, spanning half an hour or more. And rather than being triggered by a relatively constitutively-produced inducer, mitotic events are controlled by an inducer whose levels gradually ramp up over the course of

approximately 45 minutes. In Chapter 3, I discussed work investigating how this process is regulated. By providing titrated, stable pulses of inducer (Clb2-CDK) *in vivo* and carefully measuring the execution and kinetics of ensuing mitotic events with timelapse microscopy, I uncovered a quantitative mechanism for mitotic control. Individual events exhibit distinct requirements for Clb2-CDK, with later events requiring higher Clb2 levels than earlier events. This validates the "quantitative model" of Stern and Nurse (Stern and Nurse, 1996).

These results are consistent with recent work in mammalian systems showing that increasing mitotic cyclin-CDK levels might order events, which suggests that this mechanism is fundamental and conserved across eukaryotes (Deibler and Kirschner, 2010; Gavet and Pines, 2010). My work extends these results by providing quantitative, rather than relative, measurements of the thresholds for mitotic events, and by examining events spanning the bulk of Mitosis.

The quantitative measurement of mitotic event thresholds provides two interesting insights. The first is how little Clb2-CDK is required to trigger these events. Eighty percent of the peak level of Clb2 reliably triggers anaphase (the highest threshold), and in wild-type cells, Clb1, Clb3, and Clb4 also contribute to mitosis, with a combined protein level estimated at a few times that of Clb2 alone (Cross et al., 2002; Ghaemmaghami et al., 2003). Thus, cells appear to synthesize more mitotic cyclin than is strictly necessary. This may be due to the effect of Clb2 level on overall cell cycle frequency, described in Chapter 5 and discussed below. Alternatively, excess cyclin may serve as a buffer against noise. I observed a high degree of variability among cycling cells in peak Clb2

level; excess cyclin production may ensure that even low cyclin-expressing cells make enough to get through Mitosis.

Another explanation comes from the second insight arising from my quantitative analysis. By measuring the kinetics of mitotic events in response to Clb2 dosage, I observed a direct relationship between Clb2 level and efficiency, particularly for spindle formation and, to a lesser extent, spindle elongation. Cells with a low level of Clb2 could occasionally form a spindle, but they took much longer to do so than cells with higher Clb2 levels. This observation, combined with the fairly gradual ramp-up of Clb2 level, may help reinforce the order of events. For example, a cell with a certain low level of Clb2 may technically be capable of both depolarizing growth and forming a spindle; however, the cell will depolarize its growth much more efficiently than it will form a spindle, and the former will likely occur before the latter. A short time later, though, Clb2 levels will be higher, and spindle formation will likely occur with greater efficiency.

This reinforcement of ordering may be a common theme of mitotic control. The quantitative mechanism for cyclin-CDK ordering of events is likely supplemented by other ordering mechanisms. For growth depolarization and spindle formation, order may be reinforced by the different mechanisms of the two events, as discussed in Chapter 4. Growth depolarization may occur through Clb2-CDK activity during a sensitive period of the peripheral polarization cycle. This sensitive portion could be the "on" or polarized half of the cycle, in which case the role of Clb2-CDK activity may be to prevent the oscillator from undertaking another cycle. If this were the case, Clb2-CDK would have a significant period of time to accumulate, since polarized growth will shut off for 40 minutes even without Clb-CDK. This provides a large time buffer to correct for sporadic

cell cycles in which Clb2 expression is delayed. For spindle formation and elongation, the two events are necessarily mechanistically coupled; anaphase cannot occur without prior spindle formation, enforcing an order of the two events. In this case, the quantitative Clb2-CDK mechanism seems to enforce further separation of the events by requiring a higher Clb2 level for anaphase. This may prevent possibly deleterious effects of attempting to initiate anaphase on a morphologically incomplete spindle.

Setting Thresholds for Clb-CDK Activity

As discussed above, in Mitosis, graded Clb2-CDK levels are translated into the discrete execution of various events. How are these event thresholds set? As described in Chapter 4, I used my system for measuring Clb2-CDK requirements to test candidate targets of regulation for the process of spindle formation. It was previously suggested that stabilization of the kinesin-5 motors Cin8 and Kip1 is the only essential activity of Clb2-CDK for spindle formation (Crasta et al., 2006). However, I find that this is not the case; in fact, stabilization of Cin8 and Kip1 is not even rate-limiting for spindle formation. The discrepancy between my observations and those described previously may be attributable to the degree of overexpression; my work used a single extra copy of *CIN8* under the control of the endogenous promoter, while previous work used the extremely strong *GAL1* promoter.

I do, however, find phosphorylation of the SPB bridge protein Sfi1 to be critical. Sfi1 contains a cluster of consensus CDK phosphorylation sites, a fairly common feature of CDK targets that has been suggested to introduce easily-evolvable bulk charges that

alter protein-protein interactions rather than inducing subtle conformational changes (Holt et al., 2009). In Sfi1, this cluster occurs in the C-terminus, which may form the basis for the bridge between SPBs (Li et al., 2006). It has been hypothesized, though not shown, that phosphorylation in this region may weaken the bridge (Simmons Kovacs et al., 2008). In my experiments, the ability of charge-based phosphomimetic alleles (double glutamates) to rescue wild-type SPB separation suggests that CDK phosphorylation may indeed introduce a bulk charge that acts to disrupt the interaction between Sfi1 molecules, thereby destabilizing the bridge. These results support a role for Sfi1 as a brake on SPB separation, the release of which allows rapid spindle formation. In the continued presence of this brake (in the *sfi1-120 (sfi1^{NPVK})* allele), spindle formation requires more Clb2, and the timing of spindle formation is more variable. Interestingly, increasing the dosage of the microtubule motor *CIN8* restored normal spindle formation kinetics to *sfi1-120* cells. I combine these results with previous findings (Ma et al., 1999; Strawn and True, 2006; Anderson et al., 2007) to speculate that spindle formation is normally restrained by C-terminal Sfi1 interactions. Phosphorylation of Sfi1 weakens these interactions, and pulling by Cin8 and related motors antagonizes these interactions. If true, spindle formation could be limited by "cutting the last strand" kinetics, which would result in high variability if the number of Sfi1 bridges is small, as is believed to be the case (Li et al., 2006). This could explain the long delays observed in *sfi1-120* cells, the elimination of these delays by adding extra Cin8, the high variability in timing of spindle formation at low Clb2 levels, as well as the rapidity of spindle formation itself, which takes around six minutes regardless of whether the previous waiting time was minutes or hours.

However, there remains a critical, unidentified Clb2-CDK target in this system. This target could involve Cin8/Kip1 activation (distinct from its stabilization), a function recently attributed to Clb-CDK activity (Chee and Haase, 2010), or some other protein altogether. This unknown target is likely rate-limiting, since a strain combining two CDK bypass mutations (*SFI1*$^{5\text{-}EE}$ and *CIN8-KED*) exhibited identical kinetics to an *SFI1*^{WT} *CIN8*^{WT} strain.

The existence of multiple targets controlling spindle formation may allow for a "coincidence detector" mechanism, in which several conditions must be met in order to trigger an output. For example, according to the model above, Sfi1 must be phosphorylated and Cin8 (and likely other factors) must be sufficiently activated in order to achieve SPB separation. This mechanism has been shown previously to function in a single protein. Multisite phosphorylation of Sic1 has been proposed to lead to a steep threshold response of Sic1 degradation to increasing kinase levels (Nash et al., 2001). Analogously, multiple independent phosphorylation targets, on different proteins, could create the threshold we observe for spindle formation.

Anaphase is also controlled by at least two independent Clb-CDK-dependent steps. Clb-CDK activity activates APC^{Cdc20} (which triggers separation of sister chromatids (Rudner and Murray, 2000; Rudner et al., 2000)), and also promotes spindle elongation through a less well-understood APC-independent mechanism (Rahal and Amon, 2008). This dual target system may help restrict the initiation of anaphase to a time, late in the cell cycle, when cells have high Clb-CDK levels.

A different mechanism seems to set the Clb-CDK requirement for growth depolarization. Growth polarization (and associated budding) seems to be controlled by

an autonomous oscillator (Haase and Reed, 1999), whose frequency is modulated by the CDK oscillator to ensure the production of a single bud each cell cycle. Modeling, as described in Chapter 4, can provide useful insights into the behavior of the system, but the molecular nature of the oscillator is unknown. It is possible that cyclical cell polarization does not constitute a unique peripheral oscillator, but rather is a manifestation of the separately described transcriptional oscillator (Orlando et al., 2008). As discussed in Chapter 2, Cln2-CDK activity seems to be continuously required for polarized bud growth, and multiple rounds of Cln2 production drive multiple rounds of budding. The transcriptional oscillator, thought to reflect the periodic activation of transcription factors, is reported to cycle freely upon depletion of mitotic cyclins, and perhaps it is the resultant cycles of Cln2 transcription that drive the growth polarization behavior we observe. It will be interesting to examine this possibility further.

Setting the Frequency of the Cell Cycle Oscillator

A key prediction of the quantitative ordering mechanism described above is that the inducer (Clb-CDK) should be rate-limiting for the events it controls. In other words, increasing the Clb2 level above its endogenous range should accelerate the pace of Mitosis. My work is unique, to my knowledge, in demonstrating this to be true. I show that moderate overexpression of Clb2 from a constitutive promoter accelerates mitotic events, measured from the time of budding. Moreover, I observed that such overexpression also ultimately increases the frequency of the cell cycle oscillator as a whole. This is unexpected, due to the long-held view that growth is rate-limiting for cell

division. In this view, the oscillator's frequency should be fixed by the cell's growth rate, not by the concentration of a cell cycle regulator (Johnston et al., 1977).

I propose that these results can be reconciled with the help of the recent observation that the cell's growth rate is decreased during periods of the cell cycle when the cortex is polarized (Goranov et al., 2009). I believe that premature growth depolarization in cells overexpressing Clb2 increases the average growth rate by dramatically reducing the amount of time cells spend in the slower, polarized growth regime.

A faster cell doubling time might confer a fitness advantage. It is possible that this increased growth rate is one reason cells make more Clb2 than is strictly necessary to trigger mitotic events (see above). But why not make even more Clb2? My work suggests that there is a fitness cost associated with overexpression of Clb2, although the exact nature of this cost remains to be determined. Since *GALL:CLB2* cells proliferate faster than wild-type cells in exponential growth, it is likely that the fitness defect observed in single-step competition assays is due to an impaired ability to cope with nutrient deprivation and undergo the diauxic shift to respiration (Herman, 2002).

Together, this work underscores the central role of the Clb-CDK mitotic regulator, which I have shown controls not only the relative timing of individual cell cycle events, but also the growth rate of the cell, and the overall frequency of the cell cycle oscillator.

APPENDIX – MATERIALS AND METHODS

I. EXPERIMENTAL PROCEDURES

Strain Construction

All strains were derived from W303 and constructed using standard mating and transformation methods. *MET3pr-Venus*, *MET3pr-Venus- CLN2$_{PEST}$* and *MET3pr-CLN2* constructs were integrated at the *URA3* locus by StuI digestion of pCL25, pCL10, and pCL17, respectively. *MET3pr-Venus-CLN2$_{PEST}$* was integrated at the *TRP1* locus by XbaI digestion of pGC25D. *MET3pr-mCherry* and *MET3pr-Venus* were integrated at the *MET3* locus by MfeI digestion of pCL13 and BsmI digestion of pGC25, respectively. *GALL-CLB2* and *GALL-CLB2-YFP* strains were constructed by integration of the zapper plasmid pCL3 (containing a large 3' deletion in *CLB2*) digested with BlpI. *ADH1pr-GAL4rMR* was integrated at the *ADH1* locus by PacI digestion of pCL5. *SPA2-GFP* was integrated at the *LEU2* locus by XcmI digestion of pCL30. *CIN8* and *CIN8-KED* constructs were integrated at the *LEU2* locus by AflII digestion of pCL20 and pCL22, respectively.

Mutant alleles of *SFI1* were obtained as synthesized sequences corresponding to the 3' region of *SFI1*, containing the desired mutations (marked with restriction sites), and flanked by HindIII and KpnI sites (Epoch Biolabs, Missouri City, TX). Syntheses were provided in pBSK and verified by sequencing. Integrating plasmids were constructed by cloning the HindIII-KpnI fragment of each into pRS406. *sfi1-120(NPVK)*, *SFI1^{EEVK}*, and *SFI1$^{5\text{-}EE}$* strains were constructed by digestion of pCL33,

pCL36, and pCL42, respectively, with AgeI to integrate at the *SFI1* locus. The *sfi1-120(NPVK)* mutant was based on the published sequence(Anderson et al., 2007). Integrations were verified by digestion of diagnostic PCR fragments.

Timecourses

Alpha-factor Synchronization

Strains containing a *bar1*Δ mutation were grown to mid-log phase in appropriate media. Cells were arrested with 10nM alpha-factor for two hours at 30^{o}C. Alpha-factor was removed by three cold washes in appropriate media, and cells were resuspended in pre-warmed media.

GALL-CLB2-YFP Pulsing

Strains containing *GALL-CLB2-YFP* and *ADH1-GAL4rMR* were grown to mid-log phase in Synthetic Complete media lacking methionine and supplemented with 2% dextrose (SCD-Met) containing 5mM deoxycorticosterone (DOC) at 30^{o}C. To arrest cells through Clb2-YFP depletion, DOC was removed by three cold washes in SCD-Met and cells were incubated for two hours at 30^{o}C. To deplete Cdc20, 0.4g/L Met was added to turn off *MET3-CDC20*. After an additional hour, cells were pulsed with 5mM DOC for between five and 15 minutes. To terminate the pulse, DOC was removed by three cold washes with SCD+0.4g/L Met. For timelapse imaging, cells were plated as described below, on SCD+0.4g/L Met. For anaphase timecourses, cells were incubated for two hours at 30^{o}C before Met was removed by vacuum filtration. Cells were resuspended in SCD-Met media and plated for timelapse imaging on SCD-Met.

Assaying Spindle Formation in CLB2^{WT} Cells

clb1,3,4Δ CLB2-YFP MET3-CDC20 cells carrying a *bar1Δ* mutation were synchronized as described above with 10nM alpha-factor, and released into SCD-Met. At either 45, 50, or 55 minutes post-release, 200µg/mL cycloheximide was added to stop protein translation (and thus further Clb2-YFP production). Cells were incubated for one hour at 30°C to allow full maturation of the YFP fluorophore. Cells were fixed and imaged (see below). Mean nuclear Clb2-YFP intensity was measured using custom Matlab software (briefly, background was subtracted and values normalized to the peak level of Clb2-YFP in an unperturbed cell cycle). Spindle state was assayed by eye from Tub1-CFP signal.

Microscopy

Fixed Cell Imaging

For imaging of Tub1-CFP, Tub1-GFP, Clb2-YFP, Htb2-mCherry, and/or Spc29-CFP, samples were collected by centrifugation, washed once with water, resuspended in formaldehyde fixative (4% paraformaldehyde, 3.4% sucrose, 100mM KPO_4 pH 7.5, 100µM $MgCl_2$), and incubated for ten minutes at room temperature. Cells were spun down, washed twice with sorbitol-phosphate buffer (1.2M sorbitol, 100mM KPO_4 pH 7.5, 100µM $MgCl_2$), and resuspended in 50µl sorbitol-phosphate buffer. Fixed cells were stored at 4°C and imaged within 24 hours.

To quantify growth depolarization, samples were fixed with the formaldehyde fixative described above for one hour, washed two times in sorbitol-phosphate buffer, then incubated with rhodamine-phalloidin (Invitrogen) for one hour in darkness (vortexed every 15 minutes). Cells were washed five times with sorbitol-phosphate buffer and resuspended in 50µl sorbitol-phosphate buffer.

Samples were imaged using a Zeiss Axioplan 2 inverted fluorescent microscope with a 63X N.A. 1.4 Plan Apo oil objective and a Hamamatsu camera. Images were acquired using OpenLab software (Improvision). Image intensity calibration beads (InSpeck Green, 2.5μm, ~0.3% relative intensity; Molecular Probes) were used to correct for intensity variations between imaging sessions. For fluorescently-tagged proteins, a z-stack of layers 0.5μm apart was taken (YFP and mCherry – 3 layers; CFP – 5 layers). Clb2-YFP signal intensity and spindle formation were determined using custom Matlab software. Briefly, background was subtracted from raw YFP images and values were normalized to the calibration bead reading. Nuclei were masked by a thresholding function performed on raw mCherry images. Mean YFP intensity in each nucleus was calculated and normalized to the mean from a population of cells containing peak levels of Clb2-YFP. When imaging Spc29-CFP, the number of distinct CFP signals in each cell body was automatically determined; 1 signal was scored as no spindle, 2 signals were scored as a spindle.

For phalloidin-stained cells, images were acquired as above, and polarization index was determined using custom Matlab software. Briefly, the bud contour (outer edge) was traced, and the mean fluorescent intensity of the middle third of the contour (corresponding to the bud tip) divided by the mean fluorescent intensity of the remaining two-thirds. Values around one indicate uniform cortical actin patch distribution; values greater than one indicate tip-biased (polarized) localization.

Timelapse Microscopy (Agar Slab)

Timelapse imaging was carried out using a Leica DMI6000B inverted fluorescence microscope with a 63X N.A. 1.4 oil objective and a Hamamatsu Orca-AG

camera. The objective and stage were heated to 30^{o}C. Samples were mounted on slabs containing 1.5% agar dissolved in appropriate growth media. Images were acquired every three minutes, with image acquisition and analysis carried out with custom Matlab software described previously(Charvin et al., 2008). To enhance signal intensity, 2x2 binning of CCD pixels was used. As described for fixed cell imaging, intensity calibration beads were used to correct for lamp intensity. Htb2-mCherry signal was used to mask nuclei and determine mean nuclear Clb2-YFP intensity. Clb2-YFP took up to 45 minutes to fully mature; nuclear intensity was determined by averaging the values from at least five frames after this point. For anaphase movies, Clb2-YFP was fully mature at the beginning of the movie (following a two hour incubation). Clb2-YFP nuclear intensity values were normalized to the intensity of calibration beads, unlabeled cell background (mean value obtained from cycling cells without YFP-labeled Clb2) was subtracted, and the resulting values were normalized to peak Clb2-YFP levels (from cycling cells carrying *CLB2-YFP*). The timings of spindle formation and elongation were scored by eye from Tub1-CFP signal. Since the spindle pole bodies (SPBs) did not always lie in the focal plane, it took up to three frames (nine minutes) to definitively score spindle formation. Growth depolarization was scored by eye from the rate of increase of bud length.

Timelapse Microscopy (Flow Cell)

To monitor events in real-time following changes in media conditions (leading to changes in gene expression), a microfluidic device was used in conjunction with the timelapse microscope setup described above. This device has previously been described in detail (Charvin et al., 2008; Charvin et al., 2010a). Media used were synthetic

complete (SC) supplemented with 2% dextrose, 3% raffinose, or 3% raffinose + 3% galactose and the appropriate concentration of methionine. To repress the *MET3* promoter, 0.04 g/L (2X) methionine was used, except for experiments using *MET3-Venus*, in which 10X methionine was used to lower the fluorescence level.

Mean cytoplasmic fluorescence values for various fluorescent proteins were obtained by averaging the pixel intensities within a cell contour. Nuclear fluorescence of Whi5-GFP was determined using a custom Monte Carlo routine in Matlab, described in detail elsewhere(Charvin et al., 2010b).

Immunoblotting and Kinase Assays

Western blotting was performed using standard methods. The following antibody concentrations were used: mouse anti-Pgk1, 1:10,000 (Invitrogen); rabbit anti-Clb2, 1:2,000 (Covance); goat anti-Clb5, 1:200 (Sigma); rabbit anti-c-myc (A-14), 1:10,000 (Santa Cruz), mouse anti-GFP, 1:1,000 (Roche); HRP-conjugated anti-rabbit and anti-mouse, 1:5,000 (GE); HRP-conjugated anti-goat, 1:4,000 (Sigma).

Kinase assays were performed essentially as described(Levine et al., 1996), with a few modifications. Additional phosphatase inhibitors were used: 50mM NaF, 1mM sodium-orthovanadate. Cells were broken using a FastPrep bead beater (Thermo Scientific), two times 20 seconds each on setting 5, with a one minute rest on ice in between. Rabbit anti-Clb2 antibody (Covance) was used at a 1:700 dilution.

Single-Step Competition Assays

To determine relative fitness of strains carrying *GALL-CLB2::URA3*, cells of the experimental strain and a WT strain carrying the *HIS3* auxotrophic marker were grown to mid-log phase in yeast extract peptone + 2% galactose (YPG). Approximately equal cell

numbers of the two strains were mixed into fresh YPG to a combined OD_{660} of ~0.05. As a control for differential growth caused by the auxotrophic markers, a WT strain carrying the *URA3* marker was similarly grown and mixed with the WT *HIS3* strain. Equal volumes of the resulting cultures were plated on G-Ura and G-His plates, and the resulting colonies were counted. The mixed cultures were incubated for 24 hours at 30°C, after which time equal volumes were again plated on G-Ura and G-His plates, and resulting colonies counted. The relative fitness was calculated by dividing the final Ura+ : His+ colony ratio by the initial ratio, and then normalizing to the same calculation for the WT strain mixture (markers only).

Matlab Modeling

Spindle Formation at Fixed Clb2 Levels

An ordinary differential equation (ODE) model for the *S. cerevisiae* cell cycle was previously described(Chen et al., 2004). To compare our measured Clb2 requirement for spindle formation to the prediction of that model, we isolated the ODE describing spindle formation:

$$\frac{d[SPN]}{dt} = k_s \times \frac{[CLB2]}{J_s + [CLB2]} - k_d \times [SPN]$$

where [*CLB2*] is the Clb2 level, spindle formation occurs when [*SPN*] reaches 1, and rate constants are:

$k_s = 0.1$

$J_s = 0.14$

$k_d = 0.06$

Matlab was used to solve this ODE for various fixed levels of [*CLB2*] corresponding to the stable Clb2-YFP levels provided experimentally (expressed as a fraction of the peak level in a normal cell cycle).

Clb2-CDK Phase-Locking of Independent Growth Polarization Cycle

To model Clb2-CDK entrainment of a growth polarization cycle, we adapted a mathematical phase-locking model from (Lu and Cross, 2010). The treatment of coupling between oscillators is modified from (Strogatz, 1994), adapted to describe one-way phase-locking. Essentially, a Clb2-CDK oscillator (φ) oscillates with an intrinsic frequency ($\nu(\varphi)$), which is arbitrarily set to 1. A peripheral oscillator controlling polarized growth (ψ) oscillates with its own intrinsic frequency ($\nu(\psi)$), expressed as a fraction of $\nu(\varphi)$. The peripheral cycle, ψ, is sensitive to forcing by the Clb2-CDK oscillator, φ, in a specific portion of its cycle, when $\sin(\psi) > Z_{lim}$. $Z_{lim} = 1$ means that ψ is never sensitive to forcing, -1 means that it is always sensitive, and 0 means that it is sensitive during half of its cycle. Coupling (C) characterizes the strength of the effect of φ on $\nu(\psi)$. φ_{level} denotes a fixed, stable level of φ corresponding to the fixed Clb2 levels provided experimentally. The response of ψ is described by

$$\frac{d\psi}{dt} = \psi + Z(\psi, Z_{\lim}) \times C \times \varphi_{level}$$

where

$$Z(\psi, Z_{\lim}) = \begin{cases} 1 & for \quad \sin(\psi) > Z_{\lim} \\ 0 & \end{cases}$$

Parameter values were estimated from experimental data. Specifically, $\nu(\psi)$ was calculated by dividing the frequency of budding in the absence of Clb2-CDK activity (1/80') by the total cell cycle frequency (1/100'), giving 1.25. It was assumed that the

budding cycle is sensitive during its polarized portion, which is half the total cycle time, giving $Z_{lim} = 0$. C was arbitrarily defined to be equal to 2, since this gave a response to fixed levels of φ consistent with the response observed experimentally. Simulation was carried out in Matlab.

II. EXPERIMENTAL MATERIALS

Table 1 Yeast strains used in this study. All strains are derivatives of W303.

Strain	Genotype
HTLU-H	*MATa HIS3*
HTLU-U	*MATa URA3*
RUY156	*MATα mad2::kanMX*
CL37	*MATa bar1 TUB1-GFP::HIS3 cdc20::MET3pr:HA$_3$-CDC20::TRP1 ADE2*
CL107-1	*MATα cln1::HI3 cln2::CLNpr:yEVenus::TRP1 cln3::LEU2 TRP1::MET3pr:CLN2 URA3::GAL1pr:SIC1-Δ3P CDC10-YFP::LEU2 WHI5-GFP::kanMX ADE2*
CL107-2	*MATa cln1::HIS3 cln2::CLN2pr:yEVenus-CLN2$_{PEST}$::TRP1 cln3::LEU2 TRP1::MET3pr:CLN2 CDC10-YFP::LEU2 URA3::GAL1pr:SIC1-Δ3P ADE2*
CL118	*MATa MET3::MET3pr:mCherry::URA3::MET3pr:yEVenus::TRP1 ADE2*
CL124	*MATα cln3::LEU2 bck2::HIS3 TRP1::MET3pr:CLN2 URA3::GAL1pr:SIC1Δ3P WHI5-GFP::kanMX CDC10-YFP::LEU2 CLN2pr:yEVenus-CLN2$_{PEST}$::TRP1::CLN2 ADE2*
CL142	*MATa CLN2pr:GFP::HIS3 URA3::GAL1pr:SIC1Δ3P ADE2*
CL146	*MATα cln1 cln2 cln3::LEU2 GAL1pr:CLN1::LEU2 URA3::MET3pr:CLN2 TRP1::MET3pr:yEVenus-CLN2$_{PEST}$ ADE2*
CL156	*MATa cln1 cln2 cln3::LEU2 bck2::HIS3 TRP1::MET3pr:CLN2 WHI5-GFP::kanMX CDC10-YFP::LEU2 ADE2*
CL172	*MATa clb1 clb2::GALLpr:CLB2-YFP::URA3::HIS3 clb3::TRP1 clb4::his3::kanMX cdc20::MET3pr:HA$_3$-CDC20::TRP1 ADH1pr:GAL4rMR::HIS5 TUB1-CFP::HIS3 HTB2-mCherry::HIS3 MYO1-mCherry::HIS3 ADE2*

CL174	*MATa cln1::HIS3 cln2 cln3::LEU2 bck2::HIS3 TRP1::MET3pr:CLN2 URA3::GAL1pr:SIC1Δ3P CDC10-YFP::LEU2 WHI5-GFP::kanMX*
CL177	*MATα cln1::HIS3 cln2::CLN2pr:yEVenus::TRP1 cln3::LEU2 TRP1::MET3pr:CLN2 URA3::GAL1pr:SIC1-Δ3P whi5::kanMX CDC10-YFP::LEU2 ADE2*
CL190	*MATa cln1 cln2 cln3::LEU2 GAL1pr:CLN1::LEU2 TRP1::MET3pr:CLN2 CDC10-YFP::LEU2 URA3::MET3pr:yEVenus ADE2*
CL207	*MATa clb1 clb2::GALLpr:CLB2-YFP::URA3::HIS3 clb3::TRP1 clb4::his3::kanMX cdc20::MET3pr:HA$_3$-CDC20::TRP1 ADH1pr:GAL4rMR::HIS5 SPC29-CFP::kanMX HTB2-mCherry::HIS3 ADE2*
CL218	*MATα clb1 clb2::GALLpr:CLB2-YFP::URA3::HIS3 clb3::TRP1 clb4::his3::kanMX CIN8-KED::LEU2 ADH1pr:GAL4rMR::HIS5 HTB2-mCherry::HIS3 TUB1-CFP::TRP1 ADE2*
CL219	*MATα clb1 clb2::GALLpr:CLB2-YFP::URA3::HIS3 clb3::TRP1 clb4::his3::kanMX cdc20::MET3pr:HA$_3$-CDC20::TRP1 sfi1-120 MYO1-mCherry::HIS3 TUB1-CFP::TRP1 HTB2-mCherry::HIS3 ADH1pr:GAL4rMR::HIS5 ADE2*
CL231	*MATα clb1 clb2::GALLpr:CLB2-YFP::URA3::HIS3 clb3::TRP1 clb4::his3::kanMX cdc20::MET3pr:HA$_3$-CDC20::TRP1 CIN8-KED::LEU2 ADH1pr:GAL4rMR::HIS5 TUB1-CFP::TRP1 HTB2-mCherry::HIS3 ADE2*
CL238	*MATa clb1 clb2::GALLpr:CLB2-YFP::URA3::HIS3 clb3::TRP1 clb4::his3::kanMX ADH1pr:GAL4rMR::HIS5 cdc20::MET3pr:HA$_3$-CDC20::TRP1 SFI1^{EEVK} TUB1-CFP::TRP1 HTB2-mCherry::HIS3 ADE2*
CL239	*MATa clb1 clb2::GALLpr:CLB2-YFP::URA3::HIS3 clb3::TRP1 clb4::his3::kanMX ADH1pr:GAL4rMR::HIS5 cdc20::MET3pr:HA$_3$-*

	CDC20::TRP1 swe1::URA3 TUB1-CFP::TRP1 HTB2-mCherry::HIS3 ADE2
CL240-1	*MATα clb1 clb3::TRP1 clb4::his3::kanMX cdc20::MET3pr:HA$_3$-CDC20::TRP1 TUB1-GFP::HIS3 ADE2*
CL240-2	*MATα cdc20::MET3pr:HA$_3$-CDC20::TRP1 TUB1-GFP::HIS3 ADE2*
CL243	*MATa bar1 clb1 CLB2-YFP::HIS3 clb3::TRP1 clb4::his3::kanMX cdc20::MET3pr:HA$_3$-CDC20::TRP1 MYO1-mCherry::HIS3 TUB1-mCherry::URA3 TUB1-CFP::TRP1 ADE2*
CL265	*MATα clb1 clb2::GALLpr:CLB2-YFP::URA3::HIS3 clb3::TRP1 clb4::his3::kanMX ADH1pr:GAL4rMR::HIS5 sfi1-120 LEU2::CIN8 cdc20::MET3pr::HA$_3$-CDC20::TRP1 TUB1-CFP::TRP1 HTB2-mCherry::HIS3 ADE2*
CL284	*MATa clb1 clb2::GALLpr:CLB2-YFP::URA3::HIS3 clb3::TRP1 clb4::his3::kanMX ADH1pr:GAL4rMR::HIS5 SFI1^{5EE} cdc20::MET3pr:HA$_3$-CDC20::TRP1 HTB2-mCherry::HIS3 TUB1-CFP::TRP1 ADE2*
CL303-5	*MATa bar1 clb1::URA3 clb3::TRP1 clb4::HIS5 TUB1-GFP::HIS3 ADE2*
CL303-8	*MATa bar1 clb1::URA3 clb3::TRP1 clb4::HIS5 swe1::TRP1 TUB1-GFP::HIS3 ADE2*
CL309	*MATα clb1 clb2::GALLpr:CLB2-YFP::URA3::HIS3 clb3::TRP1 clb4::his3::kanMX ADH1pr:GAL4rMR::HIS5 cdc20::MET3pr:HA$_3$-CDC20::TRP1 CIN8-KED::LEU2 SFI1^{5EE} TUB1-CFP::TRP1 HTB2-mCherry::HIS3 ADE2*
CL311	*MATa bar1 clb2::GALLpr:CLB2::URA3 TUB1-GFP::HIS3 cdc20::MET3pr:HA$_3$-CDC20::TRP1 ADE2*
CL313-1	*MATa clb2::GALLpr:CLB2::URA3*
CL313-2	*MATa clb2::GALLpr:CLB2::URA3*
CL314-1	*MATα mad2::kanMX clb2::GALLpr:CLB2::URA3*
CL314-2	*MATα mad2::kanMX clb2::GALLpr:CLB2::URA3*

Table 2 Plasmids used in this study. All plasmids are derivatives of the pRS series.

Plasmid	Description	Source
pMR5125	pRS416 – SPA2-GFP	M. Rose
pEH113	pRS315 – CIN8	M.A. Hoyt
pEH394	pRS315 – CIN8-KED	M.A. Hoyt
p313GAL4rMR	pRS313 – ADH1pr:GAL4rMR	N. Buchler
pGC25	pRS404 – MET3pr:yEVenus	G. Charvin
pGC25D	pRS404 – MET3pr:yEVenus-CLN2$_{PEST}$	This Study
pCL3	pRS406 – GALLpr:clb2Δ	This Study
pCL5	pRS403 – ADH1pr:GAL4rMR	This Study
pCL10	pRS406 – MET3pr:yEVenus-CLN2$_{PEST}$	This Study
pCL13	pRS406 – MET3pr:mCherry	This Study
pCL17	pRS406 – MET3pr:CLN2	This Study
pCL20	pRS405 – CIN8	This Study
pCL22	pRS405 – CIN8-KED	This Study
pCL25	pRS406 – MET3pr:yEVenus	This Study
pCL30	pRS405 – SPA2-GFP	This Study
pCL33	pRS406 – sfi1-120$^{(C\text{-terminus})}$	This Study
pCL36	pRS406 – SFI1$^{EEVK\ (C\text{-terminus})}$	This Study
pCL42	pRS406 – SFI1$^{5EE(C\text{-terminus})}$	This Study

REFERENCES

Adams, I. R., and Kilmartin, J. V. (1999). Localization of core spindle pole body (SPB) components during SPB duplication in Saccharomyces cerevisiae. J Cell Biol *145*, 809-823.

Amon, A., Surana, U., Muroff, I., and Nasmyth, K. (1992). Regulation of p34CDC28 tyrosine phosphorylation is not required for entry into mitosis in S. cerevisiae. Nature *355*, 368-371.

Amon, A., Tyers, M., Futcher, B., and Nasmyth, K. (1993). Mechanisms that help the yeast cell cycle clock tick: G2 cyclins transcriptionally activate G2 cyclins and repress G1 cyclins. Cell *74*, 993-1007.

Anderson, V. E., Prudden, J., Prochnik, S., Giddings, T. H. J., and Hardwick, K. G. (2007). Novel *sfi1* alleles uncover additional functions for Sfi1p in bipolar spindle assembly and function. Mol. Biol. Cell *18*, 2047-2056.

Archambault, V., Buchler, N. E., Wilmes, G. M., Jacobson, M. D., and Cross, F. R. (2005). Two-Faced Cyclins with Eyes on the Targets. Cell Cycle *4*, 125-130.

Bean, J. M., Siggia, E. D., and Cross, F. R. (2005). High Functional Overlap Between MluI Cell-Cycle Box Binding Factor and Swi4/6 Cell-Cycle Box Binding Factor in the G1/S Transcriptional Program in Saccharomyces cerevisiae. Genetics *171*, 49-61.

Bean, J. M., Siggia, E. D., and Cross, F. R. (2006). Coherence and Timing of Cell Cycle Start Examined at Single-Cell Resolution. Molecular Cell *21*, 3-14.

Biondi, E. G., Reisinger, S. J., Skerker, J. M., Arif, M., Perchuk, B. S., Ryan, K. R., and Laub, M. T. (2006). Regulation of the bacterial cell cycle by an integrated genetic circuit. Nature *444*, 899-904.

Bjarnason, G. A., and Jordan, R. (2002). Rhythms in human gastrointestinal mucosa and skin. Chronobiol Int *19*, 129-140.

Bjarnason, G. A., Jordan, R. C., Wood, P. A., Li, Q., Lincoln, D. W., Sothern, R. B., Hrushesky, W. J., and Ben-David, Y. (2001). Circadian expression of clock genes in human oral mucosa and skin: association with specific cell-cycle phases. Am J Pathol *158*, 1793-1801.

Bloom, J., and Cross, F. R. (2007). Multiple levels of cyclin specificity in cell-cycle control. Nat Rev Mol Cell Biol *8*, 149-160.

Charvin, G., Cross, F. R., and Siggia, E. D. (2008). A microfluidic device for temporally controlled gene expression and long-term fluorescent imaging in unperturbed dividing yeast cells. PLoS One *3*, e1468.

Charvin, G., Cross, F. R., and Siggia, E. D. (2009). Forced periodic expression of G1 cyclins phase-locks the budding yeast cell cycle. Proc Natl Acad Sci USA *106*, 6632-6637.

Charvin, G., Oikonomou, C., and Cross, F. (2010a). Long-term imaging in microfluidic devices. Methods Mol Biol *591*, 229-242.

Charvin, G., Oikonomou, C., Siggia, E. D., and Cross, F. R. (2010b). Origin of irreversibility of cell cycle start in budding yeast. PLoS Biol *8*, e1000284.

Chee, M. K., and Haase, S. B. (2010). B-cyclin/CDKs regulate mitotic spindle assembly by phosphorylating kinesins-5 in budding yeast. PLoS Genet *6*, e1000935.

Chen, K. C., Calzone, L., Csikasz-Nagy, A., Cross, F. R., Novak, B., and Tyson, J. J. (2004). Integrative analysis of cell cycle control in budding yeast. Mol. Biol. Cell *15*, 3841-3862.

Chen, Z., Odstrcil, E. A., Tu, B. P., and McKnight, S. L. (2007). Restriction of DNA replication to the reductive phase of the metabolic cycle protects genome integrity. Science *316*, 1916-1919.

Costanzo, M., Nishikawa, J. L., Tang, X., Millman, J. S., Schub, O., Breitkreutz, B., Dewar, D., Rupes, I., Andrews, B., and Tyers, M. (2004). CDK activity antagonizes Whi5, an inhibitor of G1/S transcription in yeast. Cell *117*, 899-913.

Crasta, K., Huang, P., Morgan, G., Winey, M., and Surana, U. (2006). Cdk1 regulates centrosome separation by restraining proteolysis of microtubule-associated proteins. EMBO *25*, 2251-2263.

Crasta, K., Lim, H. H., Giddings, T. H. J., Winey, M., and Surana, U. (2008). Inactivation of Cdh1 by synergistic action of Cdk1 and polo kinase is necessary for proper assembly of the mitotic spindle. Nat. Cell Biol. *10*, 665-675.

Cross, F. R. (1995). Starting the cell cycle: what's the point? Curr Opin Cell Biol *7*, 790-797.

Cross, F. R. (2003). Two Redundant Oscillatory Mechanisms in the Yeast Cell Cycle. Developmental Cell *4*, 741-752.

Cross, F. R., and Siggia, E. D. (2005). Mode locking the cell cycle. Physical Review E (Statistical, Nonlinear, and Soft Matter Physics) *72*, 021910.

Cross, F. R., Archambault, V., Miller, M., and Klovstad, M. (2002). Testing a Mathematical Model of the Yeast Cell Cycle. Mol. Biol. Cell *13*, 52-70.

de Bruin, R. A., McDonald, W. H., Kalashnikova, T. I., Yates, J. R., and Wittenberg, C. (2004). Cln3 activates G1-specific transcription via phosphorylation of the SBF bound repressor Whi5. Cell *117*, 887-898.

Deibler, R. W., and Kirschner, M. W. (2010). Quantitative reconstruction of mitotic CDK1 activation in somatic cell extracts. Mol. Cell *37*, 753-767.

Dekens, M. P., Santoriello, C., Vallone, D., Grassi, G., Whitmore, D., and Foulkes, N. S. (2003). Light regulates the cell cycle in zebrafish. Curr Biol *13*, 2051-2057.

Di Como, C. J., Chang, H., and Arndt, K. T. (1995). Activation of CLN1 and CLN2 G1 cyclin gene expression by BCK2. Mol Cell Biol *15*, 1835-1846.

Di Talia, S., Wang, H., Skotheim, J. M., Rosebrock, A. P., Futcher, B., and Cross, F. R. (2009). Daughter-specific transcription factors regulate cell size control in budding yeast. PLoS Biol *7*, e1000221.

Di Talia, S., Skotheim, J. M., Bean, J. M., Siggia, E. D., and Cross, F. R. (2007). The effects of molecular noise and size control on variability in the budding yeast cell cycle. Nature *448*, 947-951.

Dong, G., Yang, Q., Wang, Q., Kim, Y. I., Wood, T. L., Osteryoung, K. W., van Oudenaarden, A., and Golden, S. S. (2010). Elevated ATPase activity of KaiC applies a circadian checkpoint on cell division in *Synechococcus elongatus*. Cell *140*, 529-539.

Drapkin, B. J., Lu, Y., Procko, A. L., Timney, B. L., and Cross, F. R. (2009). Analysis of the mitotic exit control system using locked levels of stable mitotic cyclin. Mol. Syst. Biol. *5*,

Dunlap, J. C., Loros, J. J., Colot, H. V., Mehra, A., Belden, W. J., Shi, M., Hong, C. I., Larrondo, L. F., Baker, C. L., Chen, C. H., Schwerdtfeger, C., Collopy, P. D., Gamsby, J. J., and Lambreights, R. (2007). A circadian clock in Neurospora: how genes and proteins cooperate to produce a sustained, entrainable, and compensated biological oscillator with a period of about a day. Cold Spring Harb Symp Quant Biol *72*, 57-68.

Durcan, T. M., Halpin, E. S., Casaletti, L., Vaughan, K. T., Pierson, M. R., Woods, S., and Hinchliffe, E. H. (2008). Centrosome duplication proceeds during mimosine-induced G1 cell cycle arrest. J Cell Physiol *215*, 182-191.

Elowitz, M. B., and Leibler, S. (2000). A synthetic oscillatory network of transcriptional regulators. Nature *403*, 335-338.

Elowitz, M. B., Levine, A. J., Siggia, E. D., and Swain, P. S. (2002). Stochastic gene expression in a single cell. Science *297*, 1183-1186.

Epstein, C. B., and Cross, F. R. (1994). Genes that can bypass the CLN requirement for Saccharomyces cerevisiae cell cycle START. Mol Cell Biol *14*, 2041-2047.

Evans, T., Rosenthal, E. T., Youngblom, J., Distel, D., and Hunt, T. (1983). Cyclin: a protein specified by maternal mRNA in sea urchin eggs that is destroyed at each cleavage division. Cell *33*, 389-396.

Felix, M. A., Labbe, J. C., Doree, M., Hunt, T., and Karsenti, E. (1990). Triggering of cyclin degradation in interphase extracts of amphibian eggs by cdc2 kinase. Nature *346*, 379-382.

Fitch, I., Dahmann, C., Surana, U., Amon, A., Nasmyth, K., Goetsch, L., Byers, B., and Futcher, B. (1992). Characterization of four B-type cyclin genes of the budding yeast Saccharomyces cerevisiae. Mol. Biol. Cell *3*, 805-818.

Gard, D. L., Hafezi, S., Zhang, T., and Doxsey, S. J. (1990). Centrosome duplication continues in cycloheximide-treated *Xenopus* blastulae in the absence of a detectable cell cycle. J Cell Biol. *110*, 2033-2042.

Gavet, O., and Pines, J. (2010). Progressive activation of CyclinB1-Cdk1 coordinates entry to mitosis. Dev. Cell *18*, 533-543.

Ghaemmaghami, S., Huh, W., Bower, K., Howson, R. W., Belle, A., Dephoure, N., O'Shea, E. K., and Weissman, J. S. (2003). Global analysis of protein expression in yeast. Nature *425*, 737-741.

Goranov, A. I., Cook, M., Ricicova, M., Ben-Ari, G., Gonzalez, C., Hansen, C., Tyers, M., and Amon, A. (2009). The rate of cell growth is governed by cell cycle stage. Genes Dev. *23*, 1408-1422.

Haase, S. B., and Reed, S. I. (1999). Evidence that a free-running oscillator drives G1 events in the budding yeast cell cycle. Nature *401*, 394-397.

Haase, S. B., Winey, M., and Reed, S. I. (2001). Multi-step control of spindle pole body duplication by cyclin-dependent kinase. Nat Cell Biol *3*, 38-42.

Hartwell, L. H. (1971). Genetic control of the cell division cycle in yeast. II. Genes controlling DNA replication and its initiation. J Mol Biol *59*, 183-194.

Hartwell, L. H., and Unger, M. W. (1977). Unequal division in Saccharomyces cerevisiae and its implications for the control of cell division. J Cell Biol. *75*, 422-435.

Hartwell, L. H., and Weinert, T. A. (1989). Checkpoints: controls that ensure the order of cell cycle events. Science *246*, 629-634.

Harvey, S. L., Charlet, A., Haas, W., Gygi, S. P., and Kellogg, D. R. (2005). Cdk1-dependent regulation of the mitotic inhibitor Wee1. Cell *122*, 407-420.

Harvey, S. L., and Kellogg, D. R. (2003). Conservation of Mechanisms Controlling Entry into Mitosis: Budding Yeast Wee1 Delays Entry into Mitosis and Is Required for Cell Size Control. Current Biology *13*.

Herman, P. K. (2002). Stationary phase in yeast. Curr Opin Microbiol *5*, 602-607.

Hildebrandt, E. R., and Hoyt, M. A. (2000). Mitotic motors in Saccharomyces cerevisiae. Biochim Biophys Acta *1496*, 99-116.

Hildebrandt, E. R., and Hoyt, M. A. (2001). Cell cycle-dependent degradation of the *Saccharomyces cerevisiae* spindle motor Cin8p requires APC^{Cdh1} and a bipartite destruction sequence. Mol. Biol. Cell *12*, 3402-3416.

Holt, L. J., Krutchinsky, A. N., and Morgan, D. O. (2008). Positive feedback sharpens the anaphase switch. Nature *454*, 353-357.

Holt, L. J., Tuch, B. B., Villén, J., Johnson, A. D., Gygi, S. P., and Morgan, D. O. (2009). Global analysis of Cdk1 substrate phosphorylation sites provides insights into evolution. Science *325*, 1682-1686.

Hood, J. K., Hwang, W. W., and Silver, P. A. (2001). The Saccharomyces cerevisiae cyclin Clb2p is targeted to multiple subcellular locations by cis- and trans-acting determinants. J Cell Sci *114*, 589-597.

Hoyt, M. A., He, L., Loo, K. K., and Saunders, W. S. (1992). Two *Saccharomyces cerevisiae* kinesin-related gene products required for mitotic spindle assembly. J Cell Biol. *118*, 109-120.

Hu, F., and Aparicio, O. M. (2005). Swe1 regulation and transcriptional control restrict the activity of mitotic cyclins toward replication proteins in Saccharomyces cerevisiae. PNAS *102*, 8910-8915.

Johnston, G. C., Pringle, J. R., and Hartwell, L. H. (1977). Coordination of growth with cell division in the yeast Saccharomyces cerevisiae. Exp Cell Res *105*, 79-98.

Jorgensen, P., Edgington, N. P., Schneider, B. L., Rupes, I., Tyers, M., and Futcher, B. (2007). The size of the nucleus increases as yeast cells grow. Mol. Biol. Cell *18*, 3523-3532.

Keaton, M. A., and Lew, D. J. (2006). Eavesdropping on the cytoskeleton: progress and controversy in the yeast morphogenesis checkpoint. Current Opinion in Microbiology *9*, 540-546.

Kilmartin, J. V. (2003). Sfi1p has conserved centrin-binding sites and an essential function in budding yeast spindle pole body duplication. J Cell Biol *162*, 1211-1221.

King, D. P., and Takahashi, J. S. (2000). Molecular genetics of circadian rhythms in mammals. Annu Rev Neurosci *23*, 713-742.

Klevecz, R. R., Bolen, J., Forrest, G., and Murray, D. B. (2004). A genomewide oscillation in transcription gates DNA replication and cell cycle. PNAS *101*, 1200-1205.

Koch, C., Moll, T., Neuberg, M., Ahorn, H., and Nasmyth, K. (1993). A role for the transcription factors Mbp1 and Swi4 in progression from G1 to S phase. Science *261*, 1551-1557.

Lee, T. I., Rinaldi, N. J., Robert, F., Odom, D. T., Bar-Joseph, Z., Gerber, G. K., Hannett, N. M., Harbison, C. T., Thompson, C. M., Simon, I., Zeitlinger, J., Jennings, E. G., Murray, H. L., Gordon, D. B., Ren, B., Wyrick, J. J., Tagne, J. B., Volkert, T. L., Fraenkel, E., Gifford, D. K., and Young, R. A. (2002). Transcriptional regulatory networks in Saccharomyces cerevisiae. Science *298*, 799-804.

Lew, D. J., and Reed, S. I. (1993). Morphogenesis in the Yeast Cell Cycle: Regulation by Cdc28 and Cyclins. The Journal of Cell Biology *120*, 1305-1320.

Li, S., Sandercock, A. M., Conduit, P., Robinson, C. V., Williams, R. L., and Kilmartin, J. V. (2006). Structural role of Sfi1p-centrin filaments in budding yeast spindle pole body duplication. J Cell Biol *173*, 867-877.

Lim, H. H., Goh, P. Y., and Surana, U. (1996). Spindle pole body separation in Saccharomyces cerevisiae requires dephosphorylation of the tyrosine 19 residue of Cdc28. Mol Cell Biol *16*, 6385-6397.

Loog, M., and Morgan, D. O. (2005). Cyclin specificity in the phosphorylation of cyclin-dependent kinase substrates. Nature *434*, 104-108.

Lu, Y., and Cross, F. R. (2010). Periodic cyclin-Cdk activity entrains an autonomous Cdc14 release oscillator. Cell *141*, 268-279.

Ma, P., Winderickx, J., Nauwelaers, D., Dumortier, F., De Doncker, A., Thevelein, J. M., and Van Dijck, P. (1999). Deletion of *SFI1*, a novel suppressor of partial Ras-cAMP pathway deficiency in the yeast *Saccharomyces cerevisiae*, causes G_2 arrest. Yeast *15*, 1097-1109.

Manzoni, R., Montani, F., Visintin, C., Caudron, F., Ciliberto, A., and Visintin, R. (2010). Oscillations in Cdc14 release and sequestration reveal a circuit underlying mitotic exit. J Cell Biol *190*, 209-222.

Markson, J. S., and O'Shea, E. K. (2009). The molecular clockwork of a protein-based circadian oscillator. FEBS Lett *583*, 3938-3947.

Mateus, C., and Avery, S. V. (2000). Destabilized green fluorescent protein for monitoring dynamic changes in yeast gene expression with flow cytometry. Yeast *16*, 1313-1323.

Matsuo, T., Yamaguchi, S., Mitsui, S., Emi, A., Shimoda, F., and Okamura, H. (2003). Control mechanism of the circadian clock for timing of cell division in vivo. Science *302*, 255-259.

McCleland, M. L., and O'Farrell, P. H. (2008). RNAi of mitotic cyclins in *Drosophila* uncouples the nuclear and centrosome cycle. Curr Biol *18*, 245-254.

McCusker, D., Denison, C., Anderson, S., Egelhofer, T. A., Yates, J. R., Gygi, S. P., and Kellogg, D. R. (2007). Cdk1 coordinates cell-surface growth with the cell cycle. Nat Cell Biol *9*, 506-515.

McNulty, J. J., and Lew, D. J. (2005). Swe1p Responds to Cytoskeletal Perturbation, Not Bud Size, in S. cerevisiae. Current Biology *15*, 2190-2198.

Mitchison, J. M. (1958). The growth of single cells. II. Saccharomyces cerevisiae. Exp Cell Res *15*, 214-221.

Morgan, D. O. (2007). The Cell Cycle: Principles of Control (London: New Science Press, Ltd.; Oxford University Press; Sinauer Associates, Inc.).

Nagoshi, E., Saini, C., Bauer, C., Laroche, T., Naef, F., and Shibler, U. (2004). Circadian gene expression in individual fibroblasts: cell-autonomous and self-sustained oscillators pass time to daughter cells. Cell *119*, 693-705.

Nash, P., Tang, X., Orlicky, S., Chen, Q., Gertler, F. B., Mendenhall, M. D., Sicheri, F., Pawson, T., and Tyers, M. (2001). Multisite phosphorylation of a CDK inhibitor sets a threshold for the onset of DNA replication. Nature *414*, 514-521.

Novak, B., and Tyson, J. J. (2008). Design principles of biochemical oscillators. Nat Rev Mol Cell Biol *9*, 981-991.

Orlando, D. A., Lin, C. Y., Bernard, A., Wang, J. Y., Socolar, J. E. S., Iversen, E. S., Hartemink, A. J., and Haase, S. B. (2008). Global control of cell-cycle transcription by coupled CDK and network oscillators. Nature *453*, 944-947.

Peterson, J. B., and Ris, H. (1976). Electron-microscopic study of the spindle and chromosome movement in the yeast Saccharomyces cerevisiae. J Cell Sci *22*, 219-242.

Picard, D. (1999). Regulation of heterologous proteins by fusion to a hormone binding domain. In Nuclear receptors: a practical approach, Picard, D., ed. (Oxford: Oxford University Press), pp. 261-275.

Pomerening, J. R., Sontag, E. D., and Ferrell, J. E. (2003). Building a cell cycle oscillator: hysteresis and bistability in the activation of Cdc2. Nat Cell Biol *5*, 346-351.

Pringle, J. R., and Hartwell, L. H. (1981). The *Saccharomyces cerevisiae* Cell Cycle. In The Molecular Biology of the Yeast *Saccharomyces*, Strathern, J. N., E. W. Jones, and J. R. Broach, eds. (Cold Spring Harbor, NY: Cold Spring Harbor Laboratory), pp. 97-144.

Rahal, R., and Amon, A. (2008). Mitotic CDKs control the metaphase-anaphase transition and trigger spindle elongation. Genes Dev. *22*, 1534-1548.

Richard, P. (2003). The rhythm of yeast. FEMS Microbiol. Rev. *27*, 547-557.

Richardson, H., Lew, D. J., Henze, M., Sugimoto, K., and Reed, S. I. (1992). Cyclin-B homologs in *Saccharomyces cerevisiae* function in S phase and in G2. Genes Dev. *6*, 2021-2034.

Robbins, J. A., and Cross, F. R. (2010). Requirements and reasons for effective inhibition of the anaphase promoting complex activator CDH1. Mol. Biol. Cell *21*, 914-925.

Roof, D. M., Meluh, P. B., and Rose, M. D. (1992). Kinesin-related proteins required for assembly of the mitotic spindle. J Cell Biol. *118*, 95-108.

Rudner, A. D., Hardwick, K. G., and Murray, A. W. (2000). Cdc28 activates exit from mitosis in budding yeast. JCB *149*, 1361-1376.

Rudner, A. D., and Murray, A. W. (2000). Phosphorylation by Cdc28 activates the Cdc20-dependent activity of the Anaphase-Promoting Complex. JCB *149*, 1377-1390.

Schneider, B. L., Yang, Q. H., and Futcher, A. B. (1996). Linkage of replication to start by the Cdk inhibitor Sic1. Science *272*, 560-562.

Schneider, B. L., Zhang, J., Markwadt, J., Tokiwa, G., Volpe, T., Honey, S., and Futcher, B. (2004). Growth rate and cell size modulate the synthesis of, and requirement for, G1-phase cyclins at start. Mol Cell Biol *24*, 10802-10813.

Schwob, E., Bohm, T., Mendenhall, M. D., and Nasmyth, K. (1994). The B-type cyclin kinase inhibitor p40SIC1 controls the G1 to S transition in S. cerevisiae. Cell *79*, 233-244.

Silverman, S. J., Petti, A. A., Slavov, N., Parsons, L., Briehof, R., Thiberge, S. Y., Zenklusen, D., Gandhi, S. J., Larson, D. R., Singer, R. H., and Botstein, D. (2010). Metabolic cycling in single yeast cells from unsynchronized steady-state populations limited on glucose or phosphate. PNAS *107*, 6946-6951.

Simmons Kovacs, L. A., Nelson, C. L., and Haase, S. B. (2008). Intrinsic and Cyclin-dependent Kinase-dependent Control of Spindle Pole Body Duplication in Budding Yeast. Mol. Biol. Cell *19*, 3243-3253.

Skotheim, J. M., Di Talia, S., Siggia, E. D., and Cross, F. R. (2008). Positive feedback of G1 cyclins ensures coherent cell cycle entry. Nature *454*, 291-296.

Sluder, G., and Lewis, K. (1987). Relationship between nuclear DNA synthesis and centrosome reproduction in sea urchin eggs. J Exp Zool *244*, 89-100.

Sluder, G., Miller, F. J., Cole, R., and Rieder, C. L. (1990). Protein synthesis and the cell cycle: centrosome reproduction in sea urchin eggs is not under translational control. J Cell Biol. *110*, 2025-2032.

Smaaland, R., Sothern, R. B., Laerum, O. D., and Abrahamsen, J. F. (2002). Rhythms in human bone marrow and blood cells. Chronobiol Int *19*, 101-127.

Snyder, M. (1989). The SPA2 protein of yeast localizes to sites of cell growth. J Cell Biol *108*, 1419-1429.

Spellman, P. T., Sherlock, G., Zhang, M. Q., Iyer, V. R., Anders, K., Eisen, M. B., Brown, P. O., Botstein, D., and Futcher, B. (1998). Comprehensive identification of cell cycle-regulated genes of the yeast Saccharomyces cerevisiae by microarray hybridization. Mol Biol Cell *9*, 3273-3297.

Stern, B., and Nurse, P. (1996). A Quantitative Model for the cdc2 Control of S Phase and Mitosis in Fission Yeast. Trends in Genetics *12*, 345-350.

Strawn, L. A., and True, H. L. (2006). Deletion of *RNQ1* gene reveals novel functional relationship between divergently transcribed Bik1p/CLIP-170 and Sfi1p in spindle pole body separation. Curr. Genet. *50*, 347-366.

Strickfaden, S. C., Winters, M., J., Ben-Ari, G., Lamson, R. E., Tyers, M., and Pryciak, P. M. (2007). A mechanism for cell-cycle regulation of MAP kinase signaling in a yeast differentiation pathway. Cell *128*, 519-531.

Strogatz, S. H. (1994). Nonlinear Dynamics and Chaos (Cambridge, MA: Westview Press).

Surana, U., Amon, A., Dowzer, C., McGrew, J., Byers, B., and Nasmyth, K. (1993). Destruction of the CDC28/CLB mitotic kinase is not required for the metaphase to anaphase transition in budding yeast. EMBO J *12*, 1969-1978.

Thornton, B. R., and Toczyski, D. P. (2003). Securin and B-cyclin/CDK are the only essential targets of the APC. Nat Cell Biol *5*, 1090-1094.

Tsai, T. Y., Choi, Y. S., Ma, W., Pomerening, J. R., Tang, C., and Ferrell, J. E. J. (2008). Robust, tunable biological oscillations from interlinked positive and negative feedback loops. Science *321*, 126-129.

Tu, B. P., Kudlicki, A., Rowicka, M., and McKnight, S. L. (2005). Logic of the yeast metabolic cycle: temporal compartmentalization of cellular processes. Science *10*, 1152-1158.

Ubersax, J. A., Woodbury, E. L., Quang, P. N., Paraz, M., Blethrow, J. D., Shah, K., Shokat, K. M., and Morgan, D. O. (2003). Targets of the cyclin-dependent kinase Cdk1. Nature *425*, 859-864.

van Drogen, F., and Peter, M. (2002). Spa2p functions as a scaffold-like protein to recruit the Mpk1p MAP kinase module to sites of polarized growth. Curr Biol *12*, 1698-1703.

Verma, R., Annan, R. S., Huddleston, M. J., Carr, S. A., Reynard, G., and Deshaies, R. J. (1997). Phosphorylation of Sic1p by G1 Cdk required for its degradation and entry into S phase. Science *278*, 455-460.

Wang, H., Carey, L. B., Cai, Y., Wijnen, H., and Futcher, B. (2009). Recruitment of Cln3 cyclin to promoters controls cell cycle entry via histone deacetylase and other targets. PLoS Biol *7*, e1000189.

Weinert, T. A., Kiser, G. L., and Hartwell, L. H. (1994). Mitotic checkpoint genes in budding yeast and the dependence of mitosis on DNA replication and repair. Genes Dev. *8*, 652-665.

Winey, M., Mamay, C. L., O'Toole, E. T., Mastronarde, D. N., Giddings, T. H. J., McDonald, K. L., and McIntosh, J. R. (1995). Three-dimensional ultrastructural analysis of the Saccharomyces cerevisiae mitotic spindle. J Cell Biol *129*, 1601-1615.

Wittenberg, C., and Reed, S. I. (2005). Cell cycle-dependent transcription in yeast: promoters, transcription factors, and transcriptomes. Oncogene *24*, 2746-2755.

Yang, Q., Pando, B. F., Dong, G., Golden, S. S., and van Oudenaarden, A. (2010). Circadian gating of the cell cycle revealed in single cyanobacterial cells. Science *327*, 1522-1526.

Yeong, F. M., Lim, H. H., Wang, Y., and Surana, U. (2001). Early expressed Clb proteins allow accumulation of mitotic cyclin by inactivating proteolytic machinery during S phase. Mol. Cell. Biol. *21*, 5071-5081.

Zachariae, W., Schwab, M., Nasmyth, K., and Seufert, W. (1998). Control of cyclin ubiquitination by CDK-regulated binding of Hct1 to the anaphase promoting complex. Science *282*, 1721-1724.